Ex Vivo- and In Vivo-Based Computational Methods to Model Muscle Structure and Study 2D Ultrasound Measurements of 3D Muscle Architecture

---

A

Dissertation

Presented to

the faculty of the School of Engineering and Applied Science

University of Virginia

---

in partial fulfillment

of the requirements for the degree

Doctor of Philosophy

by

Adrienne F.O. Williams

August 2022

APPROVAL SHEET

This

Dissertation

is submitted in partial fulfillment of the requirements
for the degree of

Doctor of Philosophy

Author: Adrienne F.O. Williams

This Dissertation has been read and approved by the examing committee:

Advisor: Silvia S. Blemker

Advisor:

Committee Member: Shayn Peirce-Cottler

Committee Member: Jason Kerrigan

Committee Member: Rebecca Scharf

Committee Member: Jeffrey Saucerman

Committee Member:

Committee Member:

Accepted for the School of Engineering and Applied Science:

Jennifer L. West, School of Engineering and Applied Science

August 2022

Abstract

In this dissertation, we present novel computational modeling techniques that enable us to (1) create 3D models without medical imaging data in order to study muscle fascicle behavior during contraction, and (2) directly compare 2D ultrasound muscle architecture measurements to 3D model architecture, allowing us to validate model-predicted changes in architecture during contraction as well as study and improve our understanding of these commonly used ultrasound measurements.

Muscle architecture – the arrangement of fascicles (fiber bundles) within a muscle – determines a muscle's ability to contract to produce force and enable movement. Cadaver dissections can determine these properties *ex vivo*, and magnetic resonance diffusion tensor imaging (MR-DTI) is used to study *in vivo* three-dimensional (3D) muscle architecture. However, neither of these methods can inherently measure changes in fascicle behavior during contraction. Brightness-mode ultrasound (US) imaging is commonly used to measure changes in architecture in contracting muscle. However, these US measurements are two-dimensional (2D) while muscles' architecture is 3D. Physics-based computational methods enable us to model 3D muscle form and architecture in order to study fascicle behavior contraction.

In project 1, we developed a method to create simple 3D CAD muscle models using cadaver architecture data. With a simple model of the medial gastrocnemius (MG), we demonstrated that we can capture the varied fascicle lengths and angles throughout a muscle and a apply a realistic material model to perform simulations of contraction in order to study muscle mechanics. In project 2, we created a method to simulate 2D ultrasound measurements using an MRI-based 3D MG model we developed. Our model successfully captured fascicle behavior that agreed with *in vivo* ultrasound data, enabling us to use our model for virtual experiments. In project 3, we applied our US simulation method to examine how

the simplifications made during typical 2D ultrasound architecture measurements impact the accuracy of the 2D measurements relative to 3D architecture. We found that the difference between 2D/linearized and 3D fascicle length decreases as the percentage of the fascicle in the US field of view increases. This suggests that linearized fascicle lengths (as in US architecture measurements) more accurately represent 3D fascicle lengths when majority of the fascicle is captured in the FOV.

My dissertation research advances our ability to 1) create 3D muscle models without *in vivo* data, and 2) explore the impact of current limitations of ultrasound on the interpretation of 2D architecture measurements of 3D muscle architecture.

Acknowledgements

First of all, thank you God. From my acceptance into this program on that last possible day in 2015, to now, only You could have cleared this path for me and seen me through, putting resources for me at each step of the way.

When I got to Charlottesville, Virginia in 2015, I had only been in the U.S. for the previous two years during a Master's program. Before 2014, I had never even heard of Charlottesville and I wish to credit those who helped to change the course of my life in that short time. Thank you to Dr Stephenson and Dr Aiken from the University of the West Indies, Mona in Jamaica for helping me to get to the US because of your role in my undergraduate education and providing letters of recommendation. Thanks to Mr Alford, and Dr McCullough from North Carolina A&T State University, for the mechanics, engineering and research training that converted me from physicist to engineer. Dr M, thank you for the research training, mentorship and the encouragement that prepared me to come into this PhD program at the University of Virginia. Dr Knisley, thanks for your encouragement and support.

To the people who mentored me and helped me find my way in grad school at UVA, I am grateful for you. I especially want to thank Deborah Johnson (and Sam), Keisha John, Keisha Jones-Tibbs, Gordon Laurie, and Kelly Cunningham. Next to Silvia, you all provided mentorship and resources, and helped me to feel like I belonged in my program, could keep going, and could finish. Kelly, you facilitated some major opportunities and growth for me, by creating space for me to grow in your Peer Review Groups and Grad Writing Lab programs, by being Co-PI for my communication activity (Speak Easy), and for being a font of resources. Most of all, thanks for the hours of your time when I dropped by your office to discuss development ideas for Speak Easy while I ate snacks leftover from your events. I really admire how much you have done with the SEAS GWL since you've been here.

To other students at UVA with whom I shared many experiences, I appreciate you. Xueying, I really enjoyed developing our research communication together in PRG and since then, getting to know you outside of school. You were one of my first Speak Easy supporters. I also want to thank my other Speak Easy supporters and Organization for Underrepresented Students (OURS)-goers Merci Best, Maria Ali, Bethany Gordon, Ciara Horne, Zollie White and Darius Carter, and Yoni Aberra. I learned so much from you all. To Sam Perez, thanks for being willing to share that inaugural GBMES DEI co-chair position with me. You didn't have to, and I am proud of the conversations and frameworks we started in our department. When I pass the all-gender bathroom in our department, I think of you. Latisha Ross, you and I met at the end of your post-doc at UVA, but I appreciate your encouragement and enjoy our Zoom check-ins. To my conference buddies Carla Davis and Mukti Chowkwale, those experiences were memorable because of you.

To my non-UVA Charlottesville community, you were critical to my welfare. My doulas, Selena Cozart and Latoria White, thank you for being our support when we had Naomi and even since then. Our former neighbors Jerrie and Chad (and the kids), thanks for lunch dates, letting me do my dissertation proposal from your apartment without prior notice, when I had technical issues on the day, and for Naomi drop-off/pick-ups when I had Enam. To my community outside of Charlottesville, I would like to thank you for your faith in me. To Dr James, CJ DARK KATS (friend group from high school), Dominique Rose, Jessie Amick and Aunt Maureen. I haven't seen many of you for years, but I feel no less love or support. Rashena, thanks for keeping me company over video calls when we both had to work overnight or on weekends.

To my lab mates. I have learned so much from you all about research and communicating our work, but also about showing up for colleagues and helping each other to put our best foot forward. Vi, I love your positivity and adaptability. I think you have one of the coolest personal, academic and professional backgrounds ever. Never doubt that you're a star. Katie P, like most people, I enjoyed your

warmth and genuine curiosity and to me, your grad school into professional career path was exemplary of not being afraid to try new things. Katie K, your deep knowledge and productivity was always inspirational. You are one of those people who was made to be a great scholar and teacher. I look forward to reading all the cool work from your future lab. Kelley and Amanda, you are excellent project managers and I respect how you knew your strengths and leveraged them efficiently. Hunter, even though we sat back-to-back and never talked much, you were a calming influence for me. I appreciate that you didn't outwardly judge me when I was perpetually having mishaps like spraying the ceiling with a soda can by accident or repeatedly dashing out the lab then coming back immediately to get something I forgot. It was funny how you and Vi would know that while I might not verbally contribute to most conversations, I would always quietly laugh at the jokes. Evan, we'd sit across from each other but just send instant messages to chat instead. Before Hunter, you were my calming influence and you showed me that it's OK to choose your happiness, to go for what you want, rather than what is expected. Ridhi, in addition to your awesome work and humility, I love how aesthetically pleasing everything you do is. Your presentations are some of my favorites. As a tea lover, Ridhi-bucks was my favorite addition to our lab space during my time there. Matthew, thanks for being a positive presence --chill and funny. Allie, we didn't spend too much time on our projects together, but I enjoyed the time that we did get. Megan, my fellow standing desker, it was nice to catch you in lab on those few weekends. Mario, it's been so nice to meet you. You all were the best lab mates.

To Xiao, you deserve a special shout out for all you have done for me and our lab. Thank you for your help at those crucial times I had in this program. You were there when I was first picking my project and while it is customary for post-docs to help new lab members get orientated, I want to acknowledge that you really helped me understand the work flow when there was little documentation. You were there whenever I had questions or needed advice. You really were the rock in our lab and your

presentations were a masterclass in “less is more”. You should also know that Naomi still has the blanket that you, Aaron and Guoman gifted her when she was born.

To my Committee, thank you for your grace and kindness during my two comprehensive exam attempts and three attempts to get this dissertation wrapped up. To Rebecca, thank you for always being willing to meet with me despite your busy clinical schedule. Thanks for always making us (grad students) feel welcome in Clinic, even when you were seeing patients. It was always a pleasure to bump into you in the MR5 or Pinn hallways. To Jason, thanks for your effort to learn all our names in Continuum and for always being willing to meet for course or research discussions. Your genuine curiosity and excitement when learning about our work always made me feel more excited about my research. To Shayn, thanks for always being there for so many of the grad student in the department, as a committee member or chair. Thanks for always helping us to keep the bigger picture of our work in mind. We know that we should have an idea of the paper(s) we expect from our work before talking to you. You gave me a unique opportunity to write an entire exam for the BME grad program Physiology core course with you, and I really enjoyed the process. To Jeff, thanks for being willing to join my committee later on. I really learned a lot from you when I was your TA for Computational Biomedical Engineering, and I appreciate your kindness over the years.

Silvia, you are the best advisor I could have ever had. I want to thank you the most for not being a dream killer. If what I was attempting was possible, you never brought up whether or not it was probable, but let me try. You alone—your belief in me and my potential-- kept me in the graduate program all this time. Thank you for showing me and so many others that one can be an excellent scientist with impactful work, and still be humble, kind and a good person. Over the years multiple people have asked if you are as cool as you seem, and I am always pleased to report that you are. Thank you for seeing all your students and postdocs as people/individuals, and not seeing our personal circumstances as

limitations or hindrances to our work. I have watched how adaptable and positive you are and I think the thing that I have learned most from you is that once we're doing the work "it will all work out".

To Kristen, thanks for BME Easter eggs each year and for always having candy in that bowl by your desk for anyone who wants it. Thanks for carrot cake with cream cheese frosting for my birthday each year—not too sweet, like I like it. When I look back, we spent months on Zoom for 90 minutes on most days in late 2021 and early 2022 co-working and motivating each other. You've been the social glue many times in the Biotech Training Program, the BME department, for BME Ravens, organizing girls Secret Santa every year and we appreciate you for it. Most recently, you've really supported me and helped watch the kids on some evenings so I could work. You really helped me get to this finish line. Naomi already asks for you all the time, so I know she will miss playing with you when you move away for work and so will I. I appreciate you, always caring for others with your big warm smile.

To Katie Gorick, I think you're cool and I wish we got to hang out more. You were present during many memorable things I did in grad school like playing for team Purple "Osas" in the C'ville women's soccer and indoor leagues and doing that one group exercise class that was not what you and Vi expected. Thank you for staying with Nomi that time Imano and I went to a comedy show at JPJ. Thanks for inviting Imano and I to your family Thanksgiving that year that we lived in Culpeper and for letting me come with you and your sister to Halloween events one year. Thanks for random lunches and conversations that were very deep, considering how rarely we hung out. All these things are memorable for me because you didn't have to be kind to a stranger.

To Bonnie and Kris, thank you for being true friends. I don't even remember how or when we started our daily health system circuit walks and too-long lunches, but you both know that next to Silvia, you eased the anxiety of this journey for me. I was never not excited when you came to lab for me, or bummed if I missed you when you came by. I learned so much from you and still look up to you both as

scientists and professionals. Bonnie, between Bible study and your hosting stuff, you helped me get out of my house. Kris, may we forever send each other funny tweets at any hour. Thanks for being godparents to our “Nomi” and “Enny Penny”.

To my family, thank you for always seeing the best in me. Grandma Fay, Grandma Cherry and Granddad Watson, thanks for being there for us and checking on us. You were the geographically closest relatives we had in the U.S. and though we were not psychically close, we knew you were always there. To the Daleys, thanks for enabling me to come home as much as I could to recharge. Dad, you never knew exactly what was going on, but you were ever confident that I could do it. Mum-Bot, my prayer warrior, when people ask how I persevere with everything I have going on, I say that you pray for me. You are the reason I am here today, because whenever I have expressed a desire to do or try something, you never discouraged me and always made a way, even if no one else got it at the time. In that regard, it’s funny that you and Silvia have birthdays days apart, because you both allowed me to dream. Jeff, thanks for being the best brother and life advisor. You were my grad application essay reviewer and now, my defense flyer creator, and I hope that I can have at least a portion of the positive impact you have had on me. May we always sing and dance together, and maintain the promise to call each other out when the familial mental instability is showing. To Shan, you’re the best sister-in-law. You always know just what to say and I appreciate your constant encouragement and active work to help me own my achievements.

To Imano, since we have been in the U.S. we have been far away from relatives. Being in PhD programs, having children, and even being married are life events that typically take a village. The truth is that we have been our own village for of these to-date. I am so proud of us and all that we have accomplished. Naomi was home with you from the time I went back to lab at 6 weeks until she was almost 2 years old. The pictures you sent me every day kept me going and I had a certain peace I couldn’t have had otherwise because she was with you at home while I couldn’t be. You’re inspirational for many reasons, but finishing most of your PhD research while caring for her for that long was an amazing feat.

We haven't known what it's like to be together without one or both of us being in school, and I look forward to life with you as free elves. You're always there for me, while pushing me to improve and I absolutely love working side by side with you every day in our home office. May work from home never end for us homebodies.

To my beautiful children, Naomi (Nomi) and Enam (Enny Penny), you may not understand the meaning of this work or what daddy and I have achieved for years to come, but thank you for being the best motivators and the best stress-relievers and mental health boosters. People say that you both are/will be extra smart because I carried you while studying, but I would also like to believe that I am smarter because I have you two to teach me every day. Nomi, you no longer have to lose sleep when you wake up in the middle of the night and find that I'm not where you expect me to be. Most times you refused to leave me and go back to bed, so the compromise was to set up a mat and blanket on the floor so I could work and you could rest. For your wellness, I wanted you to go back in the actual bed each time, but I was always glad for you and your teddy bear's company in those wee hours.

To Adrienne, you may have already forgotten some of the challenges you have faced and overcome, and even some of the many things that you have learned. I am most proud of you not for what you have accomplished academically while raising a family and later, while working full-time, but for your personal growth. You did it, despite psychological challenges such as: experiencing culture shock, micro-aggressions and racism for the first time in your life, then first-time and recurring clinical depression, and learning at the end of your program when adaptive strategies might no longer matter, that your brain does not process information "typically". Keep embracing your warmth, empathy, eccentricity, creativity, and desire to learn. The intangibles are your greatest strength.

Table of Contents

List of Figures

List of Tables

List of Equations

1 Chapter 1

Introduction

1.1 Overview

Muscle morphology and architecture, intrinsic muscle properties and determinants of function, differ greatly between individuals (Ward et al., 2009; Wickiewicz et al., 1983). A muscle's biomechanical function, i.e. its ability to produce force, is dependent on its fascicle arrangement, called muscle architecture. Real-time brightness-mode ultrasonography is quick, relatively inexpensive and commonly used to provide informative 2D measurements of these muscle properties in both healthy populations (Cronin & Lichtwark, 2013; Kawakami et al., 1998; Lichtwark et al., 2007; Maganaris, 2005; Narici et al., 1996) and those with myopathies (Barber et al., 2017; Morse et al., 2015) in superficial muscles such as the medial gastrocnemius in the leg. However, these US measurements are limited in that they do not give insight into muscle's complex 3D structure. The state-of-the-art technique for evaluating 3D fascicle arrangement is magnetic resonance diffusion tensor imaging (MR DTI), which capitalizes on principal water diffusion along muscle fibers to determine fiber direction and reconstruct fiber trajectories in muscles (Bolsterlee et al., 2017; Charles et al., 2019; Fouré et al., 2018; Sinha et al., 2015). DTI provides helpful insight into 3D architecture, but scan time is too long for subjects to sustain contractions, so only data at a resting condition are available. Computational models are powerful because they can leverage *in vivo* MRI, US and muscle strength data to examine and quantify changes in 3D muscle, architecture (fascicle length, pennation, curvature) and fascicle strain that occur with contraction.

Three-dimensional (3D) image-based finite element (FE) muscle models enable simulations of muscle contractions in order to study changes in 3D architecture. These models can also capture muscle and tendon structure interactions, giving further insight into the relationship between tissue mechanics and function. These models need to be validated with in vivo data for changes in architecture. Since there are currently no 3D methods that provide contracted architecture information, we look to ultrasound measurements of muscle architecture. Since ultrasound measurements are 2D, we cannot directly compare them to a model's 3D structure. We have identified a need to enable direct comparisons

between model architecture and US measurements, and we proposed to emulate the 2D US architecture measurements from the 3D model. Once validated with US, 3D model predictions can be used to further investigate the relationship between muscle structure and function, as well as use our method study how some of the assumptions made during ultrasound measurements may affect the accuracy of the 2D measurements with respect to 3D architecture.

1.2 Dissertation Outline

It is not yet feasible to experimentally study *in vivo* changes in 3D fascicle behavior with contraction. The field currently relies on 2D measurements of fascicle behavior, but the relationship between the 2D and 3D (expected measurements is not yet known. There is an opportunity to leverage computational modeling to gain insights into this relationship. The goal of my dissertation is to create methods for using 3D computer models of muscle to investigate the complex architecture of muscles as well as *in vivo* measurements of architecture changes with contraction, and use these methods to reveal the relationship between 3D fascicle behavior and 2D ultrasound measurements.

The remainder of this dissertation contains five chapters. Chapter 2 provides background knowledge needed for the work we present in this dissertation, including synopses of: finite element and constitutive modeling of muscle and aponeurosis, muscle fascicle arrangement and its important in muscle function, and experimental methods for studying fascicle arrangement. In Chapter 3, we present a novel method to 3D computer muscle models with 3D fascicle arrangement when no MR images or *in vivo* data are available, and we applied our method to model the medial gastrocnemius muscle. We co-authored this work with Xiao Hu, Samuel Ward, Richard Lieber and Silvia S. Blemker, and presented it as a poster at the 2017 Annual Meeting of the American Society of Biomechanics. In Chapter 4, we describe how we developed 1) a 3D MRI-based finite element model of the medial gastrocnemius and 2) a method for simulating ultrasound images and architecture measurements using the 3D model. We use the 3D to

test how aponeurosis stiffness affects changes in fascicle architecture with contraction. We co-authored this work with William H. Clark, Jeroen B. Waanders, Jason R. Franz, and Silvia S. Blemker, and presented it as a poster at the virtual 2020 Annual Meeting of the American Society of Biomechanics. Chapter 5 presents the results from using our ultrasound simulation method to investigate the relationship between 3D fascicle behavior with contraction and 2D ultrasound measurements of same. We are preparing this work for submission to the Journal of Biomechanics, with co-authors William H. Clark, Jeroen B. Waanders, Jason R. Franz and Silvia S. Blemker. In Chapter 6, the Conclusion, we summarize the work presented, highlighting key contributions to the field of biomechanics. We also discuss additional applications of this research, and propose future research directions.

2 Chapter 2

Background

2.1 Skeletal muscle structure and function

Skeletal muscles enable movement by transferring force to bones via connective tissue, specifically tendons. Muscle is a hierarchical structure (Figure 2.1), made up of tens of thousands of the micrometer-scale fundamental force-producing unit, the sarcomere. In myofibrils, sarcomeres are joined in series and enclosed by endomysium, making cylindrical muscle fibers, the cellular unit of muscle. Muscle fibers are micrometer scale in diameter and milli- to centimeter-scale in length. The sum of the individual fiber contractions permits movement. Hundreds to thousands of these fibers bundled together and surrounded by perimysium, make fascicles, which are the smallest structure of the muscle hierarchy that we can see with the visible eye. At the highest level of the structure, the fiber bundles are contained within the epimysium, forming the muscle belly.

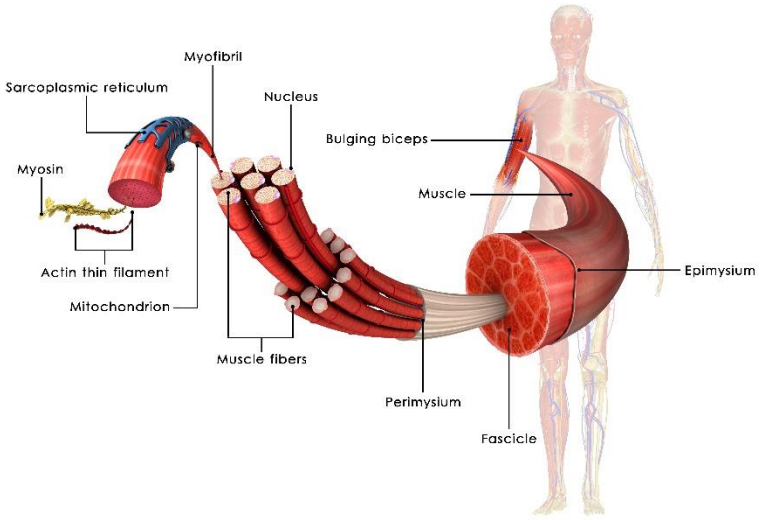

Figure 2.1:Heirarchical structure of skeletal muscle.

This diagram illustrates the hierarchical structure of skeletal muscle and its connective tissue, from the whole muscle down to the cell-level structures.

The form of skeletal muscles, also known as the morphology or geometry, varies by size and shape. The arrangement of fibers within a muscle, called muscle architecture, also varies, and it determines a muscle's ability to generate force or moments about a joint and to ultimately effect

movement. Muscle architecture is defined as the arrangement of muscle fibers within a muscle relative to its i) force generating axis or ii) tendinous tissue (Lieber & Friden, 2000; Zajac, 1989). Typical architecture measurements include fascicle length and pennation angle, as most muscles have fibers bundles that are oriented at an angle to its line of action (Figure 2.2). Hill-type muscle models have also simplified connections to tendinous tissue, so that muscle fascicles are in series with tendon and aponeuroses (Delp et al., 1990; Zajac, 1989).

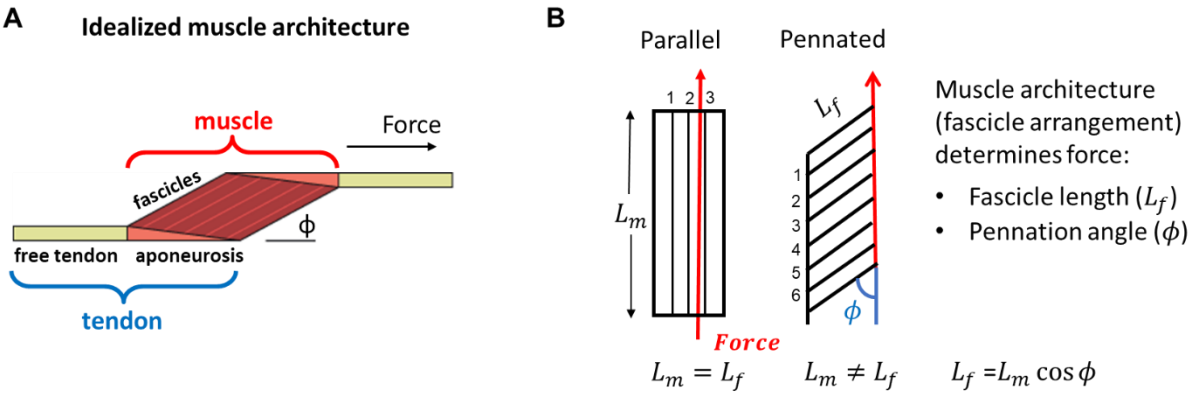

Figure 2.2. Simplified muscle architecture

Generally, muscles with short fibers will have higher PCSA per unit muscle mass, thus greater force production, while muscle with long fibers will have lower PCSA per unit muscle mass, thus lower force production. Given experimental limitations, there is still a lot that we do not understand about the relationship between muscle structure and function.

Medial gastrocnemius

The medial gastrocnemius (Figure 2.3) is one of three members of the triceps surae, often called the calf muscles, located in the superficial posterior compartment of the lower leg. The medial gastrocnemius (MG) originates proximally in the postero-superior region of the corresponding femoral

condyle (Dalmau-Pastor et al., 2014). The lateral gastrocnemius and soleus muscles complete the triceps surae, and together, all three muscles insert to the heel via the Achilles tendon. Therefore, the medial gastrocnemius is biarticular, meaning it crosses two joints. It contributes to foot plantarflexion at the ankle joint and flexion at the knee joint. The MG is important for vertical body support and swing initiation during gait (Anderson & Pandy, 2003; Clark et al., 2021; Neptune et al., 2001).

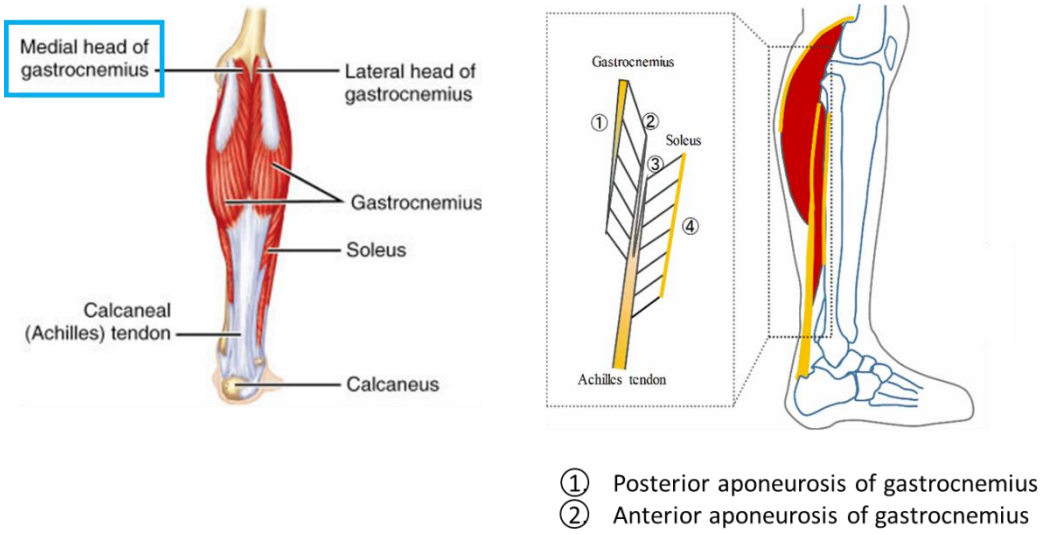

Figure 2.3. Medial gastrocnemius muscle and aponeurosis anatomy.

In this dissertation, we modeled the medial gastrocnemius in order to improve our understanding of the mechanics of this muscle. The MG is commonly studied because of its importance in gait, because it is affected in many myopathies, and because it is superficial, thus easy to access for imaging. This provides literature for us to consult during our research. Medial gastrocnemius muscle morphology and architecture (volume, pennation angles, fascicle lengths, aponeurosis structure) have been measured by cadaver (Shan et al., 2019; Ward et al., 2009), and *in vivo* by US (Fukunaga et al., 1997; Herbert et al., 2015; Maganaris, 2003; Narici et al., 1996), and DTI studies (Bolsterlee et al., 2016a, 2017; Handsfield et al., 2017).

2.2 Ultrasound for studying muscle structure and function *in vivo*

Non-invasive imaging methods allow for *in vivo* measurements of changes in muscle geometry and architecture during motion (Fukunaga et al., 1997; Narici et al., 1996). Real-time brightness-mode ultrasonography is quick, relatively inexpensive and commonly used to provide informative two-dimensional (2D) measurements of these muscle properties in superficial muscles such as the medial gastrocnemius (Cronin & Lichtwark, 2013; Kawakami et al., 1998; Lichtwark et al., 2007; Maganaris, 2003; Narici et al., 1996). Muscle fascicles (fiber bundles) appear in b-mode ultrasound images as dark/hypoechoic linear structures which are surrounded by hyperechoic connective tissues. From these 2D images, researchers digitize fascicles to measure fascicle length, fascicle pennation angle, and muscle thickness (Fukunaga et al., 1997; Kawakami et al., 1998; Maganaris et al., 1998). While changes in fascicle length, strains and pennation angle can be measured from 2D ultrasound (US) images, the efficacy of US to examine changes in muscle architecture with contraction is limited as it: i) only captures a single fascicle in a small region of the muscle that is in the US probe's field-of-view (FOV); ii) does not evaluate the muscle's 3D architecture; and iii) cannot evaluate all fascicles simultaneously.

Two-dimensional (2D) ultrasound (US) measurements of fascicle kinematics assume that a fascicle identified in the US field of view (FOV) at a relaxed state, remains completely in the same FOV or in the same plane while the fascicle contracts (Cronin et al., 2011; Farris & Lichtwark, 2016). In published figures illustrating US images with architecture measurements, the anechoic (fascicles) or hyperechoic (perimysium) tissues do not form a complete line from aponeurosis to aponeurosis, though research construct that line for fascicle length and pennation calculations. Hyperechoic tissues appear to be on a linear path but seem go in and out curve or rotate in and out of the US FOV (Figure 2.4), indicating that either the transducer is not well aligned with the fascicle or the 3D structure does not translate on the 2D imaging system.

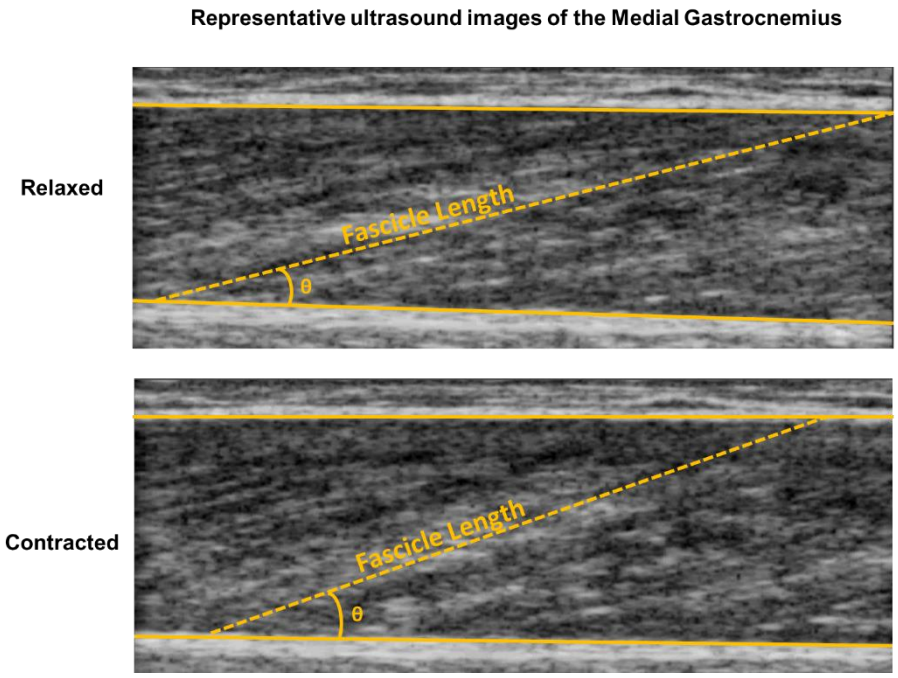

Figure 2.4. 2D ultrasound images of MG muscle when relaxed and contracted.

Fascicle paths are not always i) continuous or ii) linear from aponeurosis to aponeurosis (solid lines), but fascicle length and pennation angle (ϑ) are often determined from such images nonetheless (dashed line)

The 2D measurements are assumed to represent the muscle's 3D structure, and while the measurements are highly repeatable (Kwah et al., 2013; May et al., 2021), the relative error associated with the 2D simplification is not known because it is not physically possible to study. It is very challenging to understand the impact of the 2D assumption from ultrasound imaging alone, but it is important to understand this relationship as well as the experimental/measurement system.

Imaging maximum voluntary isometric contractions

In isometric (fixed-length) contractions, the muscle-tendon unit does not change length, because the joint angles are fixed. However, the muscle can change length during contraction, and it is assumed that the change in muscle length complements the change in in-series tendon length. For example, in the medial gastrocnemius, the muscle length shortens and the Achilles tendon lengthens. During this kind of contraction, ultrasound can image muscle-tendon junction displacement, which is the measure of muscle

shortening, and fascicle kinematics concurrently to determine how much fascicle length and orientation are changing in conjunction with change in whole muscle length.

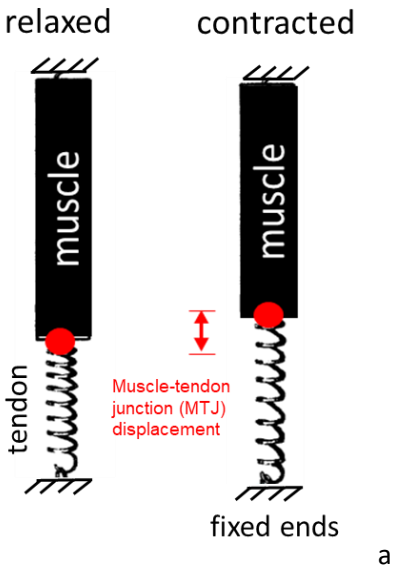

Figure 2.5. Isometric (fixed-MTU-length) contraction.

During an isometric contraction, MTJ displacement indicates how muscle (black box) shortens or tendon (spring) lengthens independent of joint movement.

2.3 Three-dimensional computational modeling of muscle and aponeuroses

Three-dimensional (3D) finite element (FE) models allow image-based modeling of muscles and simulations of muscle contractions in order capture muscle and tendon tissue structure and the mechanics of the relationship between tissue and function. In addition to the complex 3D geometry and fascicle arrangement, this type of 3D model includes fiber properties list], volume preservation, and along- and cross- fiber shear properties (Blemker et al., 2005; Blemker & Delp, 2005).

Modeling geometry and fascicle arrangement

The current state of subject-specific three-dimensional (3D) whole-muscle finite element (FE) modeling framework includes incorporating geometrical, architectural and kinematic information from medical imaging to accurately model muscle. Axial MR images are segmented using in-house software (Handsfield et al., 2014; Knaus et al., 2020) in order to create 3D muscle and aponeurosis geometries.

Models that represent the three-dimensional arrangement of muscle fibers more closely represent the *in vivo* behavior of muscle because they allow for variations in fiber lengths and moment arms. The state-of-the-art technique for evaluating 3D fascicle arrangement is magnetic resonance diffusion tensor imaging (MR DTI), which capitalizes on principal water diffusion along muscle fibers to determine fiber direction and reconstruct fiber trajectories in muscles (Bolsterlee et al., 2017; Charles et al., 2019; Fouré et al., 2018; Sinha et al., 2015). DTI is not an accessible technique. Our lab has used Laplacian computational fluid dynamics (CFD) simulations to model fiber directions and found good agreement with fiber directions determined *in vivo* with DTI (Handsfield et al., 2017). The CFD-predicted fiber directions have successfully used fascicle reconstruction algorithm used for DTI (Bolsterlee et al., 2017, 2018), showing compatibility with other methods used to generate fascicles from vector data. CFD can also be used to model tendinous tissue fiber directions, including aponeuroses.

To enable movement, muscles transmit their forces to bone via tendinous tissue: tendons (external) and aponeuroses (internal). Therefore, it is important to model these structures with the muscle. While MG muscle-tendon interactions have been widely studied (Bolsterlee et al., 2015; Fukunaga, Kubo, et al., 2001; Herbert et al., 2002, 2011), much is still unknown about muscle-aponeurosis interactions. Tendon stiffness and muscle-tendon interactions affect how much fascicles shorten or lengthen during contractions (fascicle strains) and subsequently how much force can be transmitted. Research has shown that MG fascicle length changes are often smaller than muscle-tendon unit length changes due to series elasticity, i.e. tendon's storage and release of energy (Bolsterlee et al., 2015; Fukunaga, Kubo, et al., 2001; Herbert et al., 2002, 2011). Internal tendon (aponeurosis) may behave similarly but this needs to be studied quantitatively. We included aponeurosis structures in our model (Chapter 3) to be able to study how its material stiffness affects architecture changes with contraction.

Modeling material properties.

Finite element models can predict changes in muscle shape, based on the defined constitutive behavior of the muscle and connective tissue and the physical interactions between all modeled structures. We modeled the stress-strain properties of muscle and aponeuroses using quasi-incompressible, hyperelastic, transversely isotropic materials (Blemker et al., 2005; C. Criscione et al., 2001; Weiss et al., 1996). This model separates the dilatational (volumetric – Φvol) and deviatoric (distortional – Φiso) tissue responses and uses physically-based strain invariants (Criscione, Douglas, and Hunter 2001; 28 Weiss et al. 1996) that relate material parameters to physically meaningful measures resulting in the following strain energy density function (Equation 1). The deviatoric (Φiso) term has three components: along fiber stretch ($W_3(\lambda, \alpha)$), and along- ($W_1(B_1)$) and cross-fiber shear ($W_2(B_2)$) (Equation 1). The amount of along fiber stretch is based on the muscle activation (α) and fiber length (λ) with peak isometric stress (σ_{max}) assumed to occur at optimal fiber length (λ). The dilatation (Φvol) is described in relation to the bulk modulus of the muscle tissue (K) and the relative change in volume (J). The muscle material model represents the active (contractile) and passive force-generating properties independently, so that muscle activation occurs in the fascicle direction and can be varied between 0 (no activation) and 1 (maximal activation), as is necessary for simulation of a maximum voluntary isometric contraction (MVIC).

Equation 1. Muscle constitutive equation

transversely isotropic, hyperelastic, quasi-incompressible material

$$\Phi = \Phi_{iso} + \Phi_{vol} = deformation + volume$$

$$\Phi_{iso} = \boldsymbol{W_1(C, a_0)} + \boldsymbol{W_2(C, a_0)} + \boldsymbol{W_3(C, a_0, \alpha)}$$

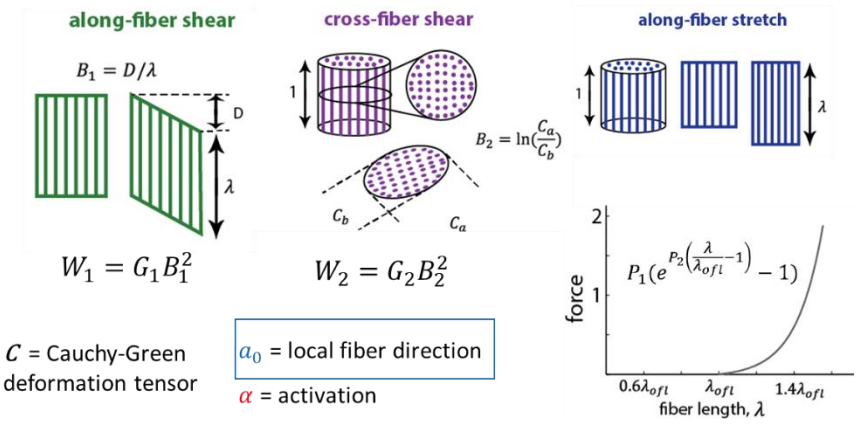

Computational models are able to leverage the 3D geometries of muscles generated from MR images and the 2D US measurements of fascicle architecture and strains to produce quantitative predictions of 3D changes in these measurements with contraction. When fortified with experimental data, physics-based computational modeling allows us to represent complex three-dimensional (3D) muscle and tendinous tissue in order to answer questions about muscle structure and biomechanical function. With models we can perform virtual experiments to investigate how muscle or tendon tissue properties affect fascicle behavior, for example, or evaluate architecture measurement systems and the validity of measurements.

3 Chapter 3

A 3D Model of the Medial Gastrocnemius Created Based on *Ex Vivo* Architectural Measurements

Acknowledgements: Xiao Hu[1], Samuel Ward[2], Richard Lieber[2], Silvia S. Blemker[1]

[1]University of Virginia, Charlottesville, VA, USA
[2]University of California, San Diego, CA, USA

3.1 Abstract

Three-dimensional models of muscle architecture are used to examine the relationship between muscle structure and function and are typically built from medical images such as MRI. However, MR or other medical images of muscles are not always available. Cadaver studies have been conducted to provide physical and fascicle arrangement measurements for most muscles, though these measurements are generally only incorporated into simplified, 2D models of muscle. In this study, we created a method to use muscle-tendon and fascicle arrangement measurements from cadaver studies to build 3D muscle geometries. We demonstrated the method by using a combination of photographs and muscle architecture and physical measurements of the *ex vivo* medial gastrocnemius (MG) from a 52-year-old cadaver to create a 3D model. We used computer-aided drawing (CAD) to generate a volume by drawing an outline of the muscle from the photograph, and extruding it to a uniform thickness given by the mean thickness of a cadaveric medial gastrocnemius. Once the 3D model was created, we generated muscle fibers by creating streamlines from the resulting vectors from a Laplacian flow simulation. We calculated key architectural parameters of the model such as physiological cross-sectional area, volume, fiber length and pennation angle, and compared these model values to those of the *ex vivo* muscle. Our 3D MG model recapitulated the *ex vivo* fiber length and PCSA well, but not the pennation angle or volume as closely. Therefore, we have shown that this method can generate 3D muscle models, in the absence of costly medical images, that represent *ex vivo* muscle well. Models created by this method can be used for *in silico* muscle experiments, to provide important insights into muscle mechanics. This method can be implemented for other muscles, as long as the relevant photographs and *ex vivo* data are available.

3.2 Introduction

Muscle structure is complex and it affects function (operating range of motion and force output) directly. Since direct measurements of muscle force are not possible in humans, computational models are needed for biomechanical studies of muscle function during everyday activities. Computational

models that allow for the incorporation of the complex three-dimensional arrangement and inhomogeneity of muscle fiber architecture are essential for us to be able to effectively study the relationship between muscle structure and function in individual muscles. These high-fidelity models can further our understanding of how individual muscle fibers interact and function to contribute to whole muscle function. Representing variations in three-dimensional structure between different muscles, provides insights into how structure influences normal functional differences. Additionally, functional changes due to muscle pathologies can be studied, once changes in muscle structure due to disease, including fiber arrangement, have been modeled.

The most commonly used computational models that represent whole muscle do not incorporate the 3D structure of individual fibers, as they represent muscle geometry as a series of line segments (Anderson & Pandy, 1999; Delp et al., 1990, 2007). One reason that these models are popular is because they are able to leverage physical and architectural muscle measurements from cadavers. Such cadaveric measurements are very accessible from the literature. High-fidelity three-dimensional finite element models that represent complex muscle geometry and fiber arrangement have been developed to study muscle mechanics (Blemker et al., 2005; Fiorentino et al., 2014; Inouye et al., 2015). These 3D models, used to study phenomena that we cannot study *in vivo*, require *in vivo* experimental data for development and validation. The state-of-the-art process for 3D muscle model-building involves creating subject-specific models based on medical imaging data, such as MRI and ultrasound, for muscle morphology and internal structure. However, often medical images and/or *in vivo* data are not available because of the high cost of medical imaging systems or the lack of experimental expertise to capture the data, or the lack of comprehensive data available from literature for a muscle of interest. These challenges prevent the broad adoption of 3D muscle models. Still, there remains a need to begin developing a muscle model towards a continuum representation of the muscle that can predict changes in shape or fiber arrangement with contraction or movement.

We propose a new solution— to use a simple model or low-fidelity models that can include varied fascicle lengths throughout a muscle and a realistic material model. By using simple models, we can still learn about some muscle mechanics, muscle-tendon interactions and perform model optimization before high resolution in vivo data becomes available. We leverage experimental data to develop and validate 3D muscle models in order to computationally study phenomena that we cannot study *in vivo*. The application and clinical relevance of the models depends on the data that is available to create and validate them. The state-of-the-art process for 3D muscle model-building involves building subject-specific models based on medical imaging data. For example, many individual lower limb muscles have been modeled using MR images (Blemker & Delp, 2005; Handsfield et al., 2014). However, sometimes medical images and/or *in vivo* data are not available, but there is a need to begin developing a muscle model towards a continuum representation of the muscle that can predict changes in shape or fiber arrangement with contraction or movement. In this case we can still learn about some muscle mechanics, muscle-tendon interactions and perform model optimization using simple models. Simple models are an excellent means by which to conduct preliminary research, as they allow for method refinement before investing resources into acquiring further images (MRI, ultrasound, etc.), processing and complex model building.

The goal of this work was to create a method for developing simple 3D computer muscle models with representative architecture that can be created without imaging or *in vivo*/kinematics data. Using our method and computer-aided design (CAD) tools, we modeled the human medial gastrocnemius (MG) muscle based on published architectural data measured *ex vivo* by anatomical inspection and ultrasound (Narici et al., 1996; Ward et al., 2009; Wickiewicz et al., 1983).

3.3 Methods

3.3.1 Physical parameters and architecture measurements from *ex vivo* muscle

To create the model geometry, we used *ex vivo* medial gastrocnemius muscle physical measurements and fiber architecture data from a cadaver study (Ward et al., 2009). Ward et al. conducted this study of lower limb muscle architecture directly measured from 21 cadaver subjects of known size (height: 168.4 ± 9.3 cm, weight: 82.7 ± 15.3 kg), sex (9 males, 12 females) and age (83 ± 9 years). In these experiments, they disassembled 27 muscles from 21 formaldehyde-fixed human lower extremities to characterize muscle fiber length and physiological cross-sectional area, which define the excursion and force-generating capacities of a muscle. To facilitate the development of high-resolution computational muscle models, they created "maps" for each muscle, which are photographs illustrated with dotted lines, to indicate the location of the physical measurements, i.e. muscle fiber sampling (1 to 3 fibers for each muscle) and muscle length (Lm) measurements.

From the measurements taken for each lower limb muscle, the following muscle measurements were relevant for this work: mass, muscle length (Lm), raw fiber length (Lf'), pennation angle (two-dimensional; at muscle surface) and physiological cross-sectional area (PCSA). The mass of each excised muscle was measured after external tendons, connective tissue, and fat were removed. Muscle length (Lm) was defined as the distance from the origin of the most proximal fibers to insertion of the most distal fibers. Raw fiber length (Lf') was measured from the previously mapped three to five regions in each muscle using a digital caliper (accuracy: 0.01 mm). Muscle fiber bundles were dissected from the proximal tendon to the distal tendon of each mapped muscle region. Surface pennation angle was measured in each of these regions with a standard goniometer, as the angle between the fibers in each region with respect to the distal muscle tendon. Because fibers project at a three-dimensional (3D) angle relative to the distal tendon, muscles were placed in a single plane, facilitating 2D pennation angle measurements. Finally, physiological cross-sectional area (PCSA) was calculated using the **Error! Reference source not found.** equation (Wickiewicz et al., 1983):

Equation 2: Physiological cross-sectional area (PCSA)

$$\boldsymbol{PCSA}\ (\boldsymbol{cm^2}) = \frac{mass\ (g)}{density\ (\frac{g}{cm^3})} \times \frac{\cos\theta}{fiber\ length\ (cm)}$$

where θ is the pennation angle of the muscle.

From this multi-cadaver lower limb muscle dataset, we obtained the corresponding photograph, map, physical parameter and architectural measurement data for the medial gastrocnemius (MG) muscle of one cadaver, as well as the muscle's internal proximal (L_{TIP}) and distal (L_{TID}) tendon lengths (Table 1, below). These data were collected for a 52-year-old male subject (height: 170.18 cm, weight: 74.84 kg) (Ward et al., 2009). We selected data for this subject because all the data for model building were available, including a photograph of the muscle with tendon intact, and the physical and architectural measurements. We used the mass of the *ex vivo* specimen to calculate its volume (Equation 3), assuming that the density of muscle is 1.056 g/cm^3 (Ward & Lieber, 2005).

Equation 3: Muscle volume

$$\boldsymbol{Muscle\ volume}\ (\boldsymbol{cm^3}) = \frac{mass\ (g)}{density\ (\frac{g}{cm^3})}$$

Table 1: Physical measurements of the ex vivo medial gastrocnemius used to create the simple model. LM = muscle length, LTIP = length internal proximal tendon, LTID = length internal distal tendon.

Architectural Property	Measurement
$Mass_{NoTendon}$ (g)	175.73
L_M (mm)	276.73
L_{TIP} (mm)	210.80
L_{TID} (mm)	211.35

3.3.2 Developing 3D MG model based on *ex vivo* architecture

We imported the photograph of the medial gastrocnemius (Figure 3.1A) into Autodesk Inventor (Autodesk Inc., San Rafael, CA), a computer-aided design (CAD) software, and used interpolated splines to sketch a 2D outline of the muscle and proximal tendon in the photo to provide the frontal shape of the

muscle model. We scaled the drawing according to the cadaveric MG muscle and tendon lengths (Table 1). We then extruded the 2D drawing along the frontal axis to create an 11.43 mm thick 3D object. This thickness was selected based on the mean thickness of an *ex vivo* MG muscle from a 62 year old male specimen, measured by anatomical inspection (Narici et al., 1996). To prepare the 3D muscle model for fiber tractography, we divided the model into 3 parts (proximal, central and distal) by two 0.5 mm wide angled planar cuts that a) ran from one-third the length of the proximal tendon to one-third the length of the distal tendon and b) ran parallel to the first, and halved the remaining two-thirds of both tendons, respectively (Figure 3.1B).

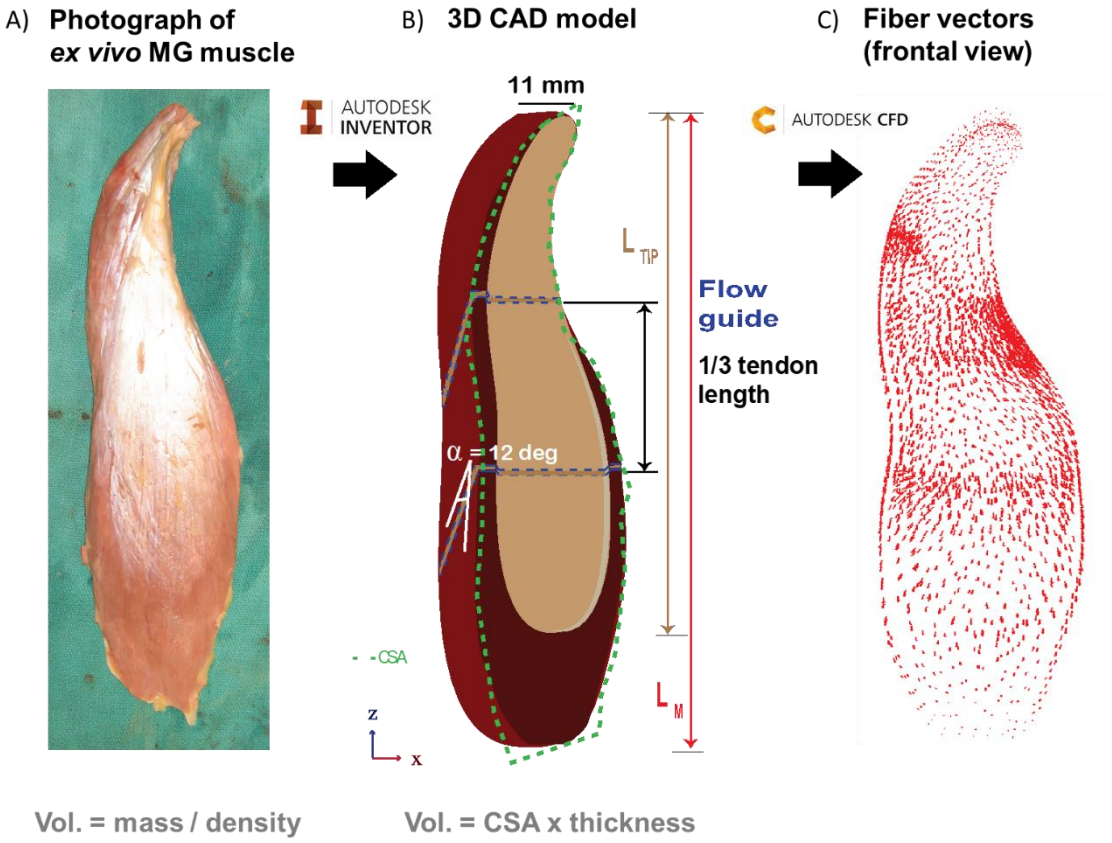

Figure 3.1: Using ex vivo muscle measurements and computer aided drawing (CAD) to build a simple 3D model of the medial gastrocnemius (MG).

A) Photograph of the ex vivo MG. B) 3D CAD model of the MG, created using the photograph and scaled to architectural measurements from the same specimen. C) Frontal view of the fiber vectors throughout the 3D MG model as determined by a computational fluid dynamics simulation.

3.3.3 Modeling fiber tracts and muscle architecture

We exported the model to Simulation CFD (Autodesk Inc., San Rafael, CA, USA) software and used computational fluid dynamics (CFD) to determine the preferred fiber direction throughout the model's geometry by implementing an established Laplacian fluid simulation approach (Handsfield et al., 2017). We assigned the CFD simulation material parameters to highly viscous and incompressible by setting fluid density and viscosity set to 1 g/cm^3 and 1000 Pa-s, respectively, to ensure laminar flow. To simulate muscle fascicles running from origin (via proximal tendon) to insertion (via distal tendon), we set inlet boundary conditions of 1 Pa pressure at the proximal aponeurosis and an outlet condition of 0 Pa pressure at the distal aponeurosis. All other surfaces were given a slip condition, also to ensure laminar flow. The planar cuts in the 3D geometry served as "flow guides" to constrain computational fluid dynamics (CFD) simulations and enforce fascicle orientations that are consistent with the cadaver architecture measurements. The software's automatic mesh function was used to generate a fine mesh throughout the model volume, for which we obtained fluid velocity vectors for each element in the mesh upon completion of the flow simulation (Figure 3.1C).

To generate muscle fascicle arrangement, we performed fiber tractography in MATLAB (Mathworks Inc., MA, USA) by generating streamlines using the CFD velocity vector output and calculating the resulting tract lengths and angles. We generated the streamlines (fiber tracts) from seed points set along the mid-frontal plane of the model and determined the model's fiber lengths by calculating the lengths of the streamlines. We averaged the mean fiber length in the three regions of the model (purple dashed boxes, Figure 3.2B) which visually corresponded to the muscle map locations where the *ex vivo* specimen architecture measurements were taken (green lines, Figure 3.2A) (Ward et al., 2009). We determined pennation angle (θ) as the angle between the flow guides and the coronal face of the model. Model PCSA was calculated using the **Error! Reference source not found.** formula (Wickiewicz et al., 1

983), accounting for pennation angle. We used the cross-sectional area (CSA) of the coronal face and the thickness of the model to calculate the model volume (Equation 4).

Equation 4: Volume of ex vivo-based model

$$\boldsymbol{Model\ volume}\ (\boldsymbol{cm^3}) = cross\ sectional\ area\ (cm^2) \times thickness\ (cm)$$

3.4 Results

3.4.1 3D model fiber distribution

There was a large range in fiber lengths throughout the model, between 1 and 90 mm. The distribution of fiber lengths throughout the model shows that longer fibers are located on the medial and lateral edges of the model, while the shortest fibers are located along the mid-sagittal region (Figure 3.2B). From a frequency plot, we saw that the distribution of all fascicles in the model is Gaussian and that the mode of the model fascicle lengths is around 45 mm (Figure 3.2C).

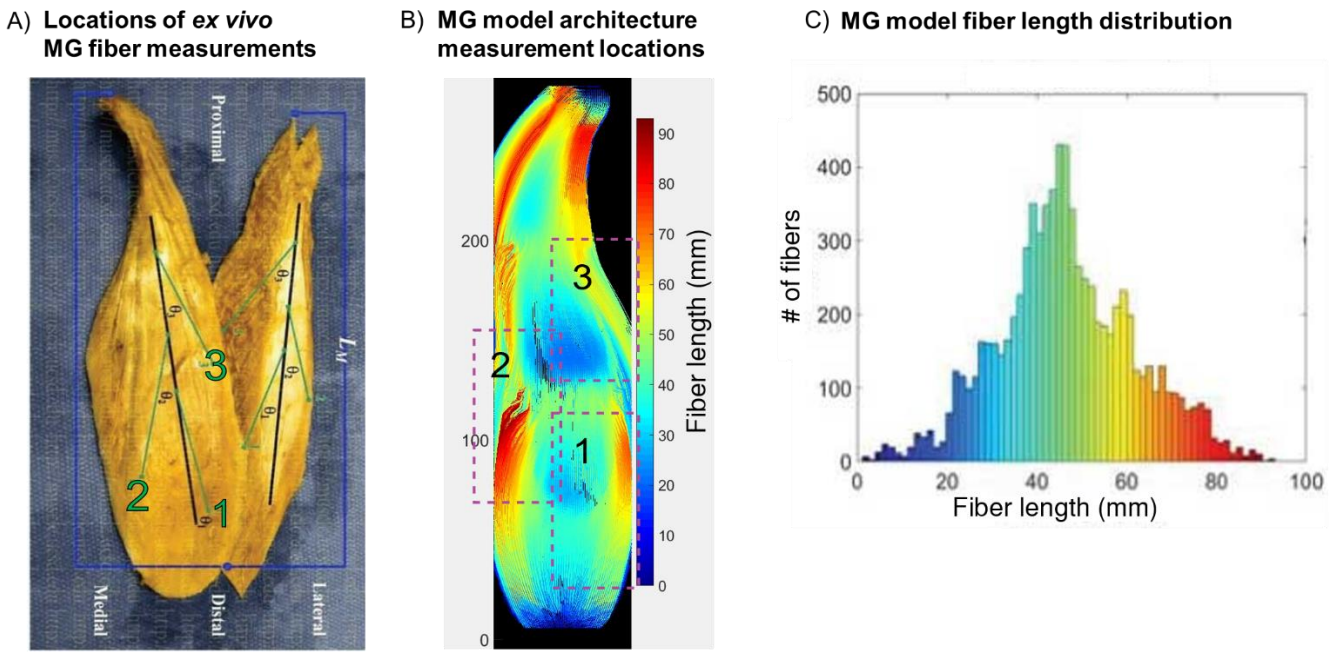

Figure 3.2: Ex vivo MG architecture measurement locations and corresponding model architecture.

Green lines indicate the locations of the three fibers where architecture measurements were taken. B) Frontal view of the fiber tracts throughout the 3D MG model as determined by creating streamlines using fiber vectors. Purple dashed boxes indicate the three regions corresponding to the locations where ex vivo architecture measurements were taken. The color bar represents fiber lengths from 0 to 90 mm, and also corresponds to the C) fiber length distribution of all tracts in the model.

3.4.2 Comparison of cadaver and model architecture

We compared the MG model architecture to the *ex vivo* measurements to evaluate how well the model matched the *ex vivo* muscle (Figure 3.3). The 3D model had a volume of 153.1 cm^3, while the cadaver muscle had a volume of 166.41 cm^3. The model had an average fiber length of 51.67 mm, while the cadaver MG had an average fiber length of 51.86 ± 5.38 mm. The model had a pennation angle of 11.96°, while the cadaver muscle had a pennation of 18.33 ± 2.36°. Finally, the MG model had a PCSA of 28.99 cm^2, while the cadaver MG had a PCSA of 30.52 cm^2.

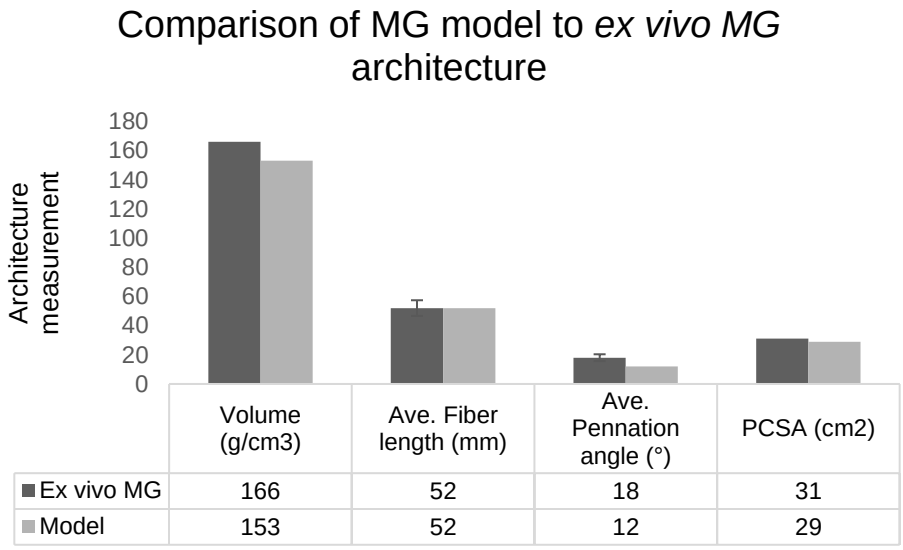

Figure 3.3: Comparison of the ex vivo medial gastrocnemius (MG) muscle architecture data and corresponding architecture measurements of the simple model.

The average fiber length measurement from the muscle specimen is the average of only 3 fibers from 3 different locations, while the model's average fiber length is the average of all fibers at the same 3 locations.

3.5 Discussion

We have created a method to build a 3D muscle model using physical muscle-tendon and fascicle arrangement measurements from *ex vivo* muscle and computer-aided design. We used our method to generate a medial gastrocnemius (MG) model with many fibers, and compared the fiber arrangement to

the mean fiber architecture measurements of the 3 fibers that were measured for the cadaveric MG. As the sample size of *ex vivo* fibers was small, we could not compare the distributions of architecture measurements. Instead, the average architecture measurements of model fibers in the three locations measured *ex vivo* were compared to the *ex vivo* fiber architecture. The key result of this project is that the model we generated with this method could recapitulate important MG cadaver architecture.

The frequency distribution of all the model's fiber lengths was Gaussian, indicating that fewer shorter and longer fibers are present than mean or near mean length fibers, which are most common in the model. In terms of the spatial distribution, the longest fibers were found on the medial and lateral sides of the model, as these fibers curved around sides of the model on the path from proximal to distal aponeurosis. The shortest fibers in the model were found along its mid-vertical line, in the vicinity of the flow guides, the planar cuts in the geometry used to enforce the fascicle arrangement. This spatial distribution of fiber lengths is consistent with that of medial gastrocnemius fibers in another study using Laplacian simulations to generate fiber architecture in a medial gastrocnemius model, validated with DTI fiber distributions (Handsfield et al., 2017).

Of the fibers in the three regions corresponding to the three sampled *ex vivo*, the average pennation angle of the model was smaller than that of the *ex vivo* MG. We attributed this difference in pennation angle to the constraints of the flow guides and the uniform thickness of the model. The flow guides dissected the model and both the proximal and distal tendons into thirds. A limitation of this model-building method is that because there is a uniform thickness, there is a trade-off between the resulting pennation angle and the fiber length due to the trigonometric relationship. In the case of this model, using flow guides to enforce an average match in fiber length to the *ex vivo* muscle resulted in a smaller average pennation angle. Increasing the angle of the flow guides to the frontal plane could have enforced the pennation angle from the specimen, but would have decreased the average fiber length. A possible solution to this trade-off and improve pennation while maintaining a better match in fiber length, could

be to use CAD methods to generate the 3D geometry by creating and adjusting a freeform volume from intersected scaled drawings of both the lateral and frontal views of the *ex vivo* muscle.

Of the fibers in the three regions corresponding to the three sampled *ex vivo*, the average fiber length (Lf) was 52 mm for both the specimen and the model and the length of the model and muscle (Lm) are the same, so the Lf/Lm ratio was 0.19 for both model and *ex vivo* muscle. The Lf/Lm ratio is an important metric used to compare a muscle's capacity for excursion (length change) capabilities independent of the absolute magnitude of muscle fiber length. Therefore, since the model's ratio is the same as the muscle, we could assume that simulating contraction with the 3D model would produce similar fiber excursions if the model was used for finite element simulations of contraction. A Lf/Lm ratio of 0.19 indicates that the average cadaver and model muscle have fibers that span less than $1/5^{th}$ of the muscle or model length, agreeing with what we know about the medial gastrocnemius and other triceps surae muscles, which is that these muscles are not designed for excursion but more so for strength. The PCSAs of both the model and the *ex vivo* MG muscle were also similar. At 29 cm^2 and 31 cm^2 respectively, these PCSAs are also larger than most shank muscles in the Ward dataset. This also symbolizes the muscle's larger capacity for force, based on the fact that PCSA is directly proportional to force (Brand et al., 1986; Fukunaga, Miyatani, et al., 2001; Narici et al., 1996).

The volume of the model was smaller than the volume of the *ex vivo* muscle. The smaller model volume was likely because the model's thickness measurement came from a 62-year-old specimen from another study, whereas as the *ex vivo* specimen we had photographs of and all other model-building measurements for was from a 52-year-old specimen the Ward study. The model thickness had to be based on another *ex vivo* MG (Narici et al., 1996), as muscle thickness was not measured in the Ward study. The volume of the older specimen is likely smaller than the younger, as muscles tend to atrophy with age (Morse et al., 2005; Narici et al., 2003). However, we were unable to make a direct comparison of both specimen volumes as the mass of the older specimen was not available to calculate its volume.

Another contributor to the difference in volume could be that while muscle specimens have non-uniform thickness, we created the model volume with a uniform thickness, extruding the frontal outline of the muscle to the mean thickness of the 62 year old cadaver MG (Narici et al., 1996). This uniform thickness and the absence of anteroposterior bulges and tapers along the length of the model could have contributed to the smaller model volume. By this model-building method, the model's fiber lengths are a function of model thickness, since thickness is uniform.

Though we did not model tendons in this study, excised tendinous tissue (external tendons and aponeuroses) could be modeled similarly, using photographs and physical measurements. Combined muscle-tendon models can then be used for computational studies of the biomechanical function of muscle-tendon units of interest. Computational studies such as finite element analyses enable whole muscle experiments that cannot be conducted *in vivo* or *ex vivo*. Typically, 3D models used for finite element simulations are built using segmentations from high resolution medical images such as MRI. With this work, we have provided a method to generate models when none of these medical images are available. The Ward lower limb *ex vivo* muscle maps and architecture measurements are publicly available and the latter has been used in Hill-type models of lower limb muscle-tendon units. We extended the use of the Ward dataset to apply our method for 3D model creation using *ex vivo* data. While, cadaver studies have provided insights into muscle structure, they are limited by the age of the specimens, as cadavers are typically from older persons. It should be noted that the models created from older muscles will be smaller than those created by specimens from younger cadavers, as younger individuals are generally more active so muscle are less atrophied. Therefore, any simulations of contractions using these models should consult literature to appropriately account for changes in specific strength based on the age of the specimen. Muscle architecture generated for models based on older cadavers will also be different from younger cadavers or *in vivo* architecture measurements such as smaller volume and PCSA, so this should be considered when reporting results of simulations of contraction using *ex vivo*-based models.

This study shows that a relatively simple 3D model, created using computer-aided drawing in the absence of medical images or *in vivo* data, can recapitulate *ex vivo* medial gastrocnemius muscle architecture data very similarly. The medial gastrocnemius model captured the average fiber length and the physiological cross-sectional area (PCSA) of the *ex vivo* specimen very well.

Chapter 4

A 3D Computational Model to Simulate 2D Ultrasound Measurements of Medial Gastrocnemius Architecture

Acknowledgements: William H. Clark[2], Jeroen B. Waanders[3], Jason R. Franz[2], Silvia S. Blemker[1]

[1]University of Virginia, Charlottesville, VA, USA
[2]UNC Chapel Hill & NC State University, Chapel Hill, NC, USA
[3]University of Groningen, Groningen, the Netherlands

4.1 Abstract

Image-based finite element models of muscle reveal how changes in function (force) relate to changes in structure (architecture) that occur during contraction. For the results of muscle models to be informative, the muscle's fiber arrangement, also known as its architecture, must be represented accurately. The accuracy of the modeled architecture for relaxed muscle can be determined by comparison to *in vivo* architecture as determined by MR-Diffusion Tensor Imaging (DTI). However, DTI cannot be used to validate architecture in models of dynamic muscle contractions, as DTI typically lacks the temporal resolution needed to study contracting muscle. Ultrasonography is used to image changes in muscle architecture throughout contraction. Therefore, it is the best option for validating three-dimensional (3D) models of contracting muscle. However, the ultrasound architecture measurements are 2D while the *in vivo* muscle and representative model are 3D. Consequently, there needs to be a way to evaluate the 3D model architecture in 2D, so that comparisons can be made with ultrasound (US) measurements. In this study, we created a method to use 3D muscle models to simulate 2D ultrasound measurements of muscle fascicle lengths and pennation angles. We built an MRI-based 3D finite element model of the medial gastrocnemius, simulated an isometric contraction, and applied our method to simulate US measurements of muscle architecture from the 3D model. We validated our 3D MG model architecture using MR-DTI architecture from published studies and validated our simulated change in 2D measurements using ultrasound data for isometric contractions from six subjects. We determined the location in the model where our model measurements recapitulated the US data. Then we used the validated model to investigate how aponeurosis stiffness affects fascicle strain in the MG. We found that mean 3D fascicle strain decreased with higher aponeurosis stiffness, but corresponding fascicle strains from simulated 2D US measurements increased with increased stiffness. The method and model that we have developed and validated will facilitate future study of the assumptions and limitations of 2D ultrasound architecture measurements of complex 3D muscle fiber arrangements.

4.2 Introduction

Computational models enable us to study the relationship between muscle structure and function, and to perform virtual biomechanics experiments that we cannot do *in vivo*. Lumped parameter musculoskeletal models have given some insight into the functional changes that occur during contraction. However, because these models assume simple line segment representations of the 3D architecture (Anderson & Pandy, 2003; Arnold et al., 2010; Delp et al., 2007), they cannot provide in depth insights into structural changes as they do not provide information for individual fascicles. Three-dimensional finite element muscle models are powerful because they can examine and quantify changes in complex 3D muscle architecture (fascicle length, pennation), tissue strains and fascicle strains that occur with contraction (Blemker et al., 2005; Blemker & Delp, 2006; Fiorentino et al., 2014; Fiorentino & Blemker, 2014; Rehorn & Blemker, 2010).

For 3D muscle model predictions to be valid, the 3D muscle geometry and architecture must be represented accurately, as these factors influence a muscle's contractile properties. Model geometries are generated using muscle segmentations from magnetic resonance images (MRI) (Blemker et al., 2005; Handsfield et al., 2014, 2017; Knaus et al., 2020). Three-dimensional muscle fiber arrangement (architecture) for relaxed muscle can also be obtained from Diffusion Tensor Imaging (DTI), an MRI technique which capitalizes on principal water diffusion along muscle fibers to determine fiber direction and reconstruct fiber trajectories in muscles (Bolsterlee et al., 2017; Charles et al., 2019; Fouré et al., 2018; Sinha et al., 2015). However, this technique cannot provide architecture data for contracted muscle or during dynamic contractions because scan time is too long for subjects to sustain contractions voluntarily. Therefore, DTI cannot be used to validate model-predicted changes in 3D architecture during muscle contraction.

Real-time brightness-mode ultrasonography is quick, relatively inexpensive and commonly used to provide informative two-dimensional (2D) measurements of these muscle properties in superficial

muscles such as the medial gastrocnemius (Cronin & Lichtwark, 2013; Kawakami et al., 1998; Lichtwark et al., 2007; Maganaris et al., 1998; Narici et al., 1996). Since ultrasound (US) can provide architecture measurements for relaxed and contracted muscle, it is the best option for validating changes in architecture in 3D finite element models of contracting muscle. However, these ultrasound measurements are 2D, so they cannot be directly compared to a model's 3D structure. To enable direct comparisons between model architecture and US measurements, there needs to be a way to emulate the 2D US architecture measurements from the 3D model. Once validated with US, 3D model predictions can be used to further investigate the relationship between muscle structure and function, including muscle-tendon interactions. For example, while medial gastrocnemius (MG) muscle-tendon interactions have been widely studied by ultrasound (Bolsterlee et al., 2015; Fukunaga, Kubo, et al., 2001; Herbert et al., 2002, 2011, 2015) and DTI (Bolsterlee et al., 2017), much is still unknown about its muscle-aponeurosis interactions. Studies in rat and wild turkey gastrocnemii suggest that changes in aponeurosis (internal tendon) properties influence muscle fascicle behavior (Eng & Roberts, 2018; Holt et al., 2016). Therefore, in addition to muscle fascicle arrangement, aponeurosis material properties and geometry likely affect fascicle behavior during contraction. This is an opportunity to leverage 3D computational models to perform relevant experiments for muscle-aponeurosis interactions that we cannot perform *in vivo,* such as how aponeurosis stiffness affects fascicle strains with contraction.

Our goal was to develop a 3D finite element (FE) model of the medial gastrocnemius muscle, validate the model by comparison with ultrasound measurements and use the model to investigate how aponeurosis stiffness affects fascicle strain measurements. To achieve these goals, we developed a method to simulate 2D ultrasound architecture measurements, and compared the 3D model predictions with 2D *in vivo* measurements of muscle architecture.

4.3 Methods

4.3.1 In vivo muscle architecture measurements

As previously described (Clark & Franz, 2018), we determined the medial gastrocnemius (MG) muscle-tendon junction (MTJ) displacements and fascicle kinematics during maximum voluntary isometric contraction (MVIC) based on cine brightness-mode ultrasound. We imaged the right MG for five subjects (age: 24.4 ± 5.1 years, mass: 74.8 ± 13.0 kg, height 1.76 ± 0.06 m, 2 females) at the University of North Carolina-Chapel Hill (Clark & Franz, 2018). We placed subjects' knee at 20°-30° flexion and ankle angle at neutral position (i.e., the foot was placed at 90° relative to the shank). We then placed a 10 MHz 60 mm Telemed Echo Blaster 128 linear array ultrasound transducer (LV7.5/60/128Z-2, UAB Telemed, Vilnius, Lithuania) along the midsagittal plane at approximately 50% of the muscle length and collected images at 61 frames per second through a longitudinal cross section, using an image depth of 65 mm. The same person performed fascicle tracking and architecture measurements (fascicle length and pennation angle) from these images, following best practices using UltraTrack software (Farris & Lichtwark, 2016). We show a summary of *in vivo* architecture measurements in Table 4.1.

Table 4.1. Summary of in vivo *ultrasound measurements of medial gastrocnemius muscle architecture from Clark and Franz, 2018.*

	Relaxed	**Contracted**	**Change**
Fascicle Length (mean ± std)	62.34 ± 1.97	57.65 ± 3.26	-4.69 ± 1.73
Pennation Angle (mean ± std)	14 ± 1.22	15.62 ± 1.76	1.62 ± 0.74

4.3.2 Developing 3D MRI-based model geometry and architecture

MR images

We used axial magnetic resonance (MR) images (Handsfield et al., 2014) of the right leg of a healthy male (height: 170 cm, weight: 76.8 kg, age: 17 years) to build a three-dimensional (3D) geometry of a healthy medial gastrocnemius muscle and its two internal tendons (aponeuroses) for finite-element (FE) modeling. To acquire the images, we used a 2D multi-slice sequence with the following scanning parameters: TE/TR/α: 3.8 ms/800 ms/90, field of view: 400 mm × 400 mm, slice thickness: 5mm, in place

spatial resolution: 1.1 mm × 1.1 mm, in a 3T scanner. The MG and aponeurosis boundaries in each MRI slice was manually outlined using in an in-house segmentation software (Handsfield et al., 2014) in MATLAB (The Mathworks, Inc. Natick, MA, US) (Figure 4.2A).

3D geometry and mesh

We lofted these axial cross-sections together in Autodesk Inventor (Autodesk Inc., San Rafael, CA, US) to create a muscle volume that was 314 mm long (Figure 4.2B). We imported the muscle volume into Trelis (Csimsoft, American Fork, UT, US) and sketched the outline of the proximal and distal aponeuroses using the boundaries of the muscle segmentation and referencing anatomical images. In order to create a model that represented the average of the ultrasound measurements, we scaled down the thickness of the muscle model to the average muscle thickness (~13 mm) of the ultrasound subjects. Then we created aponeurosis volumes by outward thickening (away from muscle surface) of the sketches to a uniform thickness of 1.5 mm (Shan et al., 2019). This ensured that adjacent surfaces had perfect intersection. In preparation of finite element meshing, we merged adjacent surfaces so that the muscle volume shared a surface with each aponeurosis. We used Trelis software (Coreform, Orem, UT, US) to mesh the three geometries together with 4-node tetrahedral elements (15,090 elements; 3,420 nodes) to make a single volume/model with three parts.

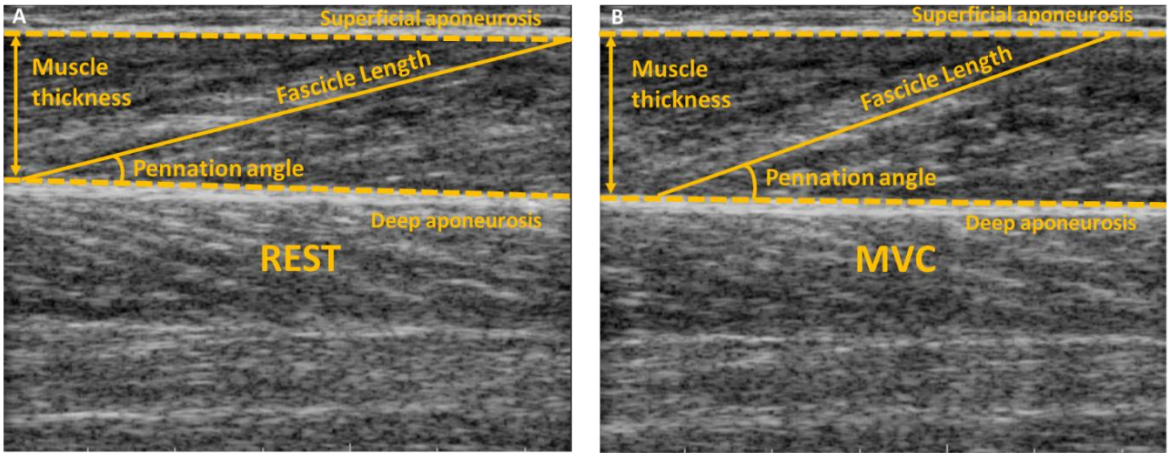

Figure 4.1. Representative ultrasound images of the medial gastrocnemius (MG) muscle.

A) At rest, reference architecture measurements are taken by measuring the length of a fascicle and its angle to the deep aponeurosis. B) At maximum voluntary contraction (MVC), the muscle thickness and pennation angle increase, while the fascicle length decreases.

We estimated muscle thickness at the location of the ultrasound image according to the following equation:

Equation 5. Estimate muscle thickness using muscle architecture measurements

$$Muscle\ thickness = Fascicle\ length \times \sin(pennation\ angle)$$

Local fiber directions

Local fiber directions are essential to the material models we applied to the tissue. We imported the muscle geometry into Autodesk CFD (Autodesk Inc., San Rafael, CA, US) where we performed Laplacian fluid simulations of highly viscous, incompressible, laminar flow to determine local fiber directions throughout the volume (Handsfield et al., 2017). To generate flow within the geometry, we prescribed pressure boundary conditions of 1 Pa and 0 Pa to the muscle fiber origins (at proximal aponeurosis surface) and insertions (at distal aponeurosis surface), respectively. We assigned local fiber directions to each mesh element of the muscle model using a nearest neighbor assignment (Figure 4.2C). For the aponeuroses, we assigned local fiber directions in a simple representation, as vertical distally-directed vectors in each mesh element.

Fascicle tracts and relaxed 3D architecture

We used vector results from the CFD simulation to generate streamlines to represent the muscle's fascicles. We calculated 3D muscle model architecture (i.e. fascicle lengths, curvatures and pennation angles at rest) in MATLAB using adapted fascicle-tracking code (Bolsterlee et al., 2017). We measured model fascicle length as the length of generated streamlines that represent fascicles, and we measured model pennation angle in multiple ways: i) the angle of the fascicle insertion point and the deep aponeurosis, ii) the angle of the fascicle origin and the superficial aponeurosis, and iii) the average of these two angles (Bolsterlee et al., 2015, 2017). We validated average 3D architecture for the undeformed

model (representing relaxed muscle) by comparing reconstructed fascicle lengths to average MG architecture from a DTI study (Bolsterlee et al., 2015).

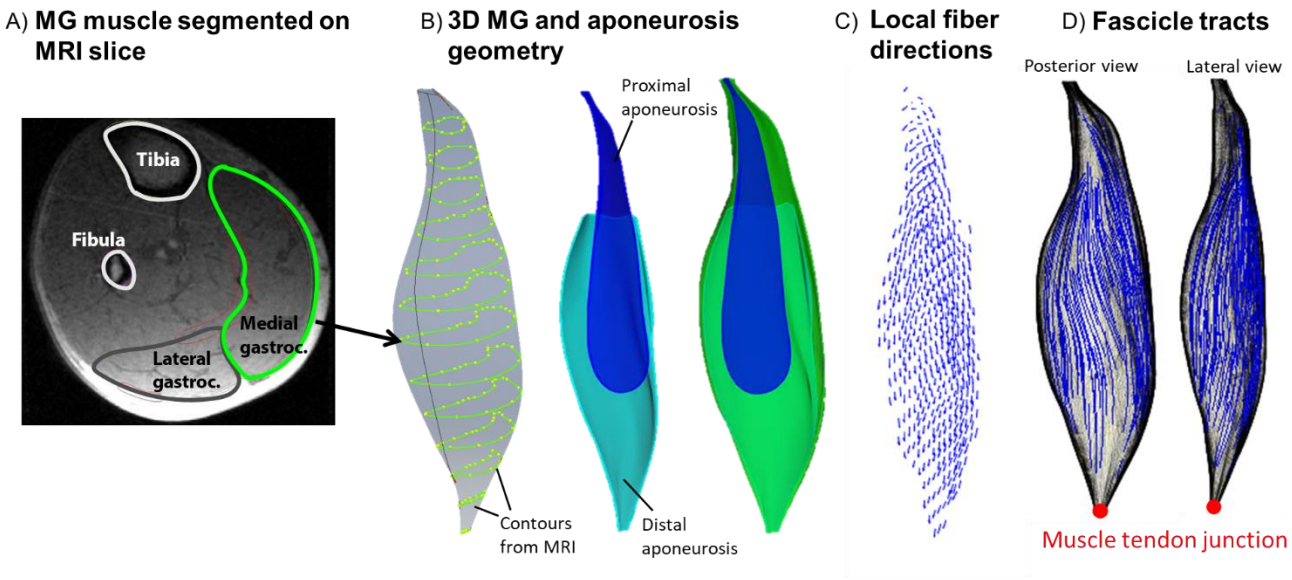

Figure 4.2: Medial gastrocnemius finite element modeling (FEM) process.

A) The MG muscle was segmented from axial MR images of the lower limb of an adult male subject. B) The 2D segmentations (green contours) were used to build a 3D MG geometry and two adjacent aponeurosis geometries. C) Local muscle fiber directions (vectors) were generated using Laplacian flow simulations and location matched to the finite element mesh. D) Fascicle tracts were created by generating streamlines using the fiber vectors. The red dots show the location of the muscle-tendon junction (MTJ) with the Achilles tendon, where ultrasound measurements of displacement due to muscle contraction were taken. In FEM simulations of isometric contraction, the proximal end of the model is fixed (representing muscle's attachment to femur) and proximal displacement is applied to the distal end/MTJ.

4.3.3 Finite element simulations of isometric contraction

Material properties

We modeled the stress-strain properties of muscle and aponeuroses using nearly-incompressible, hyper-elastic, transversely isotropic materials (Blemker et al., 2005; C. Criscione et al., 2001; Weiss et al., 1996). For muscle, we applied constitutive equations that describe the active (contractile) and passive force-generating behavior (Blemker et al., 2005). The muscle model includes the following material parameters: bulk modulus (K), along-fiber shear modulus (G_1), cross-fiber shear modulus (G_2), exponential

stress coefficient (P_1), fiber uncrimping factor (P_2), optimal fiber length ($\boldsymbol{\lambda}_{ofl}$), stretch at which the stress-strain relationship becomes linear ($\boldsymbol{\lambda}^*$), and the peak isometric stress ($\boldsymbol{\sigma}_{max}$). For the aponeuroses, we applied constitutive equations for an uncoupled solid mixture of a neo-Hookean ground matrix (parameters: Young's modulus (E) and Poisson's ratio (ν)) and fibers with an exponential power law (parameters: coefficient of exponential argument ($\boldsymbol{\alpha}$), power of exponential argument (β), and the fiber modulus (ksi)). For both muscle and aponeurosis materials, we applied material parameters (Table 4.2) in PreView pre-processing software and edited them in FEBio text files (Maas et al., 2012). We chose material parameters that predicted physiological changes in muscle architecture from the simulation.

Table 4.2. Medial gastrocnemius model dimensions and material properties.

A. Model dimensions			
	MUSCLE	SUPERFICIAL APONEUROSIS	DEEP APONEUROSIS
Length (mm)	314.24	213.77	228.90
Max. Width (mm)	85.63	49.51	84.65
Thickness (mm)	27.1 (mid-length)	1.5 (uniform)	1.5 (uniform)
Volume (cm^3)	240.22	9.11	19.70

B. Material properties			
MUSCLE		APONEUROSES	
Bulk modulus, K (MPa)	10	i) Neo-Hookean	
Along-fiber shear modulus, G_1 (MPa)	5×10^{-4}	**Young's modulus, K** (MPa)	1000
Across-fiber shear modulus, G_2 (MPa)	5×10^{-4}	**Poisson's ratio, ν**	0
Exponential stress coefficient, P_1	0.05		
Fiber uncrimping factor, P_2	6.6	ii) Fibers with exponential power law	
Optimal fiber length, λ_{ofl}	1	**Coefficient of exponential, α**	0
Stretch for straightened fibers, λ*	1.4	**Power of exponential, β**	2.5
Peak isometric stress, σ_{max} (MPa)	0.3	**Fiber modulus, ksi** (MPa)	50

Boundary conditions

We assigned boundary conditions in PreView to simulate the average muscle-tendon junction (MTJ) displacement measured by ultrasound during a maximum voluntary isometric (fixed muscle-tendon unit length) contraction at neutral (90°) ankle angle (Clark & Franz, 2018). The proximal ends of the proximal aponeurosis and muscle were fixed in all three translational and rotational degrees of freedom, symbolizing attachments to the femur. Based on the ultrasound data, we prescribed the mean proximal displacement (21.1 mm) and anterior displacement (4.1 mm) to the distal ends of the anterior aponeurosis and muscle, which represent the MG MTJ (red dot, Figure 4.2D). While boundary conditions were applied linearly, muscle activation was also linearly ramped from no (0) to maximum (1) activation during the quasi-static simulations. We performed the simulations in FEBio, a nonlinear implicit finite element solver (Maas et al., 2012).

4.3.4 Predicting changes in 3D muscle architecture

We visualized the simulation in PostView (Maas et al., 2012), then exported the model's nodal displacements for analysis in MATLAB. In the undeformed configuration, we mapped points along the fascicle tracts to the FE mesh element that they fell within. Then we used the deformation of the elements from the nodal displacements to determine the changes in fascicle arrangement post-simulation, i.e. in the deformed configuration representing maximally contracted muscle. We calculated the final length of each fascicle, and calculated fascicle strain by dividing the change in fascicle length by the initial length. We also calculated changes in pennation angle by finding the angle between the vector connecting each tract's endpoints in its initial and deformed configurations.

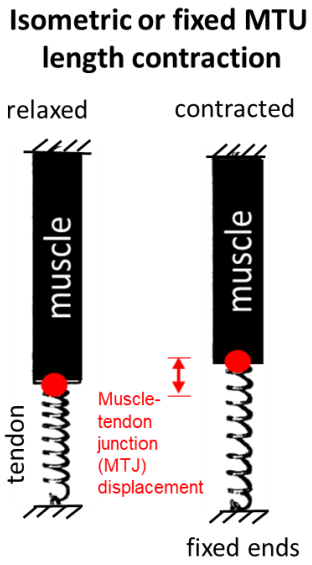

Figure 4.3: Schematic of isometric contraction for bi-articular MG.

This diagram illustrates that in isometric or fixed muscle-tendon unit (MTU) MG contractions, the muscle shortens independently of joint movement, as the knee and ankle joints are fixed. Muscle shortening is measured experimentally by proximal movement of the muscle-tendon junction (MTJ, red dot). In our FEM simulations of isometric contractions, the muscle and aponeurosis (not shown) are modeled. The Achilles tendon connecting the MG to the ankle joint is not modeled.

4.3.5 Simulating 2D US architecture measurements

We developed an algorithm to simulate ultrasound (US) architecture measurements using a 3D muscle model. The algorithm contained multiple subprocesses which took input from the model and/or prior subprocesses and output the inputs needed for subsequent subprocesses (Figure 4.4).

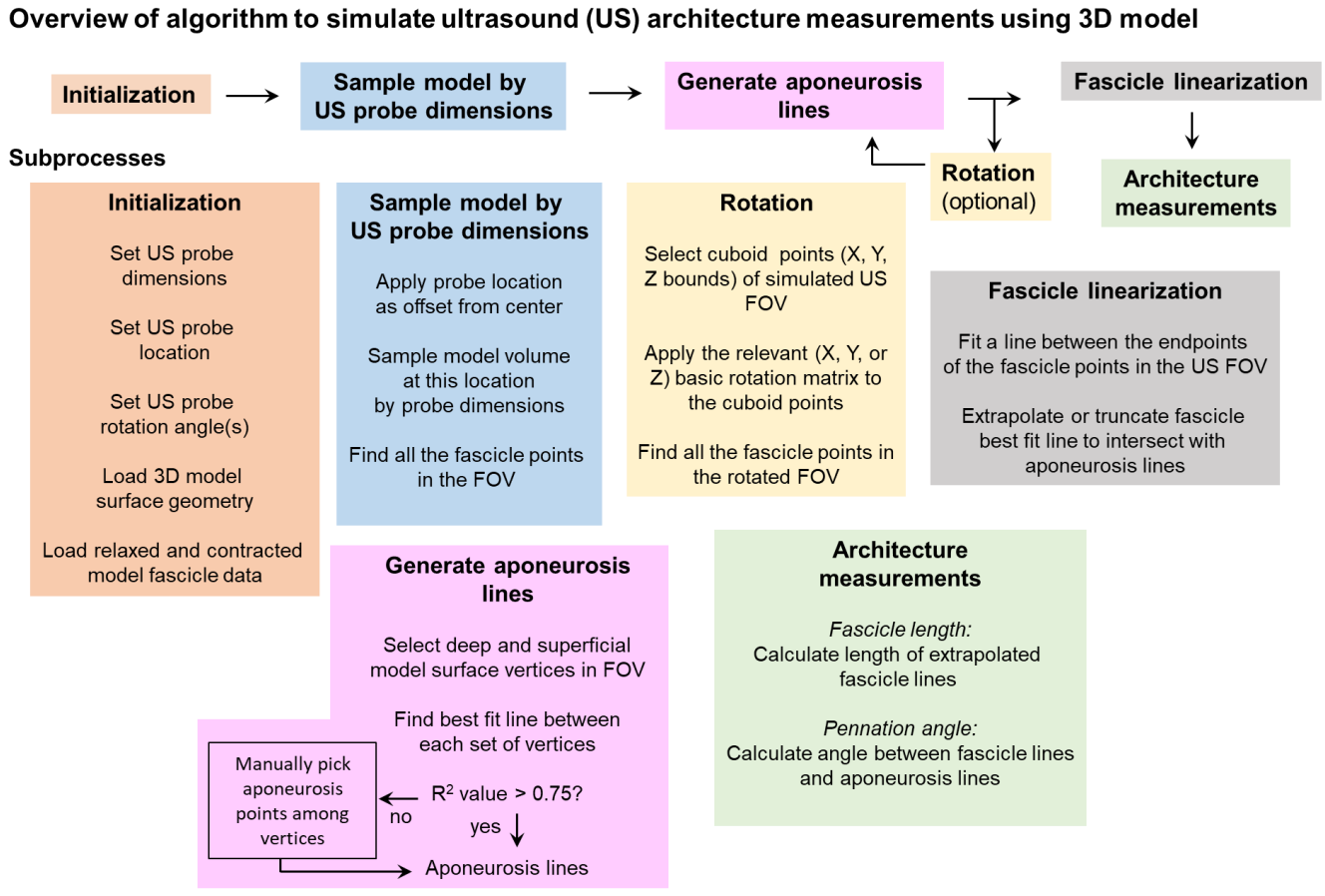

Figure 4.4: Overview of the algorithm to simulate ultrasound (US) architecture measurements using the 3D model.

In the initialization steps (orange), 3D model data are loaded and US probe size and position are set. Next, the 3D model is sampled by the US dimensions and the points along the fascicle in the sampled region are stored. The model surface points in the field-of-view (FOV) of the probe are used to generate aponeurosis lines (purple). If rotation inputs are supplied in Step 1, the US FOV is rotated (yellow), and fascicle points in the FOV are stored. A linearized fascicle is generated from stored fascicle points for each fascicle in the US FOV (gray). Finally, simulated US architecture measurements are calculated (green) from the linearized fascicles lengths and orientations to the generated aponeurosis lines.

Initialization

We created the first subprocess, initialization, to load the 3D model data and the dimensions and orientation of the ultrasound probe, including size, location, and angle. The algorithm takes input of the width, height, location and angle for the ultrasound simulation based on the size and orientation of the US probe used to measure subjects' in the experiments. Next, we input the location of the probe relative to the point of intersection of the mid-width (half of X-range) and mid-height (half of Z-range) of the geometry. This offset of the probe position from the mid-point can be input as a vector of either percentages or millimeters offset from the midpoint. If rotation is to be simulated, we input the angles for X, Y, and Z rotation as a vector. We load the fascicle tracts from the undeformed 3D model and also load the finite element model outputs of the XYZ positions and displacements of each node in the model. We determine fascicle deformation by contraction by associating each point along the fascicle with its nearest element in the deformed configuration, and using the displacement of the element's nodes to calculate displacement of the fascicle point. In this step, we also load the surface geometry of the undeformed model (STL format).

Sample model volume by US field-of-view

The next step in the algorithm is to sample the 3D model at the desired location by the US probe dimensions and orientation. At the specified location, the sampled model volume is of the entire model depth (Figure 4.5B) because the entire thickness of the MG muscle is generally imaged with ultrasound. This sample volume is reduced the two-dimensions (depth and height only), so that the fascicles are 2D but curved (Figure 4.5C). Since each fascicle is represented by a streamline connecting multiple points,

we store the points of each fascicle that are present in the US field-of-view. We also calculate the percentage of the fascicle that is present in the field-of-view.

Generate linear aponeuroses

Because ultrasound studies generally assume the aponeurosis is linear, our algorithm also generates linear aponeuroses, based on the surface points of the model in the FOV and the endpoints of fascicles in the US field of view. We determine both deep and superficial linear aponeuroses by performing linear regression to find the best fit lines through the deep and superficial surface vertices. If the R^2 value for the best fit line is greater than or equal to a magnitude of 0.75, the line is applied as the aponeurosis. If the value is less than 0.75, the aponeurosis line is created by creating a best fit line through the most superficial of the relevant points, which the user picks. When the points are picked manually, the selected points are saved to enable reproducible analyses.

Fascicle linearization

In the next algorithm step, we linearize fascicles in the FOV by removing the width dimension, projecting the fascicles to the two-dimensional plane of the ultrasound probe. Then we linearize fascicles in the FOV by interpolating a straight line between the endpoints of each fascicle. If the linearized fascicle does not meet the aponeurosis on one or both ends (i.e. it is too short), we extrapolate the fascicle line to intersect the aponeurosis/es. If the linearized fascicle intersects and extends beyond the aponeurosis (i.e. it is too long), we truncate the fascicle at the point of the intersection. We apply the linearization to relaxed and contracted fascicles.

2D architecture measurements

The final subprocess of the algorithm calculates the lengths and pennation angles of the linearized fascicles. The fascicle lengths are the lengths of the linearized lines between the deep and superficial aponeurosis. The algorithm calculates both the deep and superficial pennation angles of the linearized fascicles as the angles between the deep and superficial aponeuroses, respectively. However, only the

deep pennation angle (α) is reported, in accordance with typical US architecture measurements (Figure 4.5E).

Applying algorithm

For this study, we simulated a US probe width of 15 mm and height of 60 mm (Clark & Franz, 2018) at the model location that best matched the average experimental architecture measurements (-15mm from mid-width, 5mm from mid-length). We did not simulate probe rotation. All other steps in the algorithm were applied as described. We compared the linearized (2D) fascicle architecture with the 3D architecture.

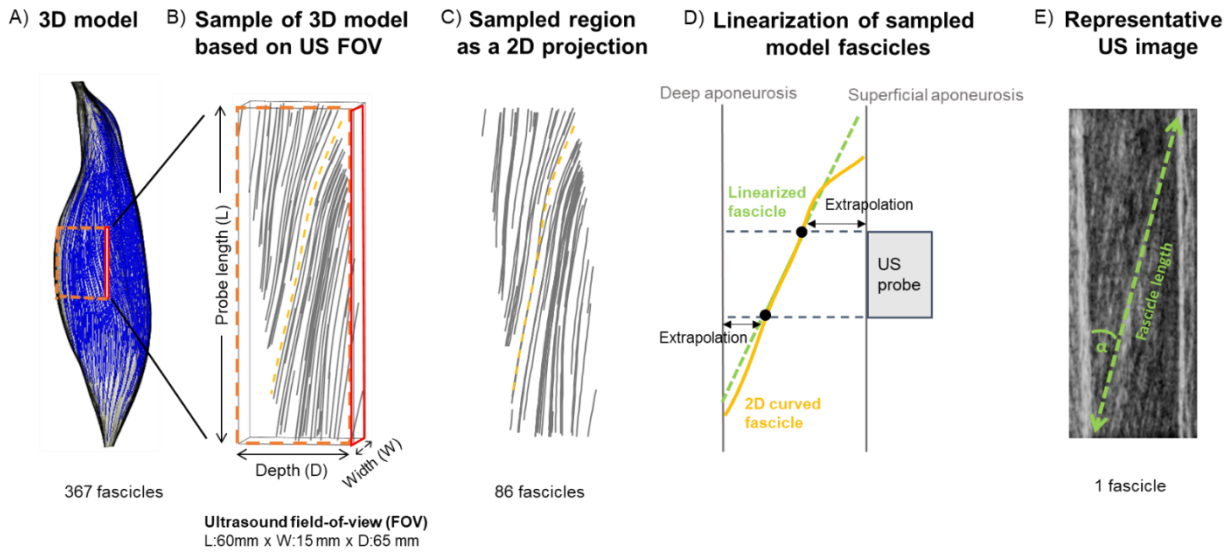

Figure 4.5. The linearization process of 3D model fascicles.

A) The red-outlined white bar represents the ultrasound probe to scale. B) The muscle is sampled by the dimensions of the US probe through the model depth. C) Sampled volume is reduced to two dimensions, showing curved 2D fascicles (yellow dashed line). D) The curved 2D fascicle (yellow line) is linearized (green dashed line) to enable model architecture comparisons with E) ultrasound architecture measurements.

4.3.6 2D model architecture validation with ultrasound

We compared predicted changes in model architecture due to isometric contraction with *in vivo* ultrasound measurements of isometric contraction (Clark & Franz, 2018). Model fascicles with 3D fascicle lengths greater than 75 mm (maximum physiological lengths for the medial gastrocnemius) and pennation

angles greater than 90 degrees were excluded from the analyses. We compared the means of the fascicle lengths, pennation angles and changes in same in the simulated/ultrasound field-of-view. We considered the model validated if the difference between ultrasound and model predictions was within one standard deviation of the mean of the experimental measurement.

4.3.7 Varying aponeurosis stiffness

We varied the effective stiffness of the aponeuroses to investigate the effects of aponeurosis stiffness on fascicle strain. We varied the aponeurosis stiffness by changing the Young's modulus of the material from 1000 MPa (original) to 50, 100, 10,000 and 100,000 MPa to investigate the effects of aponeurosis stiffness on fascicle strain. We defined fascicle strain as:

Equation 6. Fascicle strain

$$fascicle\ strain = \frac{change\ in\ fascicle\ length}{relaxed\ fascicle\ length} = \frac{l_f - l_0}{l_0}$$

4.4 Results

4.4.1 Model geometry and fascicle arrangement

The tractography algorithm we adapted (Bolsterlee et al., 2017) generated 367 complete fascicles tracts in the MG model geometry. Therefore, 367 fascicles remained throughout the model for architecture comparison and analysis (Figure 4.5A). Of these 3D fascicles, 189 (51.5%) were 75mm or shorter (i.e. were within physiological lengths (Figure 4.6 A, D)) when relaxed, and the other 49.5% of fibers (that were longer than 75 mm) were excluded from further analysis. Contracted fascicle architecture was evaluated at 50% model activation. The distribution of both relaxed and contracted 3D fascicle lengths (Figure 4.6B), indicated that most fascicles were on the longer end of the range of lengths. The average fascicle length shortened with contraction, from 57.0 mm (mean) ± 13.5 mm (STD) to 46.8 mm (mean) ± 11.9 mm (STD) (Figure 4.6B). The model-predicted pennation angles approximated a normal

distribution at rest (Figure 4.6C), which became left-skewed upon contraction, as the average pennation increased from 15.9° ± 5.3° to 20.8° ± 6.4°.

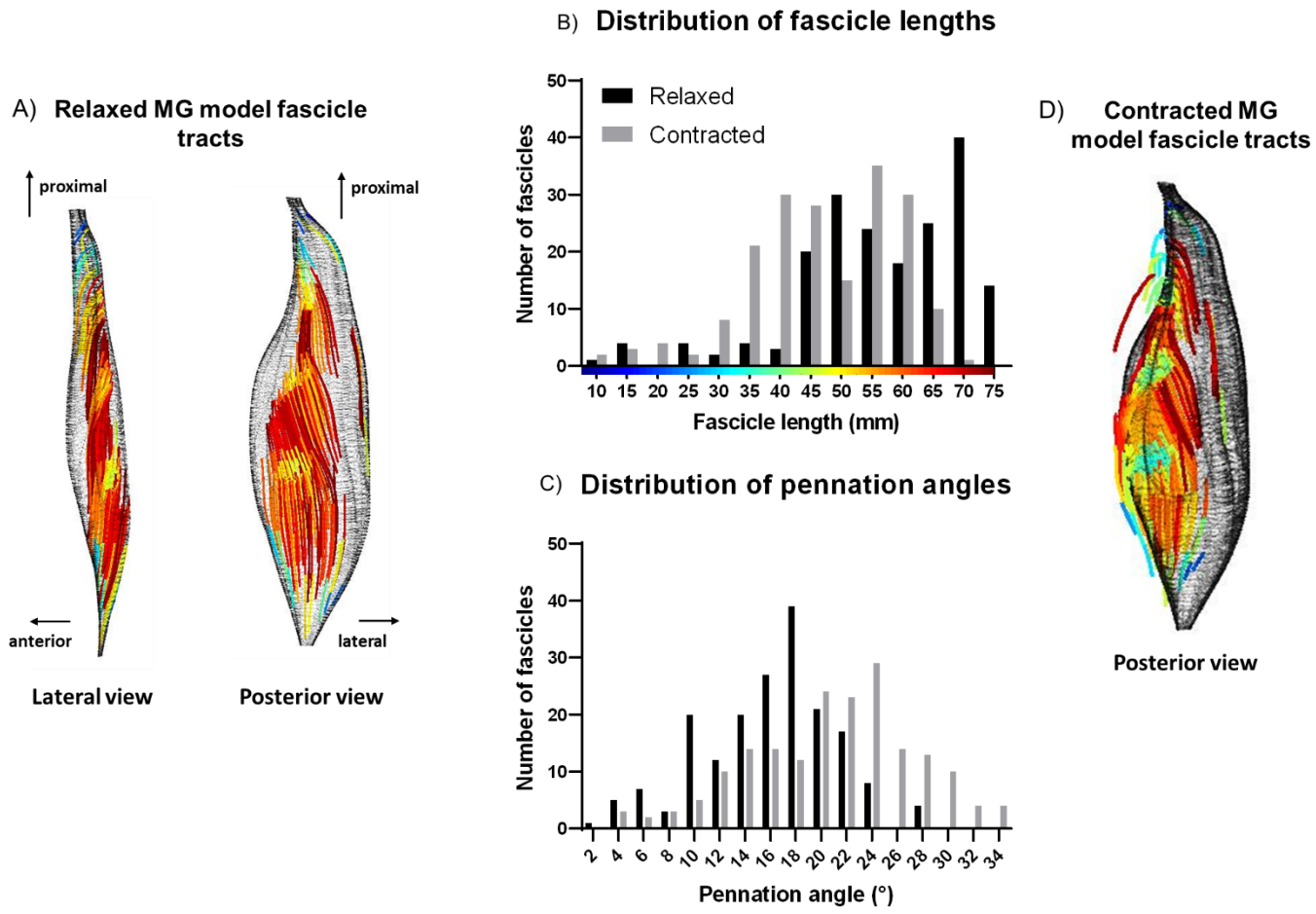

Figure 4.6: Change in MG model 3D fascicle arrangement with contraction.

Distributions of B) fascicle lengths and C) pennation angles) for the relaxed (black bars) and contracted (gray bars) 3D model. A) Relaxed medial gastrocnemius (MG) fascicle tracts within physiological lengths (≤ 75 mm) throughout the relaxed 3D geometry (black dotted volume). D) Contracted MG fascicle tract lengths, overlaid on the relaxed model geometry to show how the fascicle positions changed with contraction.

4.4.2 3D model architecture validation with DTI

Of these fascicles that were within physiological range (Figure 4.6A), the average relaxed 3D fascicle lengths (52.03 mm ± 13.48 mm) and pennation angles (19.56° ± 9.22°) were within one standard deviation of those measured with MR-DTI (Bolsterlee et al., 2015) (Figure 4.7).

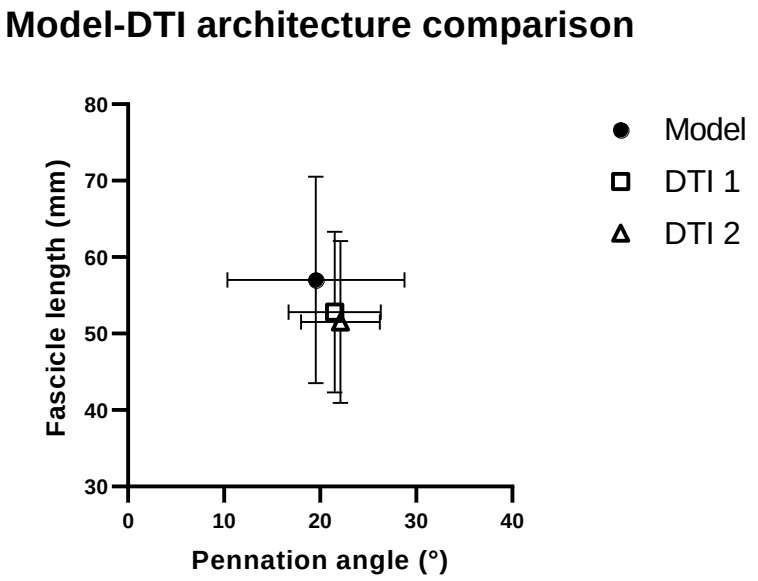

Figure 4.7: 3D model fascicle architecture was validated via comparison with architecture data from magnetic resonance diffusion tensor imaging (MR DTI) reconstructions of relaxed MG muscle architecture (Bolsterlee et al., 2015).

Mean model architecture (fascicle length and pennation angle, dot) for all fascicles were within one standard deviation of DTI architecture (square, triangle), indicating that the model architecture is representative of in vivo MG.

4.4.3 Simulated US architecture

Simulating the ultrasound field-of-view at the centroid (mid-width and mid-height, i.e. [0,0] offset) of the model (Figure 4.8) and led to architecture measurements (

Table 4.3) that was not within a standard deviation of the experimental data (Table 4.1). The location that best matched the ultrasound measurements was at 15 mm lateral and 5 mm proximal to the centroid, i.e. [15,5] offset from centroid. At this location, there were 2 linearized fascicles that were at least 75% present when relaxed, then 1 fascicle that was at least 75% present when contracted (Figure 4.9, yellow lines). In

Table 4.3, we have summarized the architecture of the fascicles present in the simulated ultrasounds at both the centroid and optimal locations. Figures for other locations we tested can be found in Appendix 1: Simulated ultrasound images at each location tested.

Table 4.3. Summary of linearized model architecture measurements in the simulated ultrasound field-of-view (FOV) at the model centroid and at the optimal location, i.e. the location that best represents experimental data

Shaded rows highlight the architecture measurements for fascicles that were 75% or greater in the US FOV and were used for comparison with US data in Table 4.1.

Measurement		Centroid, [0,0]		Optimal location, [15,5]	
		Relaxed	Contracted	Relaxed	Contracted
3D	# of fascicles ≥75% present in FOV	5	5	2	1
	# of fascicles ≥75% present in FOV when both relaxed and contracted	N/A	1	N/A	0
	mean % of 3D FL in FOV	0.84	0.86	0.82	0.83
	mean FL ± std.	55.30 ± 6.43	44.37 ± 5.93	68.96 ± 4.15	76.79
	mean PA ± std	14.74 ± 6.26	N/A	14.36 ± 0.40	N/A
Linearized	mean FL ± std.	58.88 ± 3.97	47.53 ± 3.98	64.88 ± 2.85	64.08
	mean PA ± std	17.42 ± 1.19	21.99 ± 1.19	17.58 ± 0.40	18.52 ± 0.40
	change in mean FL	N/A	-11.35	N/A	-0.80
	change in mean PA	N/A	4.57	N/A	0.93
	mean FL of all fascicles in FOV	72.66 ± 19.69	61.34 ± 19.77	60.75 ± 15.57	59.50 ± 13.47
	mean PA of all fascicles in FOV	15.12 ± 3.80	18.27 ± 4.57	19.17 ± 5.29	20.71 ± 4.25

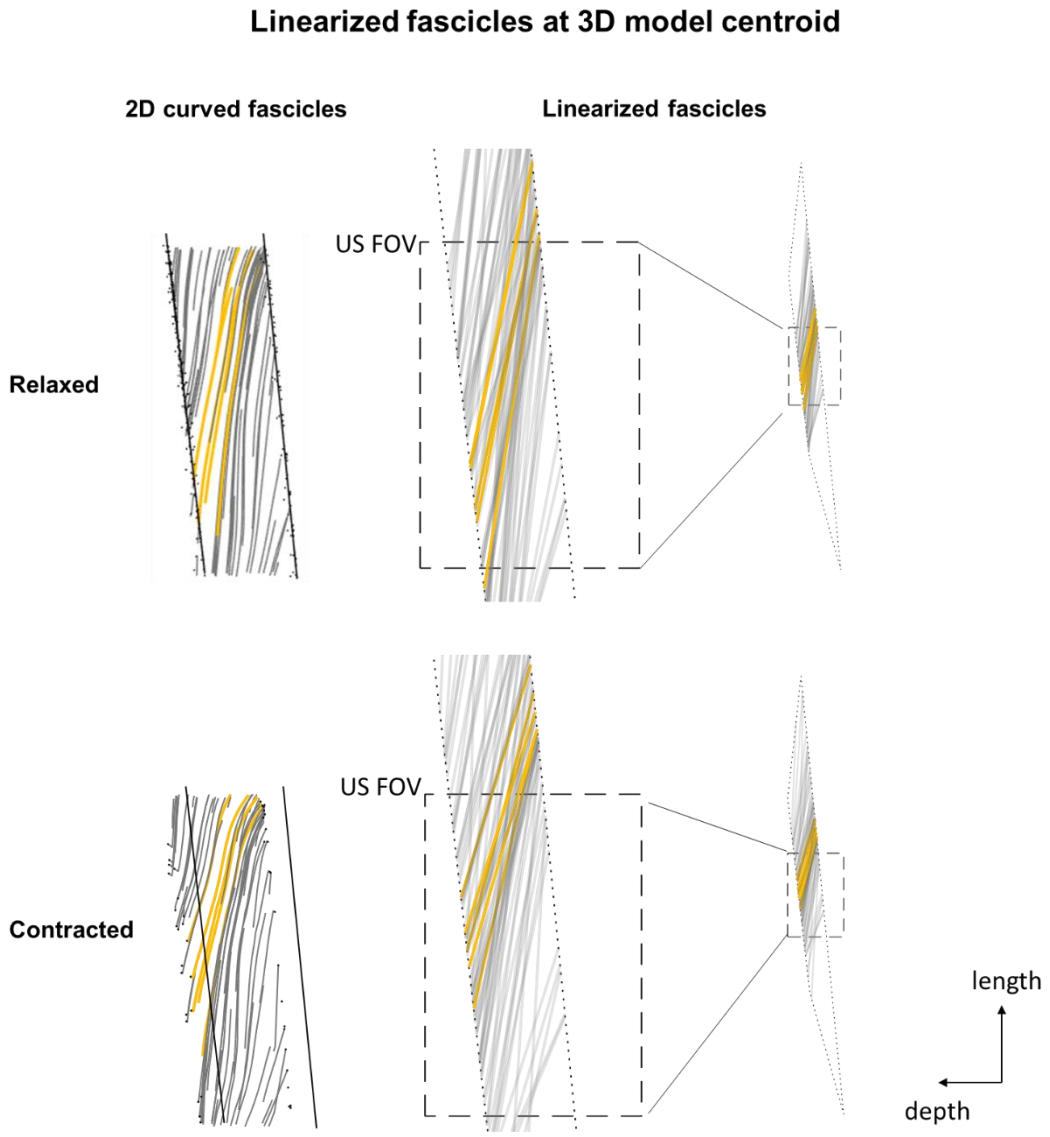

Figure 4.8. Fascicles at the model's centroid location, linearized by our algorithm.

We generated aponeuroses (black solid and dotted lines) as best fit lines through the model surface vertices (left column, black dots). The same aponeuroses were used in the linearization of the fascicles in the contracted state (bottom row) to reflect experimental practices. Fasicles at least 75% present in 3D (yellow lines) were reduced to 2D (left column), then linearized (right column) and extended or truncated as necessary to ensure fit with aponeurosis bounds. The dashed black box aound the linearized fasiscles shows the simulated ultrasound field-of-view and the portion of the fascicles in the FOV.

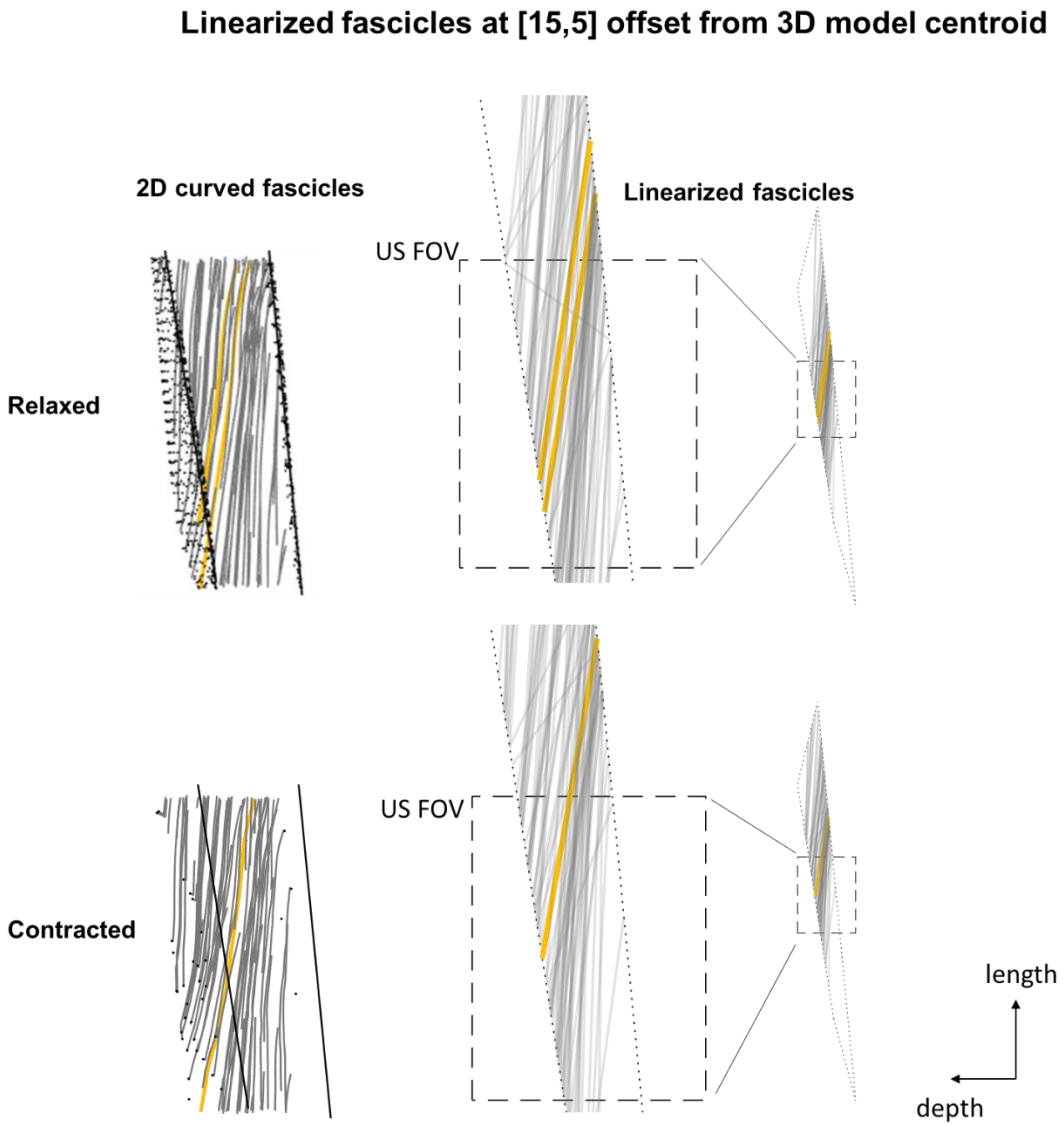

Figure 4.9. Fascicles at model's optimal match location, linearized by our algorithm.

Relative to the model centroid, fewer fascicles were at least 75% present in 3D (yellow lines) at this location. The horizontal range of model surface vertices (left column, black dots) was wider at this location than at the centroid.

4.4.4 Comparison of model and US 2D architecture

At the optimal location (15 mm medial and 5 mm proximal to model centroid, Figure 4.10A), the mean relaxed fascicle length (60.75 mm ± 15.57 mm) of the model matches experimental data well and was within 1 standard deviation of the ultrasound data (62.34 mm ± 1.97 mm). On average, fascicle lengths decreased with contraction. At this location in the model, the mean fascicle length decreased (-

1.25 mm) less than the change in ultrasound data (-4.69 mm ± 1.73 mm) (Figure 4.10B). The mean relaxed model pennation angle (19.17° ± 5.28°) was larger than the ultrasound data (14° ± 1.22°). On average, pennation angles increased with contraction. The change in mean model pennation angle (1.54°) was also larger than the change in ultrasound data (1.62° ± 0.74°) (Figure 4.10C).

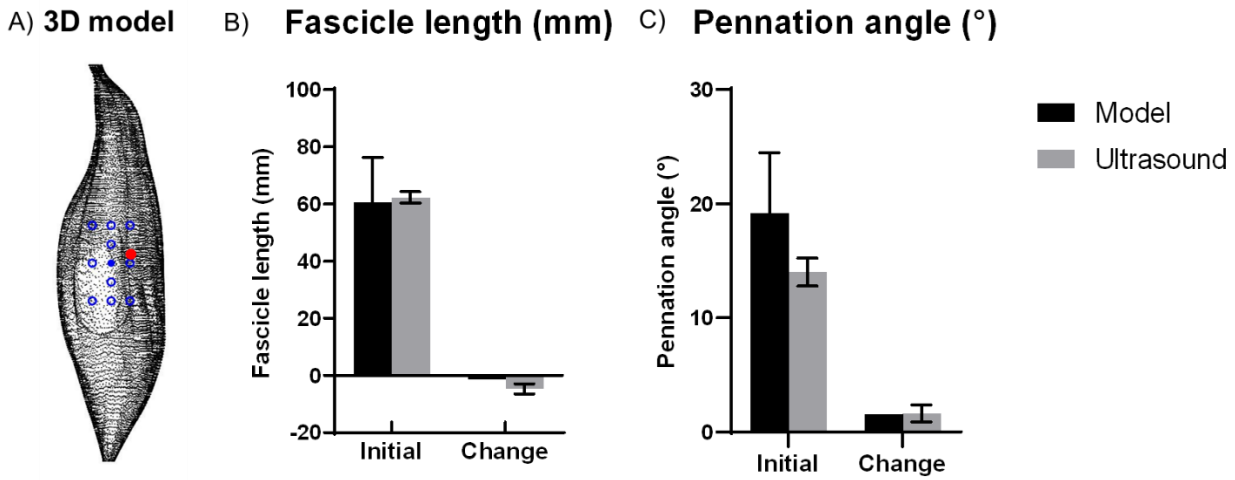

Figure 4.10. Comparison of linearized model fascicles and ultrasound architecture measurements.

A) Location (red dot) of the simulated ultrasound image and 2D architecture measurements. B) Comparison of relaxed/initial and change in fascicle lengths between model at optimal location and 50% activation (black bars), and MVIC ultrasound data (gray bars). C) Comparison of relaxed/initial and change in pennation angles between model at optimal location and 50% activation (black bars), and MVIC ultrasound data (gray bars).

4.4.5 Sensitivity to aponeurosis material properties

At the optimal location, no fascicles were present in the simulated US FOV both at rest and when contracted. Over the five tested stiffnesses, 3D and 2D mean fascicle lengths and strains were very similar (Figure 4.11). Mean linearized fascicle strains generally decreased with increasing orders of magnitude of aponeurosis stiffness, with linearized fascicle strains going from positive to negative, approaching mean 3D & 2D fascicle strains, which were all negative.

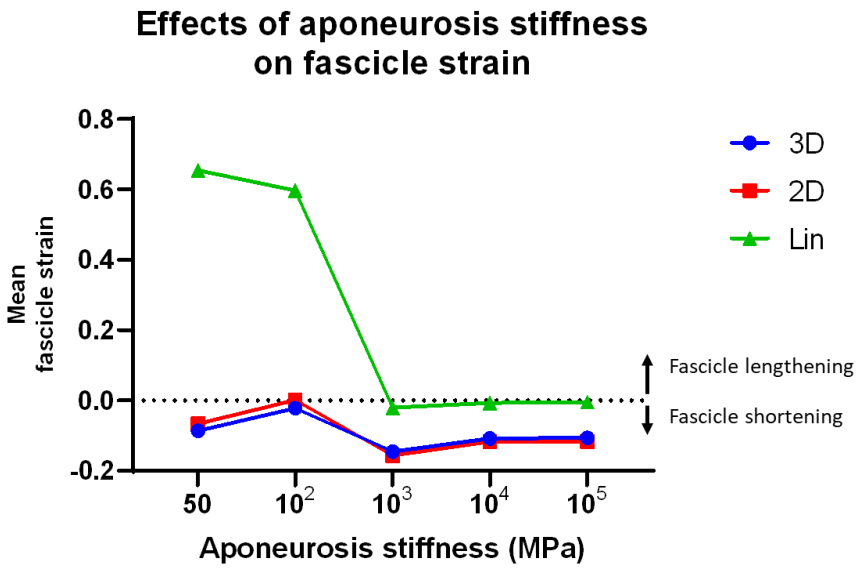

Figure 4.11. Effects of aponeurosis stiffness on model fascicle length.

The 3D (blue) and 2D (red) mean fascicle strains were consistently smaller than linearized (green) fascicle strains. With increasing aponeurosis stiffness, the 3D and 2D fascicles underwent less shortening to more shortening. At the two lowest stiffnesses, linearized fascicles underwent lengthening, but shortened at higher stiffness, though 10-15% less than the 3D and 2D fascicles shortened.

4.5 Discussion

We have created a method to simulate ultrasound images and collect 2D architecture measurements from a 3D muscle model. We created 3D medial gastrocnemius (MG) model geometry and fascicle architecture and simulated maximum voluntary isometric contractions then applied our ultrasound simulation algorithm to generate 2D architecture measurements from the model. Using this model and method, we have investigated the effects of aponeurosis stiffness on predicted 3D and 2D fascicle behavior in the MG. We found that we could recapitulate 2D US architecture measurements with our method and model. The location that our model best matched the data was not at the centroid of the model, which would correspond to muscle mid-belly where measurements were said to be taken, but at a location 15 mm proximal and 5 mm medial to the model center. Furthermore, our results indicate that it is unlikely that typical ultrasound imaging/architecture measurement reports measure the same fascicle throughout a contraction.

We built our 3D model geometry based on MR images and our model's fascicle arrangement matched relaxed 3D DTI architecture well, so we were confident that we could use our model to predict the fascicle behavior of an *in vivo* medial gastrocnemius muscle. We validated our model's relaxed/undeformed 3D architecture (fascicle lengths and pennation angles) using published MR-DTI data, enabling us to make predictions about changes in MG muscle architecture with contraction. We sampled fascicles from our 3D model to simulate 2D US images and linearize 3D fascicles, in order to compare model predictions to *in vivo* measurements of muscle architecture and fascicle strains. The predicted MVIC fascicle arrangement within the simulated probe field of view compared favorably with the ultrasound (US) images (Figure 4.1C, D). Between rest and MVIC, the average length change of all fascicles in the modelled probe region were comparable to the average *in vivo* data. We found that the location that best matched the US data was 15 mm proximal and 5 mm medial to the centroid of the muscle belly. Considering that the probe size in our study was 60 mm long and 15 mm wide, this location offset (relative to the centroid) is smaller than the probe size, and it could appear to be at the mid-belly if not measured directly. We expected the match location to be at the centroid, as US studies of the medial gastrocnemius generally claim to take the images measurements at "mid-belly" though the specific location is not typically measured or reported (Clark & Franz, 2018; Cronin et al., 2011; Darby et al., 2013). We are not exactly sure of the location where the US measurements were taken because the ultrasound probe is only capable of a narrow field of view. However, with finding that our architecture match location is not at the model's centroid demonstrates that architecture measurements are imaging site-dependent. This agrees with previous studies in other muscles (Savelberg et al., 2001; Stark & Schilling, 2010) and in the medial gastrocnemius (Rana et al., 2013). In the next chapter of this thesis, we extend the framework presented here to examine the effect of probe location on architecture measurements.

Our model and method enable us to track individual fascicle behavior throughout contraction. As is done in ultrasound experiments, we only reported architecture for fascicles that were mostly present

in fascicle (Figure 4.6). We assigned that cutoff as 75% present in the image field-of-view. It is important to note that in the ultrasound experiments, there is no way to determine how much of a fascicle is present. Our model is enabling us to measure: i) which fascicles are present and ii) how much of the fascicle is present in the FOV at each stage of a simulated contraction. We found that at the match location, the same fascicles were not present between the relaxed and contracted states. This result challenges the assumption made during ultrasound, that the same fascicle is imaged and therefore, that the architecture measurements taken at rest and when contracted are for the same fascicle. Based on the model tractography (Figure 4.6), we expected and did find that the model had more fascicles (n = 5) meeting the 75% criterion at the centroid than at the match location (2 fascicles when relaxed or 1 when contracted). This was expected as there were more fascicles towards the model center than at the edges of the model that were within physiological range (≤75mm) when relaxed. At the centroid, only one fascicle (of the 5) was present in the FOV at both relaxed and contracted, while no fascicle was present in both activation states at the match location. We found that the muscle and fascicles shifted laterally out of the FOV with contraction, so that at the medial edge of the model, the unchanged simulated US FOV captured fewer fascicles meeting the 75% presence criterion at either state. The mean linearized fascicle length of all the fascicles in the FOV at the match location (not just those meeting 75% criterion) when the model was both relaxed (60.75 mm ± 15.57 mm) and contracted (59.50 mm ± 13.47 mm) was within 1 standard deviation of the ultrasound data, whereas there was no such match at the origin. This further increased our confidence in the match location representing *in vivo* data and the possibility for future virtual experiments using the model and method. When we compared mean fascicle lengths at either activation state, we found that lengths at the centroid were consistently shorter than at the match location. The differences in means show further evidence that architecture measurements are imaging site-dependent.

Our model and method enable us to compare the 3D and 2D architecture of individual fascicles. This is important because there is currently no way to determine how well 2D ultrasound measurements

represent the 3D fascicles they measure. Our model showed that 3D fascicle lengths may be longer or shorter than linearized fascicle lengths depending on the location and orientation of the fascicles in the muscle. We compared the 3D and linearized lengths for fascicles that were at least 75% present at the match location. We found that the mean linearized fascicle lengths were longer than 3D fascicle lengths at the centroid location, but the opposite was true at the match location. At the match location, the mean 3D length of the 2 fascicles meeting the 75% presence criterion when the muscle was relaxed was larger (68.96 mm ± 4.15 mm) than the mean linearized length (64.88 mm ± 2.85 mm). When contracted, the 3D length of the only fascicle meeting the 75% presence criterion was also larger (76.79 mm) than its linearized length (64.08 mm). In summary, the mean linearized fascicle length decreased and the pennation angle increased, while the corresponding 3D fascicle length increased, going against the expected trend of decreased fascicle length with contraction. At the centroid, we saw the expected trend of fascicle length decreasing with contraction and pennation angle increasing. We know that there were fewer fascicles at the match location than at the centroid, so that the number of fascicles (discussed above) may affect the averages we compare. This highlights a challenge with ultrasound experiments relying on measuring and reporting measurements for a single fascicle (usually because it is mostly visible), rather than the summary statistics of a representative sample of fascicles visible in the field-of-view/image.

Several studies have highlighted the effects of the aponeurosis structure on the fascicle behavior during muscle contraction (Epstein et al, 2006, Eng and Roberts, 2018). We used our model and method to study interactions between MG aponeurosis stiffness and fascicle behavior with contraction, which are currently unmeasured in human muscle *in vivo*. We expected to see i) mean fascicle shortening at all stiffnesses, ii) less fascicle shortening with stiffer aponeuroses. We calculated the mean strain using the average fascicle lengths in the FOV, which were not the same fascicles at rest or activated. This is therefore not an average of individual fascicle strains, which would require us to know the change in

length of each fascicle, even if they are not in the FOV. Though our model enables tracking individual fascicles not in the FOV, we did not use this approach as US experiments do not know if they are tracking the same fascicle in the FOV. Overall, we found that increasing aponeurosis stiffness over 3 orders of magnitude increased fascicle shortening. We see for all (3D, 2D curved, linearized) the plots that across the highest 3 stiffnesses, the strains of the linearized fascicles plateaued and shortened less than 3D/2D fascicles, which generally shortened less with increasing aponeurosis stiffness. We see that the 3D and 2D curved fascicle strain curves overlap, indicating that they are almost the same. The lengthening

We wish to address some assumptions and limitations in our model and method. In terms of validating our 3D model, we found that the fascicles that remained in the model after filtering out fascicles that were longer than MG physiological length (≤75 mm) were located in the medial region of the model. This is consistent with results from DTI reconstructions (Bolsterlee et al., 2015, 2017), which use similar physiological cutoffs. Currently, the DTI technique does not allow for imaging of contracting muscles, so we were unable to validate the model's contracted 3D architecture as we did with the relaxed architecture. Another way to use DTI data to validate changes in model architecture is to perform simulations of passive (no muscle activation) lengthening and compare to DTI architecture measurements from relaxed lengthened muscle. However, we were not able to additionally validate our model this way as DTI data for similar experimental conditions, namely joint angles, were not available to us at this time. Nevertheless, we were confident in our model's ability to provide new information about MG fascicle behavior during contraction.

To gain insight into fascicle behavior during contraction, it was important to include aponeuroses with appropriate material properties in our model rather than model the muscle only. However, we modeled the aponeuroses simply, with uniform thicknesses and uniform fiber directions, as well as a neo-Hookean ground matrix. In the material definitions, we used a simple ground matrix that has a linear relationship between stress and strain, in order to easily modify material stiffness to capture the effects

of stiffness on architecture measurements. The Young's modulus that that we used in our virtual experiments was 3-4 times larger than the longitudinal Young's modulus measured from cadavers (age 82.2 ± 10.1 years) (Shan et al., 2019) and between 30%-190% larger than the stiffnesses measured in healthy young (age 37 ± 3 years) male adults (Magnusson et al., 2001). In future work, we will implement a ground matrix such as a Mooney-Rivlin material that would allow differences in longitudinal and transverse stiffnesses and perform further sensitivity analyses to fine-tune ratio of longitudinal and transverse aponeurosis properties and their relationship with our muscle material.

Although cadaver experiments show non-uniform aponeurosis thicknesses (Shan et al., 2019), the MR images that we used to build our model did not provide sufficient resolution of the variable aponeurosis thickness in order to model this property. We modeled the aponeurosis thickness uniformly within physiological range, based on the average reported thicknesses (Shan et al., 2019). We applied purely vertical fiber directions to the elements of the aponeurosis geometries. In future, we would conduct CFD simulations or assign vectors that follow the lateral edges of the aponeuroses, as this is more physiologically accurate and would likely improve the tissue and fascicle strain results of the finite element simulations. To test that we could still get expected results from our simplified aponeuroses, we tested that the average aponeurosis finite element fiber stretch, a direct output of the muscle model's constitutive model, over a simulation of maximum contraction. Average muscle fiber stretch consistently decreased with increased aponeurosis stiffness. This test gave us confidence that our model would predict changes in fascicle behavior well.

In generating linearized fascicles, the first step in our algorithm is to linearize the model's deep and superficial aponeuroses. In practice, the general approach is to identify the hyperechoic aponeuroses in the US images of relaxed muscle and define straight lines through them. The experimenter also draws a straight line through the fascicle of interest to intersect with the aponeuroses. Some semi-automated methods take manually selected lines through both aponeuroses in each ultrasound video frame over a

contraction and generate a representative fascicle based on the average of several manually selected visible fascicle portions that have a minimum length (Ekizos et al., 2013; Marzilger et al., 2018; Nikolaidou et al., n.d.). Semi-automated feature detection methods calculate architecture by first determining fascicle orientation in a selected region of interest (ROI) using Hough/wavelet or Radon transforms (Rana et al., 2009; Zhou et al., 2015). The most popular semi-automated methods are feature tracking algorithms which rely on manual identification of features (aponeuroses and fascicle endpoints) that are tracked through each US video frame (Cronin et al., 2011; Darby et al., 2013; Farris & Lichtwark, 2016; Seynnes & Cronin, 2020). These methods do not automatically track movement in the aponeuroses, but define an unchanging quadrilateral region of interest (ROI) that includes the aponeuroses as upper and lower boundaries, and uses optic flow algorithms and/or affine transformations to track behavior of a pre-defined fascicle within the ROI during contraction. In keeping with the way that these ultrasound measurements are taken, i.e., from a pre-determined region of interest, we did not readjust the aponeuroses with contraction. While our model enables us to follow changes in aponeurosis orientation in its naturally curved state, for this study we: a) linearized the aponeuroses, and b) did not update the orientation of the aponeuroses (i.e., we used the aponeurosis orientations when the muscle was relaxed), in keeping with the experimental measurement technique. In the next chapter of this thesis, we extend our framework to examine the effect of unchanged aponeurosis orientation on architecture measurements.

An assumption we made during the aponeurosis and fascicle linearization process is that once we set the "imaging" location/field-of-view, that the simulated US image was set exactly upon the surface of the model. This was not true, as neither aponeurosis was perfectly vertical (e.g. deep: 6.7° and superficial: 5.7° at the centroid) and we did not apply a corrective pitch rotation (Figure 6.1) to the simulated US probe because the angles were small and similar in value, creating close to uniform boundaries for fascicle

linearization. In future work we will account for the alignment by applying any appropriate rotation to the simulated probe to ensure perfect alignment with the model surface.

In some locations of the muscle, including the match location, one or both of the aponeuroses generated by the algorithm were stochastic, meaning that the aponeurosis line generated would be different each time the algorithm ran. This stochasticity resulted when the algorithm took user selections for [x, y] points used to generate the linearized aponeurosis, because the automatically generated line did not meet a criterion. Specifically, if the 3D model surface vertices used to generate the linearized aponeurosis did not have a best fit line with $R^2 \geq 0.75$, then the algorithm allowed the user to pick points and fit a line through it to create the aponeurosis. Once we pick the points at a location manually, we must save their coordinates to ensure that the same aponeuroses are generated for reproducible analyses. However, once these considerations are made, our method performs as expected.

This study is the first to describe a method to simulate 2D ultrasound images of pennated skeletal muscle and fascicles, and predict changes in fascicle arrangement during contraction using a 3D model, enabling fascicle by fascicle comparisons of 2D ultrasound measurements and 3D muscle architecture. To date, studies evaluating the reliability and validity of ultrasound architecture measurements take the form of literature reviews. We hope that this method will enable computational studies to aid in evaluating the ultrasound technique as well as measurements of changes in both actual/3D and linearized architecture from ultrasound data.

5 Chapter 5

A 3D Muscle Model Reveals the Relationship Between 3D Fascicle Behavior and 2D Ultrasound Measurements

Acknowledgements: William H. Clark[2], Jeroen B. Waanders[3], Jason R. Franz[2], Silvia S. Blemker[1]

[1]University of Virginia, Charlottesville, VA, USA
[2]UNC Chapel Hill & NC State University, Chapel Hill, NC, USA
[3]University of Groningen, Groningen, the Netherlands

5.1 Abstract

The field of muscle biomechanics frequently utilizes ultrasound measurements of muscle architecture (fascicle arrangement) to evaluate muscles' performance during various movements and relative to other muscles. *In vivo*, muscle fascicles are curved, and three-dimensional (3D). However, in order to make muscle architecture (fascicle length and pennation angle) measurements from 2D ultrasound (US) images, it is assumed that fascicles are straight lines. In this study we aim to evaluate the relationship between 3D architecture and 2D measurements in the medial gastrocnemius (MG), as well as the effects of US imaging variables such as probe location or imaging site on measurements. We also investigated two common assumptions made during muscle architecture measurements from 2D US images: (1) that the same fascicles are tracked in the US image as the muscle contracts, and (2) that the aponeurosis orientations remain unchanged with contraction. To do this, we leveraged the method we previously generated to use a three-dimensional (3D) model to simulate 2D ultrasound measurements of muscle architecture. We simulated 2D US images and compared model predictions of relaxed and contracted muscle architecture and fascicle strains for 3D curved, 2D curved and linearized fascicles. From studying some common US assumptions, we found that linearized fascicle lengths are more representative of 3D fascicle length (more accurate) when more of the fascicle is captured in the US image field-of-view. We found that the average of multiple linearized fascicle lengths reduced potential difference (error) compared to the 3D (expected) measurement. We found that linearized architecture measurements are location dependent within the medial gastrocnemius. At the location that we previously identified best matched US data, we found that for fascicles ≥75% present in the US FOV, there was no significant difference of architecture means between measurements taken a) from fascicles in the US FOV at final state or only those that were present at the initial state, and b) when the aponeuroses in the relaxed configuration or contracted configuration were used. Our findings are relevant to ultrasound

imaging studies of muscle, as they provide increased knowledge about how 2D measurements compare to 3D architecture and how some experimental assumptions affect the measurements.

5.2 Introduction

Quantifying changes in fascicle behavior during movement is crucial to understanding the relationship between muscle's structure and function in healthy and clinical populations. Real-time brightness-mode ultrasonography is a non-invasive, quick, inexpensive and commonly used method to provide informative two-dimensional (2D) measurements of relaxed and contracted muscle. Muscle fascicles (fiber bundles) appear in b-mode ultrasound images as dark/hypoechoic linear structures which are surrounded by hyperechoic connective tissues. From these 2D images, researchers digitize fascicles to measure fascicle length, fascicle pennation angle, and muscle thickness (Fukunaga et al., 1997; Kawakami et al., 1998; Maganaris et al., 1998). This technique is mostly performed in superficial muscles such as the medial gastrocnemius (Cronin & Lichtwark, 2013; Kawakami et al., 1998; Lichtwark et al., 2007; Maganaris et al., 1998; Narici et al., 1996).

Despite its broad use, ultrasound (US) measurements have the notable limitation that they provide 2D measurements of 3D structures. The 2D measurements are assumed to represent the muscle's 3D structure, and while the measurements are highly repeatable (Kwah et al., 2013; May et al., 2021), the relative error associated with the 2D simplification is not known because it is not physically possible to study. It is very challenging to understand the impact of the 2D assumption from ultrasound imaging alone, but it is important to understand this relationship as well as the experimental/measurement system. To date, computational and quantitative approaches to investigate this relationship are limited. There have been ultrasound (Rana et al., 2013, 2014; Rana & Wakeling, 2011), DTI (Bolsterlee et al., 2016b, 2017) and computational fluid dynamics (Handsfield et al., 2017) studies to determine 3D architecture, and there have been review studies evaluating the reliability of 2D ultrasound measurements from literature (Kwah et al., 2013; May et al., 2021). Existing studies looking at the relationship between 3D

architecture and 2D measurements gave insight into the orientation of fascicles relative to the imaging plane (Bolsterlee et al., 2015) and how to optimize imaging orientation to reduce error (Bolsterlee et al., 2016a, 2016b), but these studies were MR-DTI studies that assume highly linear fascicles and only provide static measurements of 3D muscle architecture.

Typically, MG muscle architecture measurements are reported to be taken at the muscle mid-belly and orientated to get the clearest image of the fascicles. However, we have not seen exact locations stated in the literature (e.g. (Clark & Franz, 2018; Cronin et al., 2011; Herbert et al., 2011, 2015)). In order to make the 2D architecture measurements, some assumptions must be made. Despite evidence of fascicle curvature (Darby et al., 2013; Muramatsu et al., 2002; Namburete et al., 2011; Rana et al., 2014), typical ultrasound measurements assume linear fascicles. To use manual digitization (Fukunaga et al., 1997; Lichtwark et al., 2007) or automatic fascicle tracking software (Cronin et al., 2011; Farris & Lichtwark, 2016) to make dynamic MG architecture measurements from ultrasound images, both the aponeuroses and all fascicles are assumed to be straight lines. The assumption that the aponeurosis orientation does not change significantly with contraction is necessary for some of the automatic fascicle tracking software, which tracks fascicles within a user-selected region of interest chosen in the relaxed condition (Cronin et al., 2011; Farris & Lichtwark, 2016). Like the relationship between the actual 3D arrangement and the 2D measurements, the effects of these assumptions cannot be tested directly. This is another opportunity to leverage 3D computational models to perform relevant experiments for architecture measurement sensitivity to that we cannot perform physically.

Computational models enable us to study muscle *in silico*, but also to study the experimental systems that we use to study muscle *in vivo*. There is an opportunity to leverage computational modeling to investigate the effects of the assumptions and limitations in the experimental and measurement process of taking 2D architecture measurements from ultrasound images/videos. We previously created a method to enable direct comparisons between 3D model architecture and 2D US measurements. These

3D model predictions can be used to further investigate the relationship between 3D fascicle arrangement an 2D measurements.

Our goal was to use our 3D medial gastrocnemius (MG) model with our method to simulate 2D ultrasound images and architecture measurements to investigate the: (1) relationship between 3D architecture and 2D US architecture measurements, and (2) sensitivity of 2D architecture measurements to US imaging location. We also aimed to use our framework to evaluate how typical assumptions made to enable architecture measurements from US images affect the measurements. We investigated the assumptions that: i) fascicles that architecture measurements are taken from remain in the image and are the same fascicles being tracked throughout the contraction, ii) the aponeurosis orientation does not change with contraction, and iii) how these assumptions may affect 2D architecture measurements.

5.3 Methods

We used a 3D model of the MG muscle that we developed previously, along with our method to simulate 2D ultrasound images to perform the following virtual experiments.

5.3.1 Evaluating the relationship between 3D architecture and 2D US architecture measurements

We simulated ultrasound images at 15 mm proximal and 5 mm lateral to the centroid of the 3D model. This is the location that we previously found to best match MG ultrasound measurements (Table 4.1). At this reference location, we compared relaxed measurements and post-contraction changes in 3D, 2D curved and linearized architecture (fascicle lengths and pennation angles) for the fascicles that were present (at any percentage) in the field-of-view. For pennation angle, we compared differences between 3D and linearized measurements only.

To determine how well the linearized measurements represent the 3D architecture, we evaluated the percent error between the 3D fascicle lengths and linearized measurements. We defined absolute

error as the difference between the expected fascicle length (FL_{3D}) and the observed fascicle length (FL_{Lin}). Therefore, we defined percentage error in fascicle length as:

Equation 7. Percentage difference (error) in model-predicted fascicle length.

$$Fasicle\ Length\ Percent\ Error = \left|\frac{FL_{Lin} - FL_{3D}}{FL_{3D}}\right| \times 100\%$$

We also calculated the percentage of each fascicle that was present in the ultrasound (US) field-of-view (FOV). Then, to explore whether the fascicle length percent error was due to limited presense of a fascicle in the field of view, we examined the relationship between percentage error in fascicle length and the percentage of the fascicle that is present in the ultrasound field-of-view.

5.3.2 Effects of location on 2D US architecture measurements

To determine how sensitive ultrasound architecture measurements in the MG were to the probe location, we took linearized fascicle architecture measurements at a variety of locations (

Table 4) in the relaxed and contracted 3D model and compared them to our reference location ([15,5] offset from centroid). We also compared the change in mean linearized fascicle length and pennation angle at these locations and evaluated whether any differences in means were statistically significant.

Table 4. MG model locations where we collected and compared architecture measurement predications
First column shows the reference location (red dot) and other locations (letters) where we took measurements. The other columns show the vertical and horizontal distances of each point from the model centroid. Positive values are proximal (in 3rd column) or lateral (in 4th column).

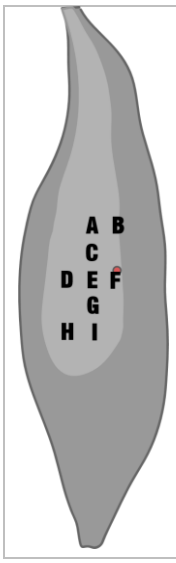

Location	Mediolateral (side-side) distance from centroid	Proximodistal (up-down) distance from centroid
Reference (red dot)	15	5
A	0	30
B	15	30
C	0	15
D	-15	0
E (centroid)	0	0
F	15	0
G	0	-15
H	-15	-30
I	0	-30

5.3.3 Evaluating the experimental method: window versus fascicle tracking

To investigate the experimental assumption that the relaxed and contracted architecture measurements come from the same fascicle in the US image, we determined the number of linearized fascicles that were 75% present in the US FOV at both relaxed and contracted states. We leveraged our model's resolution, i.e. our ability to follow the behavior of individual fascicles, to determine how linearized architecture measurements would differ if this assumption were true. To do this, we compared differences in mean architecture measurements taken by 2 methods: i) tracking the same fascicles from relaxed to contracted, and ii) tracking only the fascicles in the window or FOV at each state (relaxed or contracted). We performed a Wilcoxon matched-pairs test to evaluate if the sets of pairs (window-tracking versus fascicle-tracking) were significantly different.

5.3.4 Evaluating the experimental method: relaxed versus contracted aponeurosis

To investigate the effects of the commonly made assumption that aponeurosis orientation does not change during contraction (Cronin et al., 2011; Farris & Lichtwark, 2016), we determined the mean change in fascicle length and pennation angle taken with the aponeurosis configuration when the muscle

was either: i) relaxed or ii) contracted. We performed a Wilcoxon matched-pairs test to evaluate if the sets of pairs (using the relaxed aponeurosis versus using the changed/contracted) were significantly different from each other.

5.4 Results

5.4.1 Evaluating the relationship between 3D architecture and 2D US architecture measurements

When relaxed, there was a small difference between the 3D (blue) and 2D curved fascicle length (FL, red) for each fascicle, as seen in the overlapping data points (Figure 5.1A). The corresponding linearized fascicle lengths (green) were not consistently larger or smaller than the 3D FL (Figure 5.1A). Most linearized PA measurements were larger than the corresponding 3D PA (Figure 5.1C). The means of the linearized FL and PA were generally larger than the 3D measurements, but not significantly larger (Figure 5.1B,D). The 3D and linearized FL measurements of all fascicles (3D FL: 62.69 ± 8.0 mm; 3D PA: 16.17° ± 4.61°; Linearized FL: 62.53 ± 12.92 mm; Linearized PA: 19.17° ± 5.03°) (solid bars, Figure 5.1B,D) and the ≥75% present fascicles (3D FL: 68.96 ± 2.40 mm; 3D PA: 17.55° ± 0.84°; Linearized FL: 64.88 ± 1.64 mm; Linearized PA: 17.58 ± 0.23) (striped bars, Figure 5.1B,D) were not significantly different from each other.

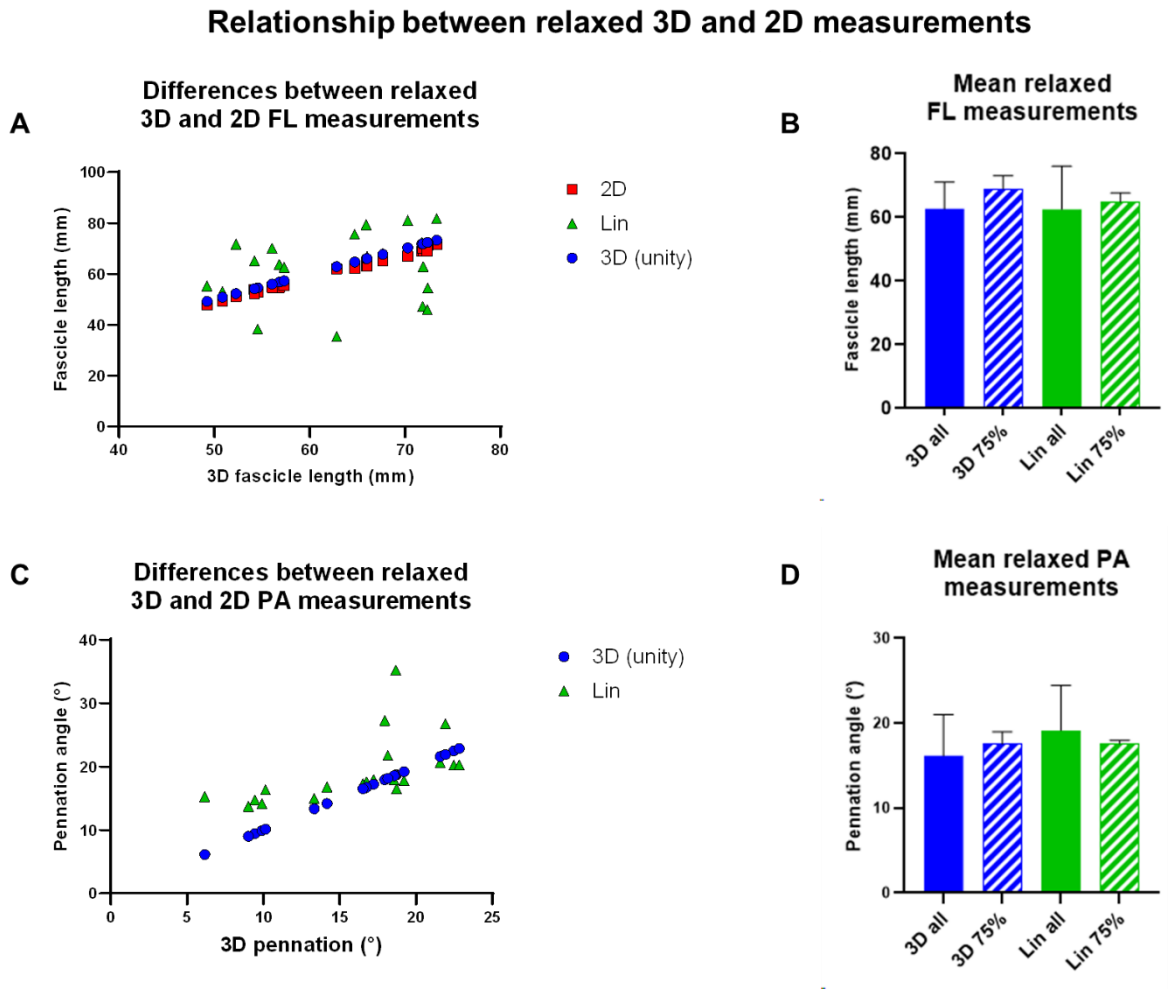

Figure 5.1. Relationship between model-predcted 3D, 2D and linearized architecture measurements, when the muscle is relaxed.

Left panels show the relationship between corresponding relaxed 3D (blue), 2D curved (red) and linearized (green) fascicle length ("FL", A) and pennation angle ("PA", C) measurements for each of the 21 fascicles present at [15,5] offset from model centroid. We compared the corresponding relaxed 3D and linearized FL and PA means for all the fascicles (solid), as well as only those fascicles that were at least 75% present (striped) in the US FOV. Error bars on the right panel indicate standard deviation.

There was generally a i) decrease in fascicle length and ii) increase in pennation angle with contraction, except for the 3D measurements for the ≥75% fascicles (Figure 5.2). The magnitude of changes in mean 3D (blue, Figure 5.2) FL and PA were generally larger than the linearized (green, Figure 5.2) measurements. The changes in mean FL (3D: -9.14 mm; Linearized: -1.25 mm) and PA (3D: 2.23°; Linearized: 1.53°) for all fascicles (solid bars) in the field of view were generally larger than the changes in

mean FL (3D: 7.84 mm; Linearized: -0.80 mm) and PA (3D: -2.66°; Linearized: 0.93°) of the ≥75% fascicles (striped bars), except for 3D pennation angle.

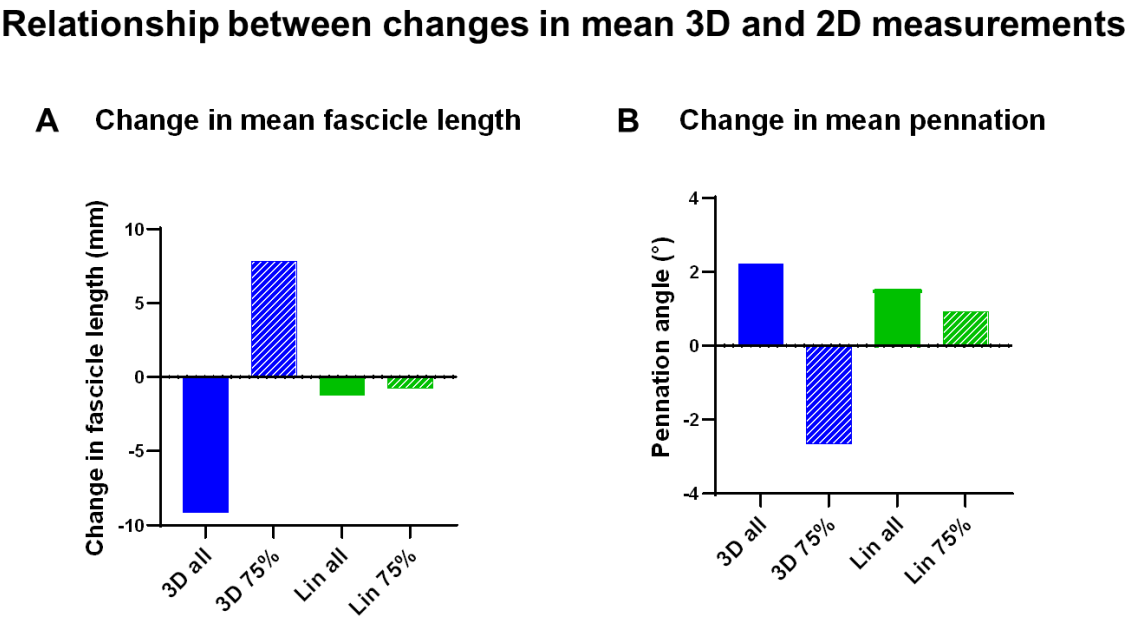

Figure 5.2. Relationship between changes in mean 3D and linearized measurements with contraction.

We compared changes in mean 3D (blue) and linearized (green) fascicle length (A) and pennation angle (B) for any fascicles present (solid) as well as only those fascicles at least 75% present (striped) in the US FOV.

Table 5 (below) summarizes the differences in architecture measurements between: a) centroid and reference location and b) 3D and Linearized measurements. At the reference location of the model, there were no fascicles that were at least 75% present in the FOV in both the contracted and relaxed states. At the centroid, there was 1 fascicle that was at least 75% present in the FOV in both the relaxed and contracted states. In general, the magnitude of percentage differences between the 3D and linearized measurements was smaller in the relaxed (initial) state than in the contracted (final) state. At either location, the magnitude of the percentage difference in measurements for i) all fascicles (

Table 4, last 2 columns) and for ii) each state (initial vs. final) was generally consistent for the FL and PA.

Table 5. Percentage difference in predicted 2D architecture measurements at the centroid location [0,0] and at the reference location [15,5], which best corresponds to US data

These measurements are taken from fascicles that were at least 75% present in the US FOV, except for the data in the last two rows, which summarize architecture for all fascicles present in the FOV at all.

Architecture measurement	3D measurement				Linearized measurement				% Difference between 3D & linearized measurements			
	[0,0] location		[15,5] location		[0,0] location		[15,5] location		[0,0] location		[15,5] location	
	Initial	Final	Initial	Final	Initial	Final	Initial	Final	Initial	Final	Initial	Final
# of 3D fascicles ≥75% present in FOV	5	5	2	1	5	5	2	1	N/A	N/A	N/A	N/A
# of fascicles ≥75% present in FOV when both relaxed and contracted	N/A	1	N/A	0	N/A	1	N/A	0	N/A	N/A	N/A	N/A
mean percentage of 3D FL in FOV	0.84	0.86	0.82	0.83	0.84	0.86	0.82	0.83	N/A	N/A	N/A	N/A
mean FL ± std.	55.30 ± 6.43	44.37 ± 5.93	68.96 ± 4.15	76.79 ± 0.00	58.88 ± 3.97	47.53 ± 3.98	64.88 ± 2.85	64.08 ± 0.00	-6%	-7%	6%	17%
mean PA ± std.	17.38 ± 4.94	23.40 ± 6.45	17.55 ± 1.45	23.33 ± 0.00	17.42 ± 1.19	21.99 ± 1.19	17.58 ± 0.40	18.52 ± 0.40	0%	6%	0%	21%
change in mean FL	N/A	-10.92	N/A	7.84	N/A	-11.35	N/A	-0.80	N/A	-4%	N/A	110%
change in mean PA	N/A	-5.76	N/A	-2.96	N/A	4.57	N/A	0.93	N/A	179%	N/A	132%
mean FL of all fascicles in FOV	61.71	52.05	62.69	53.55	72.66	61.34	60.75	59.50	-18%	-18%	3%	-11%
mean PA of all fascicles in FOV	15.84	20.68	16.17	18.71	15.12	18.27	19.17	20.71	5%	12%	-19%	-11%

We found that, in general, the higher the percentage of a fascicle's length in the US FOV, the lower the percentage difference in the linearized fascicle length measurement (compared to 3D (expected) fascicle length) (Figure 5.3). Therefore, there is an inverse relationship between percentage of fascicle length present in the simulated US FOV and the percentage difference (error) in fascicle length.

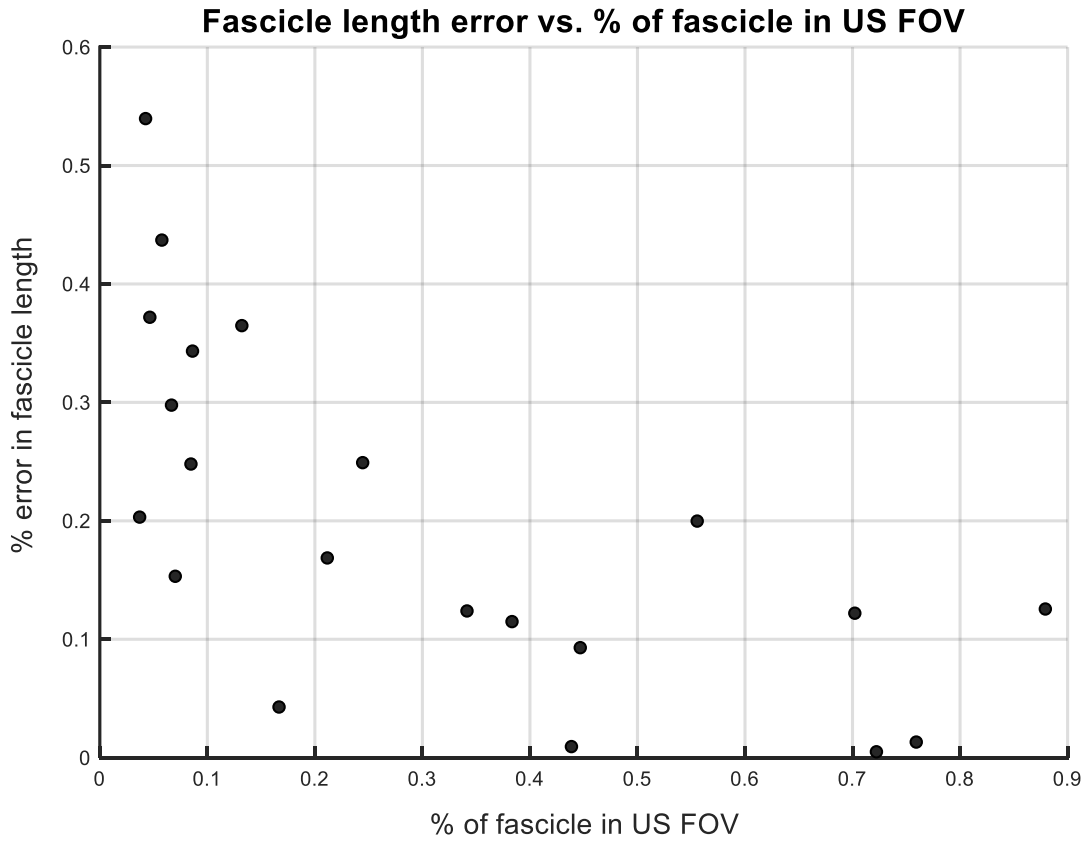

Figure 5.3. Relationship between percentage error in fascicle length and the percentage of a fascicle in the ultrasound field-of-view.

Each data point represents a fascicle visible at the reference location.

5.4.2 Effects of location on 2D US architecture measurements

When we compared fascicle length (FL) and pennation angles (PA) at various locations to the reference location [15,5], we generally found that FLs were smaller and PAs were larger, regardless of contraction (activation) state (Figure 5.4B). There were exceptions to this trend, including locations where

the measurement difference opposed these trends but were within one standard deviation of the reference location measurement (filled symbols, Figure 5.4B). We generally found larger differences in the contracted architecture than in the relaxed architecture, by up to twice as much in the fascicle lengths (Figure 5.4A). There were no relaxed linearized architecture measurements for the [15,30] or [0,-15] locations, and no contracted measurements for the [15,30]. location. Since we computed the differences relative to the [15,5] location, no differences are reported for that region.

Differences (compared to match location) in linearized architecture measurements by location

A. Table of differences by location

Location	Difference in **relaxed** linearized architecture		Difference in **contracted** linearized architecture	
	Fascicle length (mm)	**Pennation angle** (°)	**Fascicle length** (mm)	**Pennation angle** (°)
[0,30]	-4.49	1.04	-15.08	5.83
[15,30]	N/A	N/A	N/A	N/A
[0,15]	-10.27	1.53	-20.0	5.83
[-15,0]	-9.31	0.40	-20.56	5.17
[0,0]	-6.00	-0.16	-16.55	3.48
[15,0]	2.73	-0.93	0.35	-0.003
[0,-15]	N/A	N/A	-23.35	6.05
[-15,-30]	4.80	-0.27	-20.05	8.99
[0,-30]	-21.26	4.86	-28.01	9.36

B. Illustration of differences by location

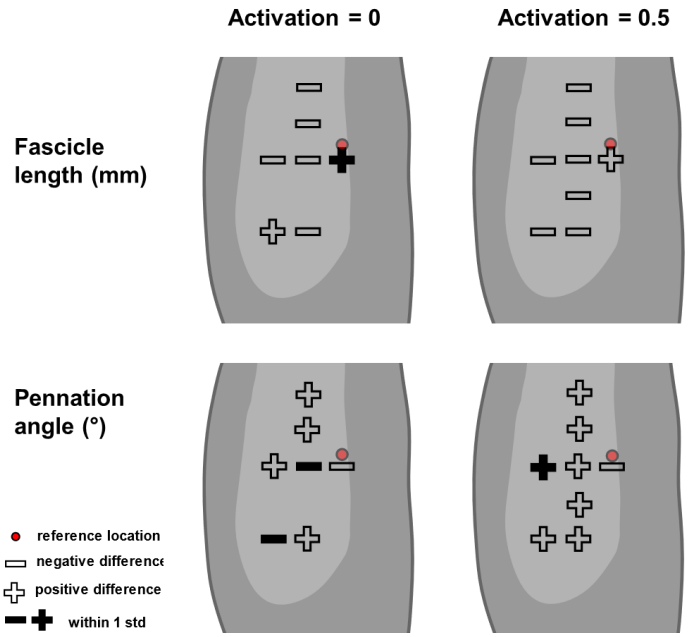

Figure 5.4. Absolute error in relaxed and contracted linearized architecture measurements by location.

Table A) and B) illustration of the errors compared to the reference location (red dot). Negative/positicve errors (location measurement smaller/larger than reference location) are represented by minus/plus symbols at the location. Filled symbols indicate that the measurement was within 1 standard deviation of the reference locatrion.

Generally, at each location, fascicle length decreased and pennation angle increased (Figure 5.5). There was an exception to this trend at the [-15,-30] and [0,-30] locations, where the pennation angle decreased instead. The change in fascicle lengths at these locations was larger for the ≥75% present mean

than the means of all the fascicles in the FOV. The magnitude in changes in mean linearized fascicle length (Figure 5.5B,D) and pennation angle (Figure 5.5C,E) by location were consistent for the any fascicles (Figure 5.5C,D) and ≥75% (Figure 5.5A,B) fascicles means. There were no FL or PA measurements at [15,30] and [0,-15], but we have mean measurements for any (all) fascicles in the FOV at these locations.

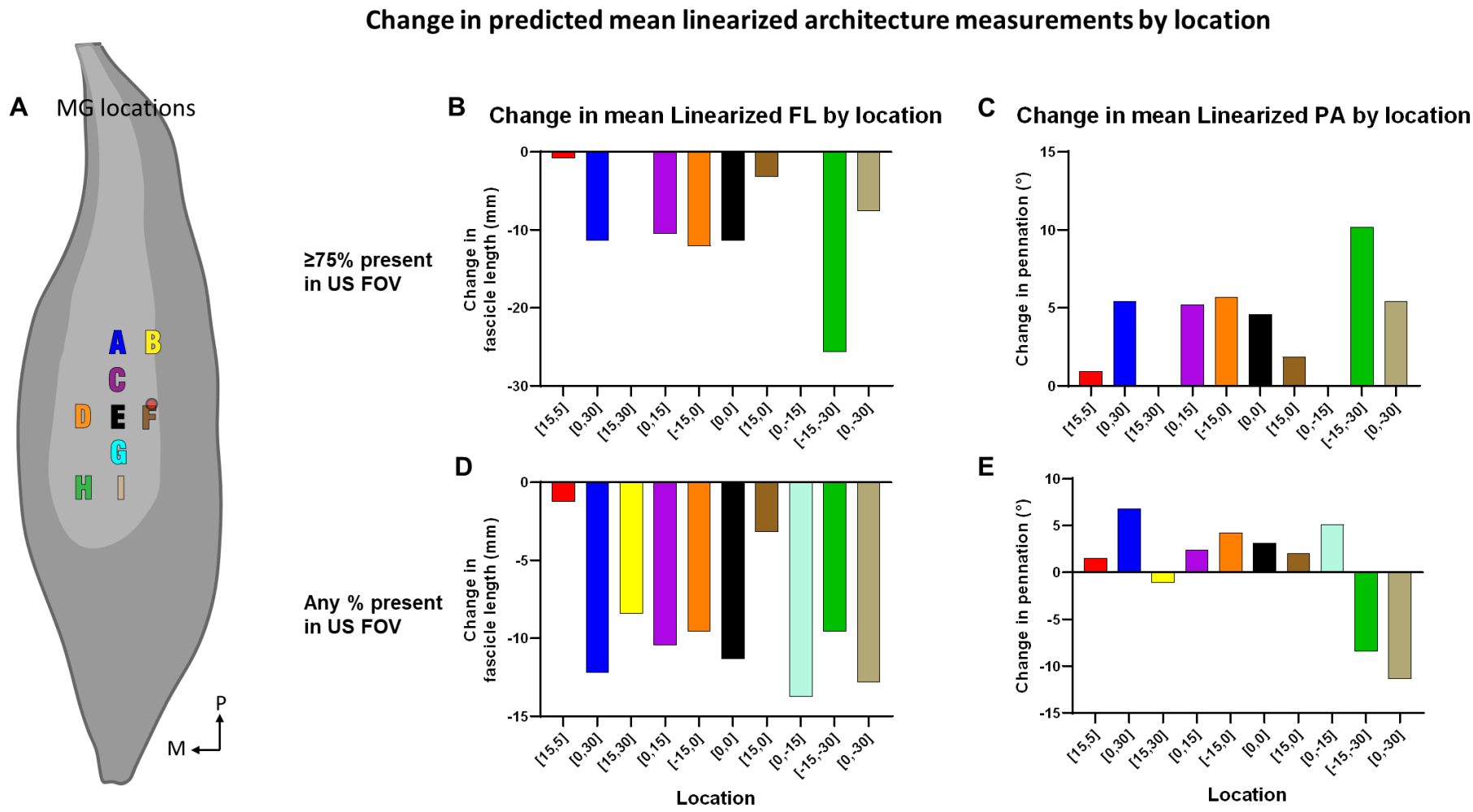

Figure 5.5. Change in model-predicted mean linearized architecture measurements by location.

A) Colors of the reference (red dot) and other locations (lettered A through I) illustrated on the MG model correspond to bar chart colors (B-E). Location distances are to scale, and location coordinates are based on their proximal (P) and medial (M) directions from the muscle centroid (location E), where ultrasound studies generally claim to take measurements. Change in mean linearized fascicle length ("FL" in graphs B,D) and pennation angle ("PA" in graphs C,E) by location, for only the fascicles at least 75% present in the FOV (B,C) and for any fascicles present in the FOV (D,E) . Note the difference in scales of the vertical axes of B and D.

5.4.3 Evaluating the method: window versus fascicle tracking

We found the that there was no significant difference between predicted fascicle length (Figure 5.6B) or pennation angle (Figure 5.6C) group means (of all locations [Figure 5.6A]) from the window (FL: -10.31 mm ± 6.58 mm; PA: 4.92° ± 2.46°) and fascicle tracking (FL: -7.62 mm ± 2.53 mm; PA: 3.86° ± 1.48°). The lines among the data represent the median measurements. Data for individual locations can be found in Appendix 2: Percentage difference between mean 2D and 3D architecture measurements by location.

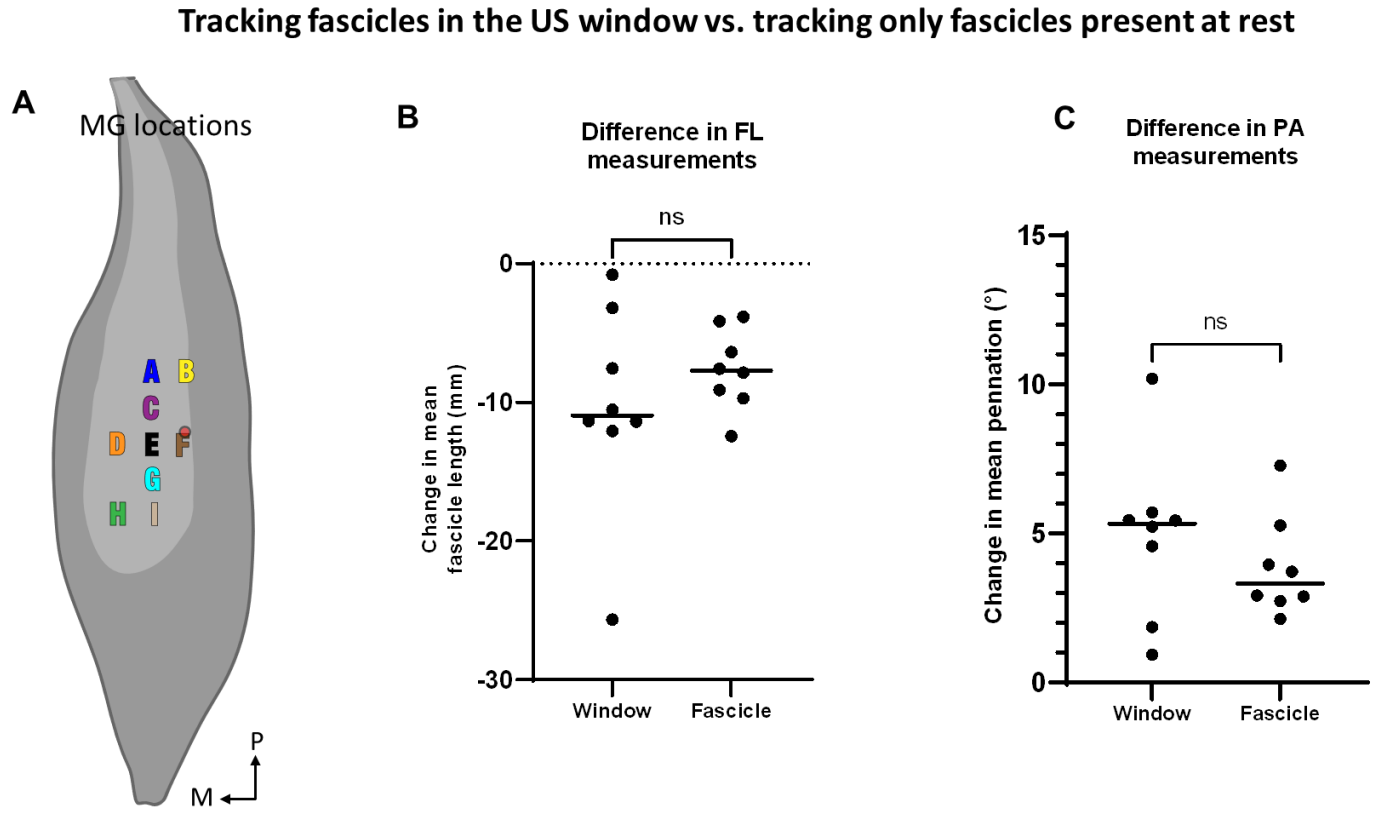

Figure 5.6. Comparing differences in changes in mean architecture measurements when we take measurements from fascicles in the US FOV/window (as is done experimentally) versus taking the change in architecture of fascicles that were present when the muscle was relaxed (cannot be done experimentally, enabled by model).

A) Colors of the reference (red dot) and other locations (lettered A through I) illustrated on the MG model correspond to bar chart colors (B-E). Location distances are to scale, and location coordinates are based on their proximal (P) and medial (M) directions from the muscle centroid (location E), where ultrasound studies generally claim to take measurements. Horizontal bars indicate the medians of data.

5.4.4 Effects of aponeurosis used

We found the that there was no significant difference between predicted fascicle length (Figure 5.7B) or pennation angle (Figure 5.7C) group means (of all locations [Figure 5.7A]) from using the unchanged/relaxed (FL: -8.58 mm ± 7.78 mm; PA: 4.92° ± 2.46°) versus changed/contracted (FL: -13.68 mm ± 6.26 mm; PA: 5.10° ± 2.83° (or with outliers, 17.88° ± 19.27)) aponeuroses. The lines among the data represent the median measurements.

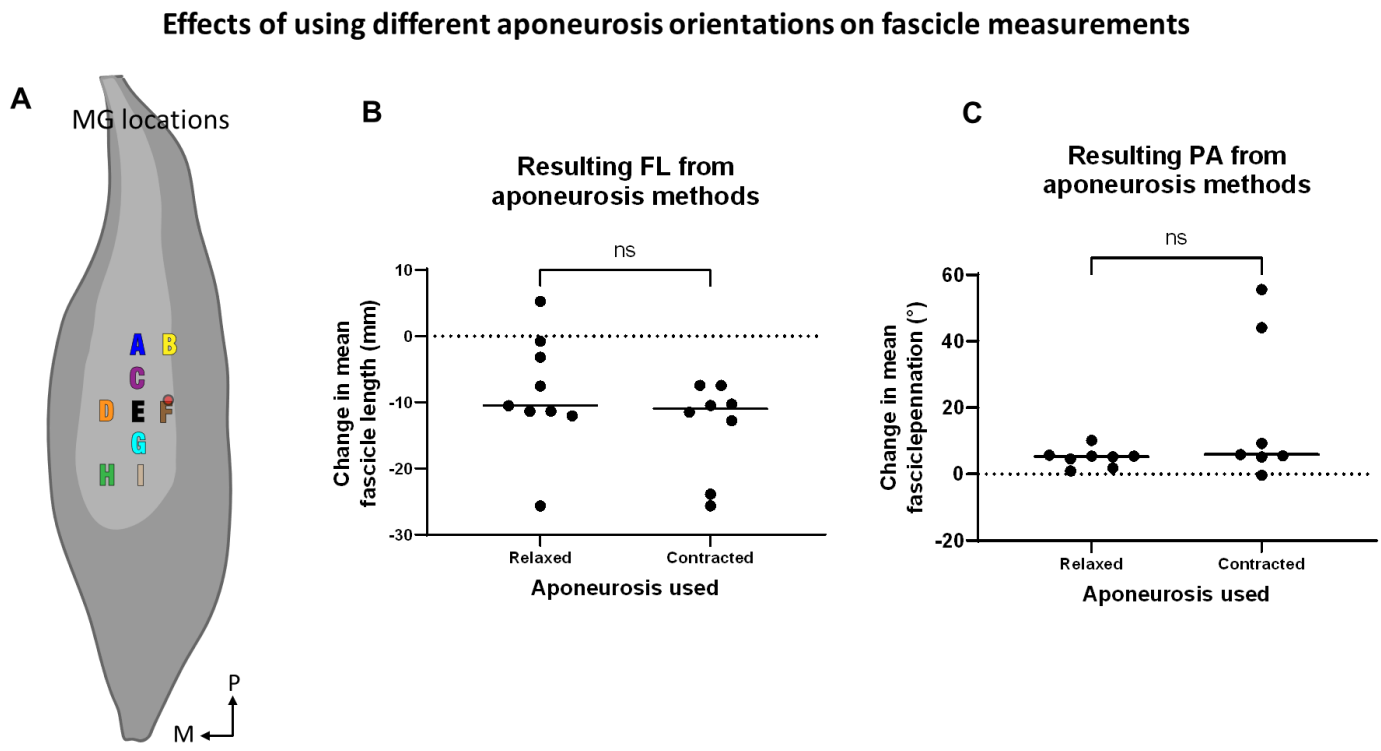

Figure 5.7. Comparing differences in changes in mean architecture measurements when we take measurements from different aponeurosis orientations: pre-contraction orientation, and post-contraction orientation.

A) Colors of the reference (red dot) and other locations (lettered A through I) illustrated on the MG model correspond to bar chart colors (B-E). Location distances are to scale, and location coordinates are based on their proximal (P, positive) and medial (M,) directions from the muscle centroid (location E), where ultrasound studies generally claim to take measurements. Horizontal bar indicated the medians of the data.

5.5 Discussion

Our model and method allow us to explore the relationship between 3D architecture and representative 2D measurements of architecture. Previously, there have been 3D US studies reporting

some 3D architecture (Rana et al., 2013, 2014), and 3D DTI - 2D US architecture comparisons (Bolsterlee et al., 2015), as well as misalignment in the measurement of architecture from 2D US and virtual US images (Bolsterlee et al., 2016a). However, no studies to our knowledge have linearized 3D fascicles to investigate how well 2D US measurements represent 3D muscle architecture with contraction. We have presented a way to do this, that uses a 3D finite element model, but could also be applied for DTI data, for example.

We conducted our primary analysis comparing 2D and 3D architecture at the [15,5] location, which we previously showed best represented *in vivo* data captured by ultrasound. We found that individual linearized measurements of relaxed fascicles were not consistently larger or smaller than the 3D measurements, but the means of the linearized fascicle lengths or pennations were not significantly different from their 3D counterparts for a) all fascicles present in the FOV, and only those ≥75% present in the FOV (Figure 5.1). As expected, there was generally a i) decrease in fascicle length and ii) increase in pennation angle with contraction, except for the 3D measurements for the ≥75% fascicles (Figure 5.2). There was one fascicle at the contracted state that met the ≥75% criterion. This fascicle was not smaller, but larger and its pennation decreased with contraction, causing the opposite of the expected changes in architecture measurement at this location (Figure 5.2). We performed error calculations, i.e., percentage differences in the linearized measurements compared to 3D, at the reference location (which matched US data) and at the centroid, for reference since most studies claim to capture measurements here. We found that linearized measurements at our match location ([15,5]) overestimated fascicle length by 6% when relaxed and almost 3 times as much when contracted. On the other hand, the centroid location underestimated fascicle length by 6% Muramatsu et al. (2002) found that under the assumption that the fascicle is straight, fascicle length was underestimated by ~6%. The error at the centroid location shows perfect agreement with this study, and the pennation angle error had the same magnitude, but an overestimation rather than an underestimation (Table 5). When we observed all 21 fascicles at our reference location, we found a inverse relationship between the percentage error of the fascicle length

measurement and the percentage of the fascicle that was in the US FOV (Figure 5.3). This finding is important because in practice, individual fascicles may not be chosen, but rather one or many clear portions of fascicles may be used to draw and measure a representative fascicle. We suggest that fascicles that appear to be mostly present will provide more accurate architecture measurements.

At all the locations we tested, we found that the magnitude of the percentage difference in linearized and 3D was <20% for fascicle length and ≤21% for pennation angle, showing consistency within the MG. Muramatsu et al. (2002) found that under the assumption that the fascicle is straight, fascicle length was underestimated by ~6%. Eight of the locations we tested had single digit magnitudes for difference in fascicle length for at least one activation state, and three of these locations had negative differences, showing some agreement with this study. The magnitudes of the errors in mean FL and PA of the ≥75% present fascicles were generally consistent within location, activation state (relaxed and contracted), and measurement (FL and PA). We found larger errors in the change in mean FL and PA measurements. When fewer fascicles were present at the contracted state than relaxed, the percentage difference in change in architecture was much larger than when an equal or greater number of fascicles were present. This suggests that accuracy change in architecture measurements improve in accuracy when more fascicles are measured at the contracted state. An interesting finding was that the site with highest mean percentage of 3D FL in the FOV had lowest mean FL and highest mean PA for fascicles ≥75% present in the FOV. In future work, we can formally test the hypothesis that the number of fascicles ≥75% present in the FOV in proportional to the percentage difference (error) in the linearized measurement, relative to the 3D measurement.

At six of the ten locations we tested, there were more fascicles present in the US field-of-view when contracted than when the muscle was relaxed (Appendix 2). This is expected, because fascicles shorten with contraction. The [15,30] location had no fascicles that were ≥75% present in the FOV at either activation state, and the [0,-15] location had no ≥75% present fascicle at rest, but had one ≥75%

present fascicle in the FOV when the muscle was contracted. This is why no data were present for differences in linearized architecture at these two locations (Figure 5.4, Figure 5.5). These data indicate that ultrasound architecture measurements are sensitive to location within the muscle. We saw that at most locations in our model, fascicle length was smaller and pennation angle was larger than at the reference ([15,5]) location, which we previously identified best represented *in vivo* data (Table 4.1). Fascicle shortening and increased pennation angles are consistent with what we expect for contracting muscle, so one reason for this trend at the other locations could be that fascicles at other locations are undergoing larger strains. The closest location to the reference location, [15,0], had larger FL and smaller PA than the reference location, opposing the trends seen in most other locations. At this location, the relaxed FL was within 1 standard deviation of the reference location's mean FL (Figure 5.4), and the changes in mean linearized architecture were similar (Figure 5.5), whereas changes in architecture at other locations were much larger for all fascicles, and for those meeting the ≥75% presence criterion (Figure 5.5). Altogether, these findings suggest that fascicle in this region of the muscle had similar architecture and may experience smaller strains that other regions. Typically, MG muscle architecture measurements are reported to be taken at the muscle mid-belly. However, we have not seen exact locations stated in the literature. We have shown that the architecture measurements and changes in these measurements are sensitive to imaging location. We will conduct further studies to determine if there are specific locations in the muscle in addition to our reference location ([15,5]) that agree with *in vivo* architecture data well.

When we leveraged our model's capability to compare changes in architecture for a) fascicles visible in the FOV at each state, versus b) following the architecture of fascicle that were in the FOV at rest, we found no significant difference in fascicle length or pennation group means, across all locations (Figure 5.6). This finding suggests that changes in architecture captured for fascicles that are mostly present in the US FOV are representative of the true change in architecture if the same fascicle(s) were

being tracked from start to end over a contraction. We have shown that the assumption that the same fascicle is being tracked is not likely, but that architecture measurements as if you were tracking the same fascicle(s) can still be achieved.

In most semi-automated fascicle tracking software, a region of interest in selected in the image of the relaxed muscle, and these boundaries are not updated unless the fascicle in completely lost during the contraction, which does not typically happen for small fields of view (Cronin et al., 2011; Farris & Lichtwark, 2016). When we leveraged our model's capability to compare changes in architecture when a) aponeuroses remain unchanged with contraction, versus b) aponeuroses changing with muscle bulging during contraction, we found no significant difference in fascicle length or pennation group means, across all locations (Figure 5.7). This finding suggests that when the linearized aponeurosis orientations were not being updated over a contraction, changes in architecture captured for fascicles that are mostly present in the US FOV are representative of the true change in architecture if linearized aponeurosis orientations were not being updated over a contraction. This implies that the assumption taken to linearize and not update aponeurosis does not significantly affect the architecture measurements.

We have outlined limitations with our model and method previously (Chapter 4.5 Discussion), and here we acknowledge some limitations in our virtual experiments. Our main challenge has been comparing summary results from our model at any location that only had one fascicle in the FOV that was ≥75% present because we could not compare a mean. An example of this is evaluating difference in linearized measurements between different and the reference location in the contracted state. There is only one fascicle at the reference location, so there is no fascicle length standard deviation within which to compare means.

At the outset of this dissertation, we aimed to discuss fascicle strains, but we have since learned that individual fascicles may not be present in the US FOV at both states, so while our model allows us to

track individual fascicle behavior we cannot obtain fascicle strains for fascicles in the FOV. We have compared changes in mean fascicle lengths and pennation angles instead. The other challenge has been that some locations, including our reference location, only had one fascicle in the FOV that was ≥75% present when contracted. Therefore, we did not compare changes in means, but calculated changes based on the single value of the sole fascicle meeting the presence criterion. For this reason, we do not make categorical claims about the relationship between 3D and linearized architecture at our reference location. We could not perform statistical analyses for any of the change in mean studies, because all tests would require at least 2 values for each, and we only had one mean value, not individual fascicle values.

It is important to note that in practice, usually a single fascicle's architecture is reported, which may also be susceptible to error. As we saw at many locations, taking the mean of multiple fascicles in the FOV reduced the error in the linearized fascicle length and pennation angle. We recommend taking sampling multiple fascicles, in the image/FOV and averaging their architecture measurements.

Chapter 6

Conclusion

6.1 Contributions

In this dissertation, we have presented novel computational modeling techniques that enable us to (1) create 3D models without medical imaging data in order to study muscle fascicle behavior during contraction, and (2) directly compare 2D ultrasound architecture measurements to 3D model architecture, allowing us to validate model-predicted changes in architecture during contraction as well as study and improve our understanding of commonly used ultrasound architecture measurements. Specifically, we have contributed the following to the field of muscle biomechanics:

A method to create 3D muscle models from photographs and *ex vivo* muscle architecture measurements

While medical images are typically used to create 3D muscle models, sometimes these images are not available. Cadaver studies have provided physical measurements of muscle structure, thereby giving insight into the its force-generating ability. We have created a method to use physical muscle-tendon and fascicle arrangement measurements from such *ex vivo* studies to build 3D models of muscle geometry. In [Chapter 1], we have shown that a relatively simple 3D model, created using computer-aided drawing in the absence of medical images or *in vivo* data, can recapitulate *ex vivo* medial gastrocnemius muscle architecture data very similarly. Models created using this novel method can be useful for performing parameter optimization and sensitivity analyses in the initial stages of image-based muscle modeling research, and including continuum-based modeling/finite element simulations. These models can also ultimately be used to conduct *in silico* experiments in order gain biomechanical insight at the whole muscle level. Other muscles with different architectural arrangements should be modeled similarly to determine if this method is applicable to other muscles and more complex fiber arrangements.

A method to simulate 2D ultrasound images and architecture measurements from a 3D muscle model, enabling experimental and model-predicted architecture comparisons

Since ultrasound (US) can provide architecture measurements for relaxed and contracted muscle, it is the best option for validating changes in architecture in 3D finite element models of contracting muscle. However, these ultrasound measurements are 2D, so they cannot be directly compared to a

model's 3D structure. We have created a method to simulate 2D ultrasound images of pennated skeletal muscle and fascicles, and predict changes in fascicle arrangement during contraction using a 3D model, enabling fascicle by fascicle comparisons of 2D ultrasound measurements and 3D muscle architecture (Chapter 3). We have found that we can successfully model medial gastrocnemius fascicle length and pennation angles that agree with *in vivo* ultrasound data, enabling us to confidently use our model to investigate fascicle behavior during contraction. To date, studies evaluating the reliability and validity of ultrasound architecture measurements take the form of literature reviews. We hope that this method will enable other computational studies evaluating the ultrasound technique as well as studying changes in 3D fascicle behavior (from 3D model) and corresponding linearized architecture from ultrasound data.

Insight into the differences between 2D ultrasound architecture measurements and 3D fascicle behavior

Our modeling approach is able to show us exactly which fascicles, and what percentage of their lengths are present in the simulated ultrasound field of view (FOV). When we evaluated all fascicles present, we saw that the difference between linearized and 3D fascicle length (i.e., the error) decreases as the percentage of the fascicle in the field of view increases. This suggests that linearized fascicle lengths (like US architecture measurements) more accurately represent 3D fascicle lengths when more of the fascicle is captured in the FOV. This is notable because in practice, it is generally not possible to know whether a fascicle is mostly or completely in the ultrasound image plane, but to take fascicle measurements, this is assumed. When we directly compare 3D architecture with linearized model architecture (which emulates 2D US measurements) we can specifically look at the architecture of fascicles that are mostly (we chose ≥75%) present in the FOV, as is assumed experimentally. We saw that the sample of fascicles that typically meet this criterion is about 5%-10% of all the fascicles present (at any percentage) in the FOV. Depending on the location in the muscle, the linearized architecture of these fascicles may be either larger or smaller than the 3D measurements.

We also found that while most US architecture measurement techniques assume that the same fascicle is being tracked from relaxed to contracted, on average, across all location we tested, only ~30% of our model's fascicles that met the ≥75% criterion were present at both activation states. At individual locations, none of the same fascicles were present at both states as they completely moved out if the FOV, while at other locations in the muscle, over 50% of the fascicles were present at both states. This suggests that the assumption that the same fascicles are always being measured throughout a contraction is not accurate. We found that when more fascicles were present at either state, there was a smaller difference between the linearized and 3D measurements. This suggests that it may improve accuracy if measurements are taken from multiple fascicles in the FOV and then the average reported, rather than the measurement of only fascicle as is done in practice.

Insight into the effects of some ultrasound assumptions on architecture measurements

We were able to investigate some common assumptions made during ultrasound architecture measurements. In addition to showing us which fascicles are present in the field of view and at what percentages, our algorithm and model enable us to track the behavior of fascicles that have moved outside the FOV. This is not possible experimentally, and we were able to use this capability to further test the assumption that the same fascicles are being imaged at both activation states. We investigated if the change in average architecture measurements of fascicles in the US FOV/window (what ultrasound would capture) differed from the change in average measurements from the fascicles that were in the FOV at the relaxed state. That is, we tracked those fascicles even if they were not in the FOV at the contracted state. There was not significant difference between the means of the FL or PA of the two groups. Therefore, our results suggest that although we know that the same fascicles are not likely being tracked by US throughout contraction, if we evaluate the fascicles that are at least 75% present in the FOV, the FL and PA averages representative of if we actually tracked the same fascicles throughout a contraction.

6.2 Future work

6.2.1 Improve our understanding of MG fascicle behavior

Investigate changes in MG muscle architecture with dynamic contractions

Our work in this dissertation was based on isometric (fixed muscle-tendon unit length) contraction of the medial gastrocnemius (MG). Dynamic contractions, where joint angles change during the motion, are observed for locomotion and most everyday movements. We would like to use our model and method to investigate if the changes in 3D and linearized architecture that we observed are consistent for more complicated contractions. For this work, we will use muscle-tendon junction displacement and architecture measurements from ultrasound images of isokinetic contractions over a range of joint angles, to conduct similar analyses we have performed for isometric contractions for isokinetic contractions. We will compare changes in architecture (fascicle length, pennation angle and fascicle strains (relative changes in fascicle length during contraction) for static (isometric) versus dynamic (isokinetic) contractions to improve our understanding of MG fascicle behavior.

Investigate effects of varying aponeurosis stiffness parameters by axis

We applied a simple material model to the aponeuroses, to begin to investigate how their stiffness affects fascicle behavior during contraction. We will implement a more complex material model for the aponeuroses, such as an uncoupled solid mixture with a Mooney-Rivlin ground matrix combined with combined with fibers with an exponential power law. We will include fiber directions determined by CFD simulations, and re-tune the model to determine the parameters that produce physiological changes in muscle architecture. This material model will allow us to test chhanes in longitudinal and transverse stiffness independently, to study how these factors affect model-predicted fascicle lengths, pennation angles and fascicle strains in the MG.

Determine relationship between 3D fascicle curvature and accuracy of linearized architecture

We could use our model to determine if there is a relationship between the amount of 3D curvature in a fascicle and the error in the linearized fascicle length or pennation of that fascicle. We will

expand our modeling framework to predict fascicle curvatures (in all planes), which is an aspect of fascicle orientation that 2D ultrasound experiments do not capture but that 3D MR-DTI studies do. We currently use 3D vector results from the computational fluid dynamics simulations to generate 3D streamlines to represent the muscle's fascicles. We will calculate fascicle curvature (expressed as 1/radius (m^{-1})) as the mean curvature of 100 equidistant points along the polynomial curve of a fascicle, using the Frenet–Serret formula (Bolsterlee et al., 2017, 2018; Rana et al., 2014). The curvature along the fascicle polynomial (p) at a point (t) will be defined as:

Equation 8. Curvature along the 3D fascicle

$$curvature\ (t)\ =\ \frac{|\dot{p}(t)\ \times\ \ddot{p}(t)|}{|\dot{p}(t)|^3}$$

We will compare mean predicted regional fascicle curvature to MG curvature from a published ultrasound study (Muramatsu et al., 2002) and compare curvature distribution of all fascicles to published DTI data (Bolsterlee et al., 2017). Muramatsu et al. (2002) that fascicle curvature was significantly correlated to pennation angle and muscle thickness. We can also leverage our approach to test this hypothesis.

6.2.2 Conduct virtual experiments in order to make recommendations for improved US architecture measurement accuracy

Simulate transducer rotation

Currently, the algorithm simulates rotation of the US probe in the X, Y, Z axis or any combination of these axes. It does so by applying the relevant rotation matrix (or matrices) to each vertex of the unrotated cuboid (Figure 6.1) representing the US field-of-view. Once the positions of the rotated vertices are calculated, the algorithm determines and stores the fascicle points in the rotated FOV. We calculate the number of fascicles in the rotated FOV and the length and percentage of these fascicles that are

present in the rotated view. If any rotation is applied, the linear aponeurosis generation (Figure 6.1) must be performed again.

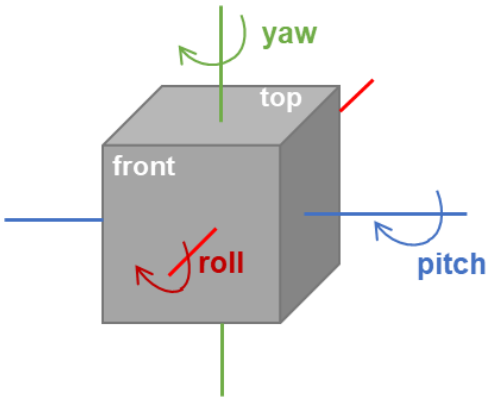

Figure 6.1: Illustration of roll, pitch and yaw rotations, as applied to simulated ultrasound field-of-view.

In Chapter 4.3.5, an assumption we made during the aponeurosis and fascicle linearization process is that once we set the "imaging" location/field-of-view, that the simulated US image was set exactly upon the surface of the model. This was not true, as neither aponeurosis was perfectly vertical (e.g. deep: 6.7° and superficial: 5.7° at the centroid) and we did not apply a corrective pitch rotation (Figure 6.1) to the simulated US probe because the angles were small and similar in value, creating close to uniform boundaries for fascicle linearization. In future work we will account for the alignment by applying any appropriate rotation to the simulated probe to ensure perfect alignment with the model surface.

We will also use our method to the study effects and potential sources of measurement error due to rotation as well as the effects of probe rotation will be studied by sampling the 3D model in the probe FOV at various angles (-40° to 40°) of the probe to the vertical axis/length of the muscle. We will study the effects of tilt by sampling the model in the probe FOV at various angles (-40° to 40°) of the probe surface to the muscle surface. All rotation and tilt simulations will be conducted at 9 equidistant sites from the mid-belly (vertical and horizontal midpoint) to determine how the combination of location and

rotation affects architecture measurements. We aim to determine which probe alignment is likely the best orientation for reducing difference between 2D and 3D measurements.

Investigating effects of probe size on architecture measurements

Others have tested the assumption that muscle fascicles lie in US plane by calculating misalignment between US image plane and DTI fascicle (Bolsterlee et al., 2015) and have created virtual US images using MRI and DTI to determine how the ultrasound transducer should be oriented to align the ultrasound image plane with muscle fascicles in the human medial gastrocnemius (Bolsterlee et al., 2016a). These studies have used a dual-probe imaging setup, that is not used in typical muscle architecture measurement studies, which use a single probe. Bolsterlee et al., use two coupled 46 mm linear array transducers generate a FOV of 110 mm and a depth of 40 mm. This US setup produces an US image with an 18 mm gap (black space) between in the middle, which gives a larger view of the muscle architecture but is not practical for capturing architecture in the hypoechoic region. We can increase the probe size that we simulate with our method and use our model to investigate: (1) how average architecture changes with an increased US FOV, and (2) whether increases the FOV affects the accuracy of the linearization predictions, i.e., we can test if the increase in FOV increases the percentage of fascicle in the FOV, which we have shown increases agreement between linearized and 3D fascicle length measurements.

6.3 Other applications

The methods we have developed can be applied to other computational research for healthy and pathological populations. We outline some potential applications below.

Study changes in architecture in the triceps surae and other muscles using our methods

In this dissertation, we have created models of the medial gastrocnemius and studied changes in its architecture with contraction as well as compared 2D and 3D architecture measurements of this muscle. The lateral gastrocnemius is the counterpart to this muscle, and with the soleus, the three muscles constitute the triceps surae. These three adjacent muscles work in tandem to plantarflex the

foot. With imaging data, we could model the other two muscles and apply our methods to investigate the differences in fascicle behavior among the three muscles. This work is needed to provide insight into the healthy biomechanics of the plantarflexors, which have applications in many sports populations and in neuromuscular disorders that affect gait.

Study muscle behavior in neuromuscular disorders using our methods

Muscle function depends on internal properties such as cross-sectional area and fascicle arrangement (length, angle, curvature). Changes in gait and contractures in individuals with neuromuscular disorders such as Duchenne muscular dystrophy (DMD) suggest that internal muscle properties also change with disease progression. While studies of changes in muscle morphology (Jones et al., 1983; Vohra et al., 2015), strength (Wokke et al., 2014) and progression (Hollingsworth et al., 2013; Torriani et al., 2012; Wren et al., 2008) have been published for ambulatory boys with DMD, we do not know much about changes in muscle architecture or fascicle strains during contraction for these children. The gastrocnemius muscles are among the most severely affected posterior lower leg muscles (Torriani et al., 2012; Wokke et al., 2014). MG pseudohypertrophy (increase in muscle cross-sectional area/total tissue, but not contractile tissue) has been well established. Because of its involvement, the MG is a good muscle to begin to study how muscle architecture adapts in ambulatory boys with DMD. There is an opportunity to use the model and method we have developed, along with a complementary model of the MG muscle of DMD patients, created from *in vivo* data, to study how DMD affects MG muscle architecture and fascicle strains.

6.4 Summary

Muscle architecture – the internal structure or arrangement of fascicles or fiber bundles within a muscle – determines a muscle's ability to contract, produce force, and enable movement. Cadaver dissections have traditionally been used to determine muscle architecture, and more recently magnetic resonance diffusion tensor imaging has become state-of-the-art for imaging muscle architecture.

However, while these methods provide complete information about fiber arrangement, they do not enable measurements of fascicle behavior during contraction. *In vivo* B-mode ultrasound is commonly used to non-invasively image muscle fascicle arrangements and measure fascicle length and orientation (pennation angle) in resting and contracting muscle. Physics-based computational modeling allows us to represent the three-dimensional (3D) form and architecture of muscle in order to study how 3D fascicle arrangement changes due to movement. Correctly representing muscle geometry and architecture in these 3D models is crucial to the models' ability to provide physiologically-relevant measurements of muscle function.

While MR images are currently the gold standard method for developing these models with representative geometry, such data are not always available for modeling the muscle of interest. In my first project, I created a solution: to use a simple or low-fidelity 3D CAD model, developed based on cadaver data, that can include the varied fascicle lengths and angles throughout a muscle and a realistic material model. I demonstrated that a simple model of the medial gastrocnemius, built from and scaled to images of *ex vivo* muscle, can recapitulate *ex vivo* architecture measurements. By using these simple models, we can still learn about some muscle mechanics, muscle-tendon interactions and perform model optimization before high resolution in vivo data becomes available.

When medical imaging data, such as MRI, is available for creating high-fidelity 3D computational models, *in vivo* data is required to validate model predictions of changes in architecture with contraction. Ultrasound imaging has become a ubiquitous tool for measuring muscle fascicle behavior during contract and these data could naturally provide model validation. However, these 2D measurements of fascicle length and orientation are not perfectly suited for validating 3D models, due to the model's additional dimension. In order to compare 3D model and 2D ultrasound architecture and explore the impact of the current limitations of ultrasound measurements, I created a method that enables simulation of 2D ultrasound measurements using a 3D model. I then used the method with a 3D model of the medial

gastrocnemius to examine how the simplifications associated with 2D ultrasound measurements impact muscle fascicle length measurements.

The work in this dissertation advances our ability to 1) create 3D muscle models without *in vivo* data, and 2) explore the impact of current limitations of ultrasound on the interpretation of 2D architecture measurements of 3D muscle architecture.

References

Anderson, F. C., & Pandy, M. G. (1999). A Dynamic Optimization Solution for Vertical Jumping in Three Dimensions. *Computer Methods in Biomechanics and Biomedical Engineering*, *2*(3), 201–231. PubMed. https://doi.org/10.1080/10255849908907988

Anderson, F. C., & Pandy, M. G. (2003). Individual muscle contributions to support in normal walking. *Gait & Posture*, *17*(2), 159–169. https://doi.org/10.1016/S0966-6362(02)00073-5

Arnold, E. M., Ward, S. R., Lieber, R. L., & Delp, S. L. (2010). A model of the lower limb for analysis of human movement. *Annals of Biomedical Engineering*, *38*(2), 269–279. https://doi.org/10.1007/s10439-009-9852-5

Barber, L., Carty, C., Modenese, L., Walsh, J., Boyd, R., & Lichtwark, G. (2017). Medial gastrocnemius and soleus muscle-tendon unit, fascicle, and tendon interaction during walking in children with cerebral palsy. *Developmental Medicine & Child Neurology*, *59*(8), 843–851. https://doi.org/10.1111/dmcn.13427

Blemker, S. S., & Delp, S. L. (2005). Three-dimensional representation of complex muscle architectures and geometries. *Annals of Biomedical Engineering*, *33*(5), 661–673.

Blemker, S. S., & Delp, S. L. (2006). Rectus femoris and vastus intermedius fiber excursions predicted by three-dimensional muscle models. *Journal of Biomechanics*, *39*(8), 1383–1391. https://doi.org/10.1016/j.jbiomech.2005.04.012

Blemker, S. S., Pinsky, P. M., & Delp, S. L. (2005). A 3D model of muscle reveals the causes of nonuniform strains in the biceps brachii. *Journal of Biomechanics*, *38*(4), 657–665. https://doi.org/10.1016/j.jbiomech.2004.04.009

Bolsterlee, B., D'Souza, A., Gandevia, S. C., & Herbert, R. D. (2017). How does passive lengthening change the architecture of the human medial gastrocnemius muscle? *Journal of Applied Physiology*, *122*(4), 727–738. https://doi.org/10.1152/japplphysiol.00976.2016

Bolsterlee, B., Finni, T., D'Souza, A., Eguchi, J., Clarke, E. C., & Herbert, R. D. (2018). Three-dimensional architecture of the whole human soleus muscle in vivo. *PeerJ*, *6*, e4610. https://doi.org/10.7717/peerj.4610

Bolsterlee, B., Gandevia, S. C., & Herbert, R. D. (2016a). Ultrasound imaging of the human medial gastrocnemius muscle: How to orient the transducer so that muscle fascicles lie in the image plane. *Journal of Biomechanics*, *49*(7), 1002–1008. https://doi.org/10.1016/j.jbiomech.2016.02.014

Bolsterlee, B., Gandevia, S. C., & Herbert, R. D. (2016b). Effect of Transducer Orientation on Errors in Ultrasound Image-Based Measurements of Human Medial Gastrocnemius Muscle Fascicle Length and Pennation. *PLOS ONE*, *11*(6), e0157273. https://doi.org/10.1371/journal.pone.0157273

Bolsterlee, B., Veeger, H. E. J. (DirkJan), van der Helm, F. C. T., Gandevia, S. C., & Herbert, R. D. (2015). Comparison of measurements of medial gastrocnemius architectural parameters from ultrasound and diffusion tensor images. *Journal of Biomechanics*, *48*(6), 1133–1140. https://doi.org/10.1016/j.jbiomech.2015.01.012

Brand, R. A., Pedersen, D. R., & Friederich, J. A. (1986). The sensitivity of muscle force predictions to changes in physiologic cross-sectional area. *Journal of Biomechanics*, *19*(8), 589–596. https://doi.org/10.1016/0021-9290(86)90164-8

C. Criscione, J., S. Douglas, A., & C. Hunter, W. (2001). Physically based strain invariant set for materials exhibiting transversely isotropic behavior. *Journal of the Mechanics and Physics of Solids*, *49*(4), 871–897. https://doi.org/10.1016/S0022-5096(00)00047-8

Charles, J. P., Suntaxi, F., & Anderst, W. J. (2019). In vivo human lower limb muscle architecture dataset obtained using diffusion tensor imaging. *PLoS ONE*, *14*(10). https://doi.org/10.1371/journal.pone.0223531

Clark, W. H., & Franz, J. R. (2018). Do triceps surae muscle dynamics govern non-uniform Achilles tendon deformations? *PeerJ*, *6*. https://doi.org/10.7717/peerj.5182

Clark, W. H., Pimentel, R. E., & Franz, J. R. (2021). Imaging and Simulation of Inter-muscular Differences in Triceps Surae Contributions to Forward Propulsion During Walking. *Annals of Biomedical Engineering*, *49*(2), 703–715. https://doi.org/10.1007/s10439-020-02594-x

Cronin, N. J., Carty, C. P., Barrett, R. S., & Lichtwark, G. (2011). Automatic tracking of medial gastrocnemius fascicle length during human locomotion. *Journal of Applied Physiology*, *111*(5), 1491–1496. https://doi.org/10.1152/japplphysiol.00530.2011

Cronin, N. J., & Lichtwark, G. (2013). The use of ultrasound to study muscle–tendon function in human posture and locomotion. *Gait & Posture*, *37*(3), 305–312. https://doi.org/10.1016/j.gaitpost.2012.07.024

Dalmau-Pastor, M., Fargues-Polo, B. J., Casanova-Martínez, D. J., Vega, J., & Golanó, P. (2014). Anatomy of the triceps surae: A pictorial essay. *Foot and Ankle Clinics*, *19*(4), 603–635. https://doi.org/10.1016/j.fcl.2014.08.002

Darby, J., Li, B., Costen, N., Loram, I., & Hodson-Tole, E. (2013). Estimating Skeletal Muscle Fascicle Curvature from B-Mode Ultrasound Image Sequences. *IEEE Transactions on Bio-Medical Engineering*, *60*(7), 1935–1945. https://doi.org/10.1109/TBME.2013.2245328

Delp, S. L., Anderson, F. C., Arnold, A. S., Loan, P., Habib, A., John, C. T., Guendelman, E., & Thelen, D. G. (2007). OpenSim: Open-source software to create and analyze dynamic simulations of movement. *IEEE Transactions on Bio-Medical Engineering*, *54*(11), 1940–1950. https://doi.org/10.1109/TBME.2007.901024

Delp, S. L., Loan, J. P., Hoy, M. G., Zajac, F. E., Topp, E. L., & Rosen, J. M. (1990). An interactive graphics-based model of the lower extremity to study orthopaedic surgical procedures. *IEEE Transactions on Biomedical Engineering*, *37*(8), 757–767. https://doi.org/10.1109/10.102791

Ekizos, A., Papatzika, F., Charcharis, G., Bohm, S., Mersmann, F., & Arampatzis, A. (2013). Ultrasound does not provide reliable results for the measurement of the patellar tendon cross sectional area. *Journal of Electromyography and Kinesiology*, *23*(6), 1278–1282. https://doi.org/10.1016/j.jelekin.2013.08.004

Eng, C. M., & Roberts, T. J. (2018). Aponeurosis influences the relationship between muscle gearing and force. *Journal of Applied Physiology*, *125*(2), 513–519. https://doi.org/10.1152/japplphysiol.00151.2018

Farris, D. J., & Lichtwark, G. A. (2016). UltraTrack: Software for semi-automated tracking of muscle fascicles in sequences of B-mode ultrasound images. *Computer Methods and Programs in Biomedicine*, *128*, 111–118. https://doi.org/10.1016/j.cmpb.2016.02.016

Fiorentino, N. M., & Blemker, S. S. (2014). Musculotendon variability influences tissue strains experienced by the biceps femoris long head muscle during high-speed running. *Journal of Biomechanics*, *47*(13), 3325–3333. https://doi.org/10.1016/j.jbiomech.2014.08.010

Fiorentino, N. M., Rehorn, M. R., Chumanov, E. S., Thelen, D. G., & Blemker, S. S. (2014). Computational Models Predict Larger Muscle Tissue Strains at Faster Sprinting Speeds. *Medicine and Science in Sports and Exercise*, *46*(4), 776–786. PMC. https://doi.org/10.1249/MSS.0000000000000172

Fouré, A., Ogier, A. C., Le Troter, A., Vilmen, C., Feiweier, T., Guye, M., Gondin, J., Besson, P., & Bendahan, D. (2018). Diffusion Properties and 3D Architecture of Human Lower Leg Muscles Assessed with Ultra-High-Field-Strength Diffusion-Tensor MR Imaging and Tractography: Reproducibility and Sensitivity to Sex Difference and Intramuscular Variability. *Radiology*, *287*(2), 592–607. https://doi.org/10.1148/radiol.2017171330

Fukunaga, T., Ichinose, Y., Ito, M., Kawakami, Y., & Fukashiro, S. (1997). Determination of fascicle length and pennation in a contracting human muscle in vivo. *Journal of Applied Physiology (Bethesda, Md. : 1985)*, *82*(1), 354–358.

Fukunaga, T., Kubo, K., Kawakami, Y., Fukashiro, S., Kanehisa, H., & Maganaris, C. N. (2001). In vivo behaviour of human muscle tendon during walking. *Proceedings of the Royal Society B: Biological Sciences*, *268*(1464), 229–233. PMC. https://doi.org/10.1098/rspb.2000.1361

Fukunaga, T., Miyatani, M., Tachi, M., Kouzaki, M., Kawakami, Y., & Kanehisa, H. (2001). Muscle volume is a major determinant of joint torque in humans. *Acta Physiologica Scandinavica*, *172*(4), 249–255. https://doi.org/10.1046/j.1365-201x.2001.00867.x

Handsfield, G. G., Bolsterlee, B., Inouye, J. M., Herbert, R. D., Besier, T. F., & Fernandez, J. W. (2017). Determining skeletal muscle architecture with Laplacian simulations: A comparison with diffusion tensor imaging. *Biomechanics and Modeling in Mechanobiology*. https://doi.org/10.1007/s10237-017-0923-5

Handsfield, G. G., Meyer, C. H., Hart, J. M., Abel, M. F., & Blemker, S. S. (2014). Relationships of 35 lower limb muscles to height and body mass quantified using MRI. *Journal of Biomechanics*, *47*(3), 631–638. https://doi.org/10.1016/j.jbiomech.2013.12.002

Herbert, R. D., Clarke, J., Kwah, L. K., Diong, J., Martin, J., Clarke, E. C., Bilston, L. E., & Gandevia, S. C. (2011). In vivo passive mechanical behaviour of muscle fascicles and tendons in human gastrocnemius muscle–tendon units. *The Journal of Physiology*, *589*(21), 5257–5267. https://doi.org/10.1113/jphysiol.2011.212175

Herbert, R. D., Héroux, M. E., Diong, J., Bilston, L. E., Gandevia, S. C., & Lichtwark, G. A. (2015). Changes in the length and three-dimensional orientation of muscle fascicles and aponeuroses with passive length changes in human gastrocnemius muscles. *The Journal of Physiology*, *593*(2), 441–455. https://doi.org/10.1113/jphysiol.2014.279166

Herbert, R. D., Moseley, A. M., Butler, J. E., & Gandevia, S. C. (2002). Change in length of relaxed muscle fascicles and tendons with knee and ankle movement in humans. *The Journal of Physiology*, *539*(2), 637–645. https://doi.org/10.1113/jphysiol.2001.012756

Hollingsworth, K. G., Garrood, P., Eagle, M., Bushby, K., & Straub, V. (2013). Magnetic resonance imaging in Duchenne muscular dystrophy: Longitudinal assessment of natural history over 18 months. *Muscle & Nerve*, *48*(4), 586–588. https://doi.org/10.1002/mus.23879

Holt, N. C., Danos, N., Roberts, T. J., & Azizi, E. (2016). Stuck in gear: Age-related loss of variable gearing in skeletal muscle. *Journal of Experimental Biology*, *219*(7), 998–1003. https://doi.org/10.1242/jeb.133009

Inouye, J. M., Pelland, C. M., Lin, K. Y., Borowitz, K. C., & Blemker, S. S. (2015). A Computational Model of Velopharyngeal Closure for Simulating Cleft Palate Repair. *Journal of Craniofacial Surgery*, *26*(3), 658–662. https://doi.org/10.1097/SCS.0000000000001441

Jones, D. A., Round, J. M., Edwards, R. H. T., Grindwood, S. R., & Tofts, P. S. (1983). Size and composition of the calf and quadriceps muscles in Duchenne muscular dystrophy: A tomographic and histochemical study. *Journal of the Neurological Sciences*, *60*(2), 307–322. https://doi.org/10.1016/0022-510X(83)90071-0

Kawakami, Y., Ichinose, Y., & Fukunaga, T. (1998). Architectural and functional features of human triceps surae muscles during contraction. *Journal of Applied Physiology*, *85*(2), 398–404. https://doi.org/10.1152/jappl.1998.85.2.398

Knaus, K. R., Ebrahimi, A., Martin, J. A., Loegering, I. F., Thelen, D. G., & Blemker, S. S. (2020). Achilles Tendon Morphology Is Related to Triceps Surae Muscle Size and Peak Plantarflexion Torques During Walking in Young but Not Older Adults. *Frontiers in Sports and Active Living*, *2*, 88. https://doi.org/10.3389/fspor.2020.00088

Kwah, L. K., Pinto, R. Z., Diong, J., & Herbert, R. D. (2013). Reliability and validity of ultrasound measurements of muscle fascicle length and pennation in humans: A systematic review. *Journal of Applied Physiology*, *114*(6), 761–769. https://doi.org/10.1152/japplphysiol.01430.2011

Lichtwark, G. A., Bougoulias, K., & Wilson, A. M. (2007). Muscle fascicle and series elastic element length changes along the length of the human gastrocnemius during walking and running. *Journal of Biomechanics*, *40*(1), 157–164. https://doi.org/10.1016/j.jbiomech.2005.10.035

Lieber, R. L., & Friden, J. (2000). Functional and clinical significance of skeletal muscle architecture. *Muscle & Nerve*, *23*(11), 1647–1666.

Maas, S. A., Ellis, B. J., Ateshian, G. A., & Weiss, J. A. (2012). FEBio: Finite Elements for Biomechanics. *Journal of Biomechanical Engineering*, *134*(1), 11005-NaN. https://doi.org/10.1115/1.4005694

Maganaris, C. N. (2003). Force-length characteristics of the in vivo human gastrocnemius muscle. *Clinical Anatomy (New York, N.Y.)*, *16*(3), 215–223. https://doi.org/10.1002/ca.10064

Maganaris, C. N. (2005). Validity of procedures involved in ultrasound-based measurement of human plantarflexor tendon elongation on contraction. *Journal of Biomechanics*, *38*(1), 9–13. https://doi.org/10.1016/j.jbiomech.2004.03.024

Maganaris, C. N., Baltzopoulos, V., & Sargeant, A. J. (1998). In vivo measurements of the triceps surae complex architecture in man: Implications for muscle function. *The Journal of Physiology*, *512*(Pt 2), 603–614. PMC. https://doi.org/10.1111/j.1469-7793.1998.603be.x

Magnusson, S. P., Aagaard, P., Rosager, S., Dyhre-Poulsen, P., & Kjaer, M. (2001). Load-displacement properties of the human triceps surae aponeurosis in vivo. *The Journal of Physiology*, *531*(1), 277–288. https://doi.org/10.1111/j.1469-7793.2001.0277j.x

Marzilger, R., Legerlotz, K., Panteli, C., Bohm, S., & Arampatzis, A. (2018). Reliability of a semi-automated algorithm for the vastus lateralis muscle architecture measurement based on ultrasound images. *European Journal of Applied Physiology*, *118*(2), 291–301. https://doi.org/10.1007/s00421-017-3769-8

May, S., Locke, S., & Kingsley, M. (2021). Reliability of ultrasonographic measurement of muscle architecture of the gastrocnemius medialis and gastrocnemius lateralis. *PLOS ONE*, *16*(9), e0258014. https://doi.org/10.1371/journal.pone.0258014

Morse, C. I., Smith, J., Denny, A., Tweedale, J., & Searle, N. D. (2015). Gastrocnemius medialis muscle architecture and physiological cross sectional area in adult males with Duchenne muscular dystrophy. *Journal of Musculoskeletal & Neuronal Interactions*, *15*(2), 154–160.

Morse, C. I., Thom, J. M., Birch, K. M., & Narici, M. V. (2005). Changes in triceps surae muscle architecture with sarcopenia. *Acta Physiologica Scandinavica*, *183*(3), 291–298. https://doi.org/10.1111/j.1365-201X.2004.01404.x

Muramatsu, T., Muraoka, T., Kawakami, Y., Shibayama, A., & Fukunaga, T. (2002). In vivo determination of fascicle curvature in contracting human skeletal muscles. *Journal of Applied Physiology*, *92*(1), 129–134. https://doi.org/10.1152/jappl.2002.92.1.129

Namburete, A. I. L., Rana, M., & Wakeling, J. M. (2011). Computational methods for quantifying in vivo muscle fascicle curvature from ultrasound images. *Journal of Biomechanics*, *44*(14), 2538–2543. https://doi.org/10.1016/j.jbiomech.2011.07.017

Narici, M. V., Binzoni, T., Hiltbrand, E., Fasel, J., Terrier, F., & Cerretelli, P. (1996). In vivo human gastrocnemius architecture with changing joint angle at rest and during graded isometric contraction. *The Journal of Physiology*, *496*(Pt 1), 287–297.

Narici, M. V., Maganaris, C. N., Reeves, N. D., & Capodaglio, P. (2003). Effect of aging on human muscle architecture. *Journal of Applied Physiology*, *95*(6), 2229–2234. https://doi.org/10.1152/japplphysiol.00433.2003

Neptune, R. R., Kautz, S. A., & Zajac, F. E. (2001). Contributions of the individual ankle plantar flexors to support, forward progression and swing initiation during walking. *Journal of Biomechanics*, *34*(11), 1387–1398. https://doi.org/10.1016/S0021-9290(01)00105-1

Nikolaidou, M. E., Marzilger, R., Bohm, S., Mersmann, F., & Arampatzis, A. (n.d.). Operating length and velocity of human M. vastus lateralis fascicles during vertical jumping. *Royal Society Open Science*, *4*(5), 170185. https://doi.org/10.1098/rsos.170185

Rana, M., Hamarneh, G., & Wakeling, J. M. (2009). Automated tracking of muscle fascicle orientation in B-mode ultrasound images. *Journal of Biomechanics*, *42*(13), 2068–2073. https://doi.org/10.1016/j.jbiomech.2009.06.003

Rana, M., Hamarneh, G., & Wakeling, J. M. (2013). 3D fascicle orientations in triceps surae. *Journal of Applied Physiology*, *115*(1), 116–125. https://doi.org/10.1152/japplphysiol.01090.2012

Rana, M., Hamarneh, G., & Wakeling, J. M. (2014). 3D curvature of muscle fascicles in triceps surae. *Journal of Applied Physiology*, *117*(11), 1388–1397. https://doi.org/10.1152/japplphysiol.00109.2013

Rana, M., & Wakeling, J. M. (2011). In-vivo determination of 3D muscle architecture of human muscle using free hand ultrasound. *Journal of Biomechanics*, *44*(11), 2129–2135. https://doi.org/10.1016/j.jbiomech.2011.05.026

Rehorn, M. R., & Blemker, S. S. (2010). The effects of aponeurosis geometry on strain injury susceptibility explored with a 3D muscle model. *Journal of Biomechanics*, *43*(13), 2574–2581. https://doi.org/10.1016/j.jbiomech.2010.05.011

Savelberg, H. H. C. M., Willems, P. J. B., Baan, G. C., & Huijing, P. A. (2001). Deformation and three-dimensional displacement of fibers in isometrically contracting rat plantaris muscles. *Journal of Morphology*, *250*(1), 89–99. https://doi.org/10.1002/jmor.1061

Seynnes, O. R., & Cronin, N. J. (2020). Simple Muscle Architecture Analysis (SMA): An ImageJ macro tool to automate measurements in B-mode ultrasound scans. *PLOS ONE*, *15*(2), e0229034. https://doi.org/10.1371/journal.pone.0229034

Shan, X., Otsuka, S., Yakura, T., Naito, M., Nakano, T., & Kawakami, Y. (2019). Morphological and mechanical properties of the human triceps surae aponeuroses taken from elderly cadavers: Implications for muscle-tendon interactions. *PLOS ONE*, *14*(2), e0211485. https://doi.org/10.1371/journal.pone.0211485

Sinha, U., Csapo, R., Malis, V., Xue, Y., & Sinha, S. (2015). Age Related Differences in Diffusion Tensor Indices and Fiber Architecture in the Medial and Lateral Gastrocnemius. *Journal of Magnetic Resonance Imaging : JMRI*, *41*(4), 941–953. https://doi.org/10.1002/jmri.24641

Stark, H., & Schilling, N. (2010). A novel method of studying fascicle architecture in relaxed and contracted muscles. *Journal of Biomechanics*, *43*(15), 2897–2903. https://doi.org/10.1016/j.jbiomech.2010.07.031

Torriani, M., Townsend, E., Thomas, B. J., Bredella, M. A., Ghomi, R. H., & Tseng, B. S. (2012). Lower leg muscle involvement in Duchenne muscular dystrophy: An MR imaging and spectroscopy study. *Skeletal Radiology*, *41*(4), 437–445. https://doi.org/10.1007/s00256-011-1240-1

Vohra, R. S., Lott, D., Mathur, S., Senesac, C., Deol, J., Germain, S., Bendixen, R., Forbes, S. C., Sweeney, H. L., Walter, G. A., & Vandenborne, K. (2015). Magnetic Resonance Assessment of Hypertrophic and Pseudo-Hypertrophic Changes in Lower Leg Muscles of Boys with Duchenne Muscular Dystrophy and Their Relationship to Functional Measurements. *PLoS ONE*, *10*(6), e0128915. PMC. https://doi.org/10.1371/journal.pone.0128915

Ward, S. R., Eng, C. M., Smallwood, L. H., & Lieber, R. L. (2009). Are Current Measurements of Lower Extremity Muscle Architecture Accurate? *Clinical Orthopaedics and Related Research*, *467*(4), 1074–1082. https://doi.org/10.1007/s11999-008-0594-8

Ward, S. R., & Lieber, R. L. (2005). Density and hydration of fresh and fixed human skeletal muscle. *Journal of Biomechanics*, *38*(11), 2317–2320. https://doi.org/10.1016/j.jbiomech.2004.10.001

Weiss, J. A., Maker, B. N., & Govindjee, S. (1996). Finite element implementation of incompressible, transversely isotropic hyperelasticity. *Computer Methods in Applied Mechanics and Engineering*, *135*(1), 107–128. https://doi.org/10.1016/0045-7825(96)01035-3

Wickiewicz, T. L., Roy, R. R., Powell, P. L., & Edgerton, V. R. (1983). Muscle architecture of the human lower limb. *Clinical Orthopaedics and Related Research*, *179*, 275–283.

Wokke, B. H., van den Bergen, J. C., Versluis, M. J., Niks, E. H., Milles, J., Webb, A. G., van Zwet, E. W., Aartsma-Rus, A., Verschuuren, J. J., & Kan, H. E. (2014). Quantitative MRI and strength measurements in the assessment of muscle quality in Duchenne muscular dystrophy. *Neuromuscular Disorders : NMD*, *24*(5), 409–416. https://doi.org/10.1016/j.nmd.2014.01.015

Wren, T. A. L., Bluml, S., Tseng-Ong, L., & Gilsanz, V. (2008). Three-point technique of fat quantification of muscle tissue as a marker of disease progression in Duchenne muscular dystrophy: Preliminary study. *AJR. American Journal of Roentgenology*, *190*(1), W8-12. https://doi.org/10.2214/AJR.07.2732

Zajac, F. E. (1989). Muscle and tendon: Properties, models, scaling, and application to biomechanics and motor control. *Critical Reviews in Biomedical Engineering*, *17*(4), 359–411.

Zhou, G.-Q., Chan, P., & Zheng, Y.-P. (2015). Automatic measurement of pennation angle and fascicle length of gastrocnemius muscles using real-time ultrasound imaging. *Ultrasonics*, *57*, 72–83. https://doi.org/10.1016/j.ultras.2014.10.020

Appendix 1: Simulated ultrasound images at each location tested

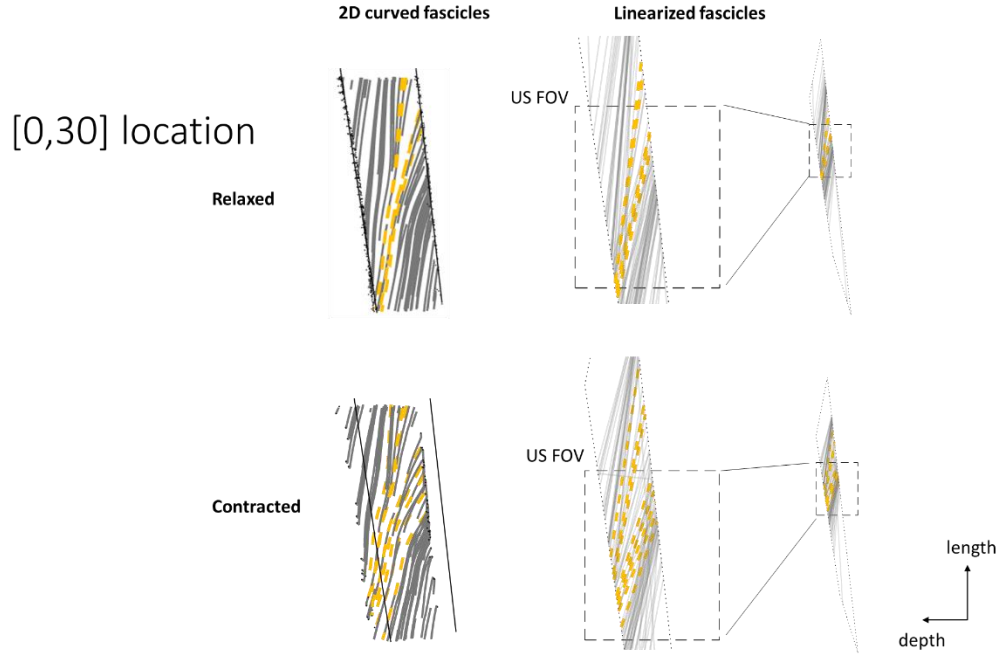

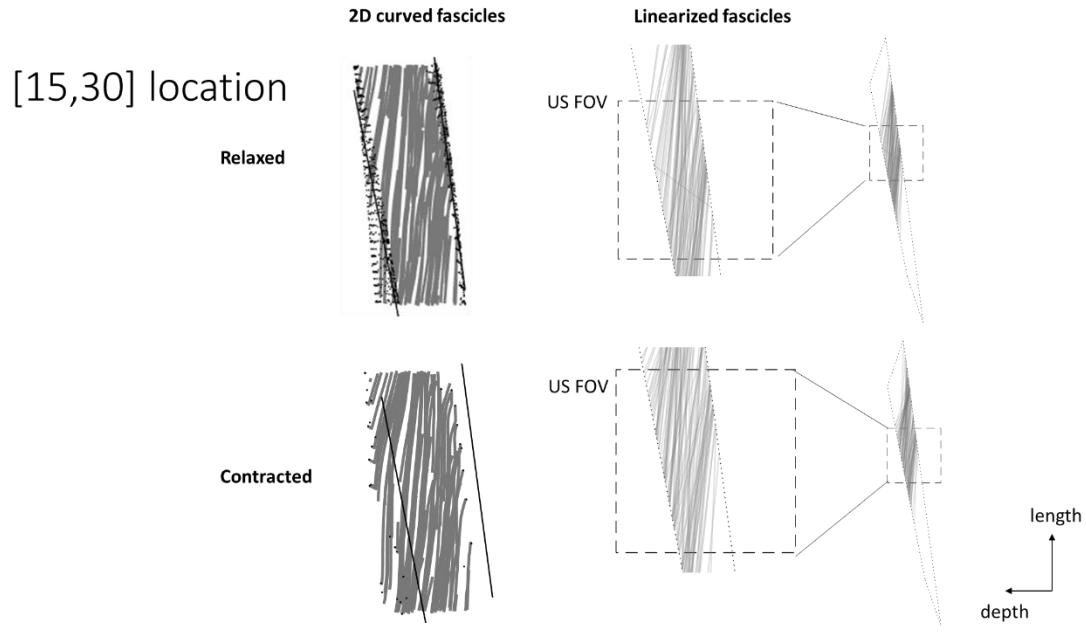

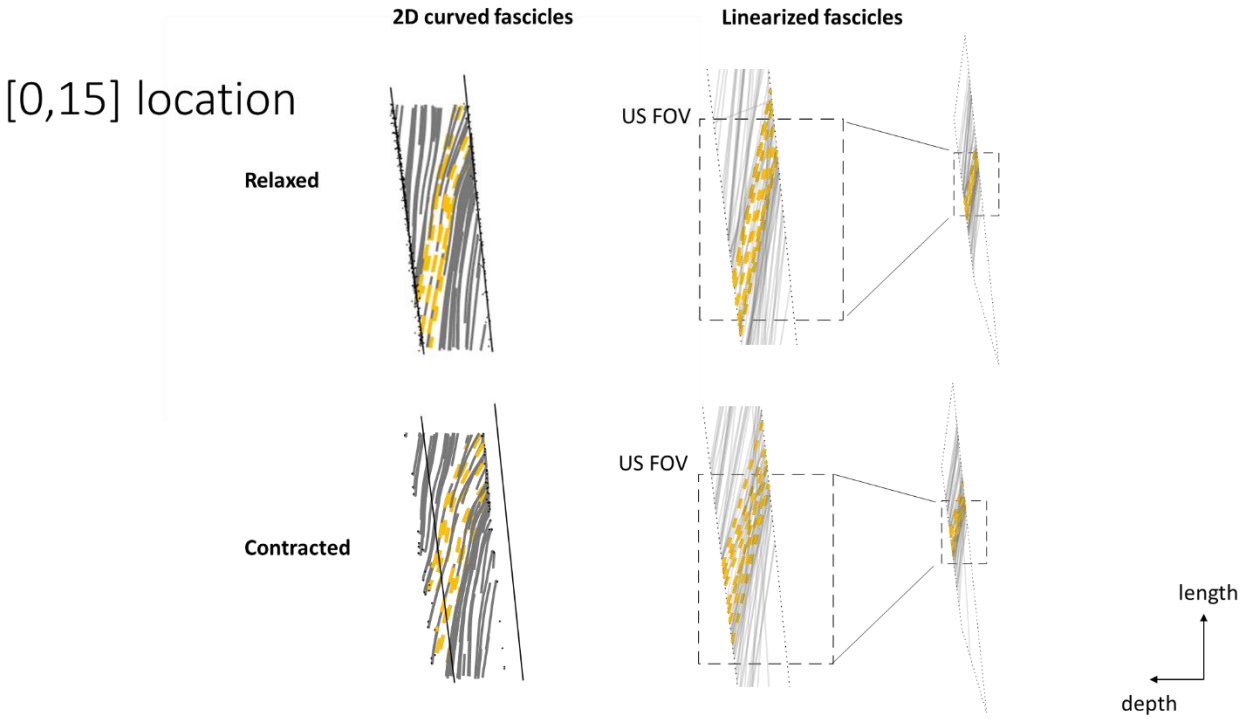
[0,15] location
2D curved fascicles
Linearized fascicles
Relaxed
Contracted
US FOV
US FOV
length
depth

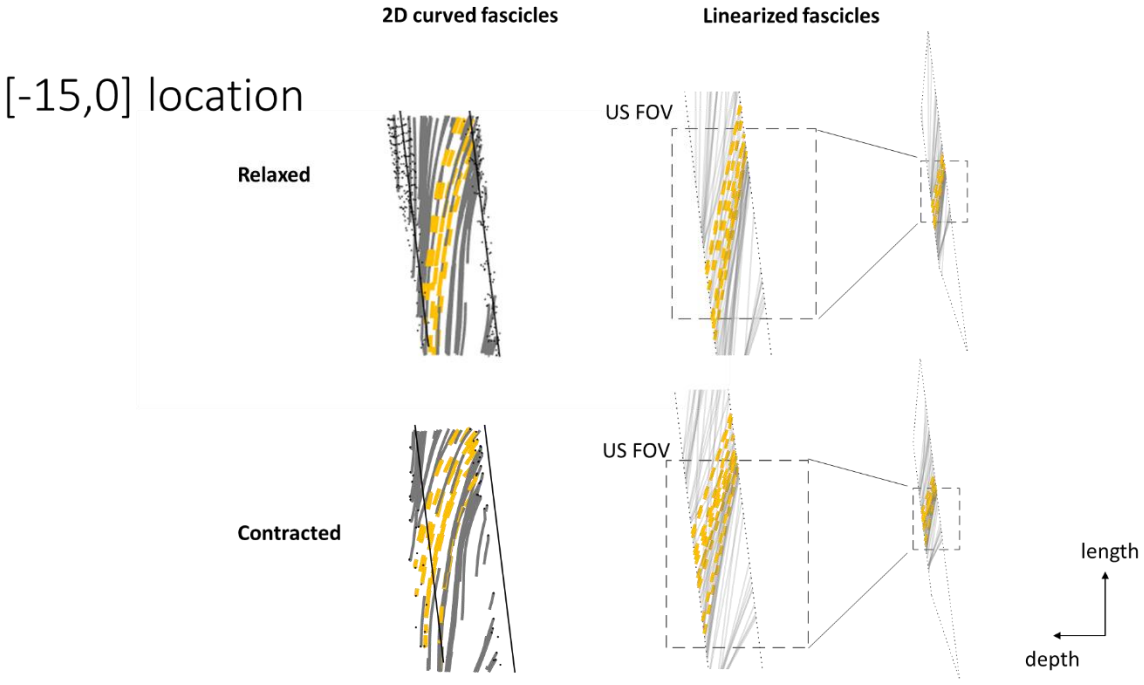
[-15,0] location
2D curved fascicles
Linearized fascicles
Relaxed
Contracted
US FOV
US FOV
length
depth

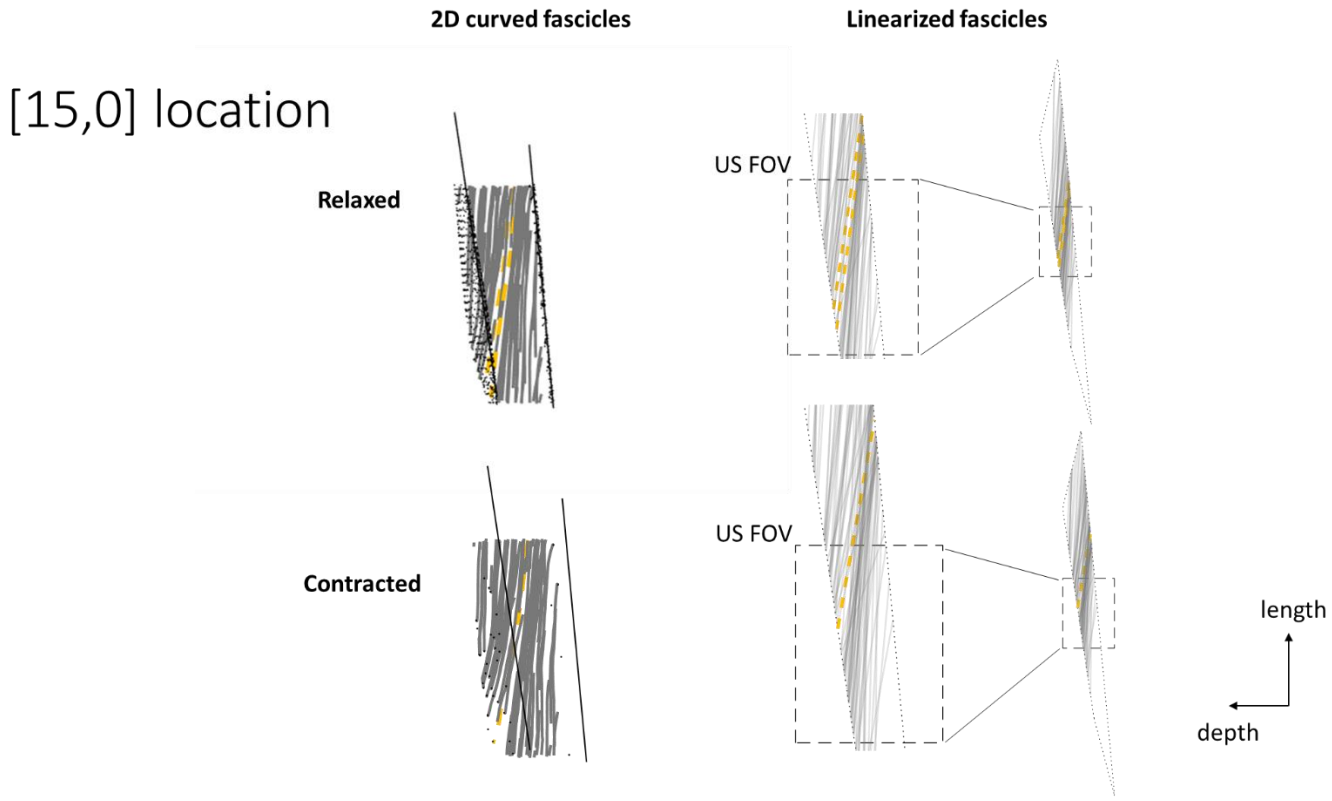
[15,0] location
2D curved fascicles
Linearized fascicles
Relaxed
Contracted
US FOV
US FOV
length
depth

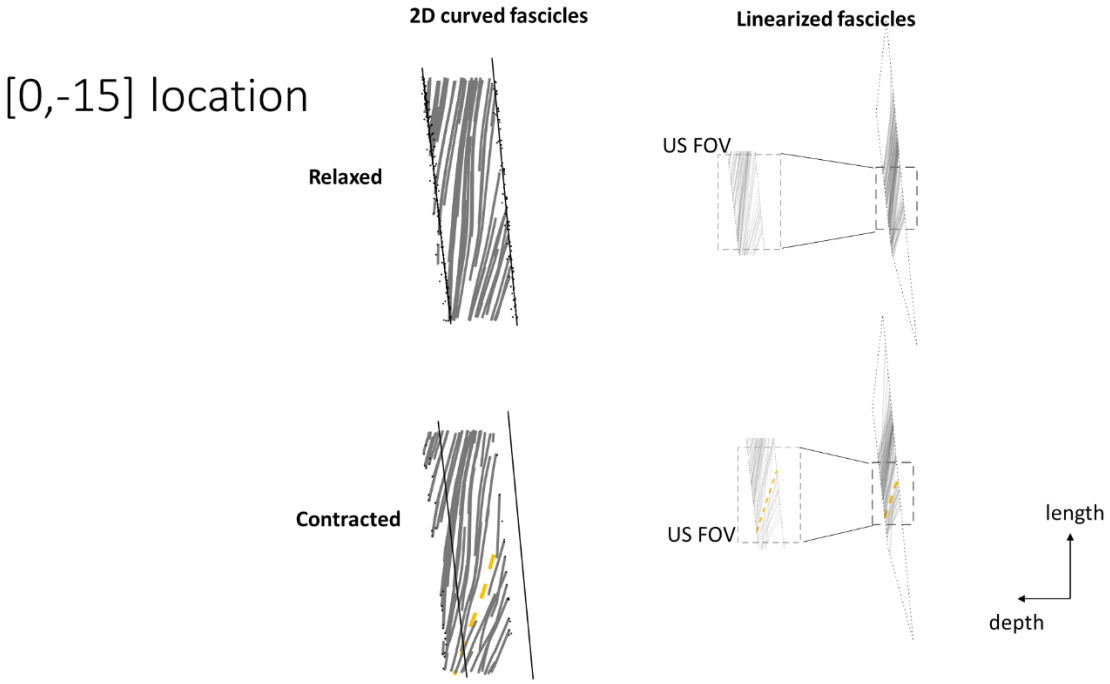
[0,-15] location
2D curved fascicles
Linearized fascicles
Relaxed
Contracted
US FOV
US FOV
length
depth

[-15,-30] location

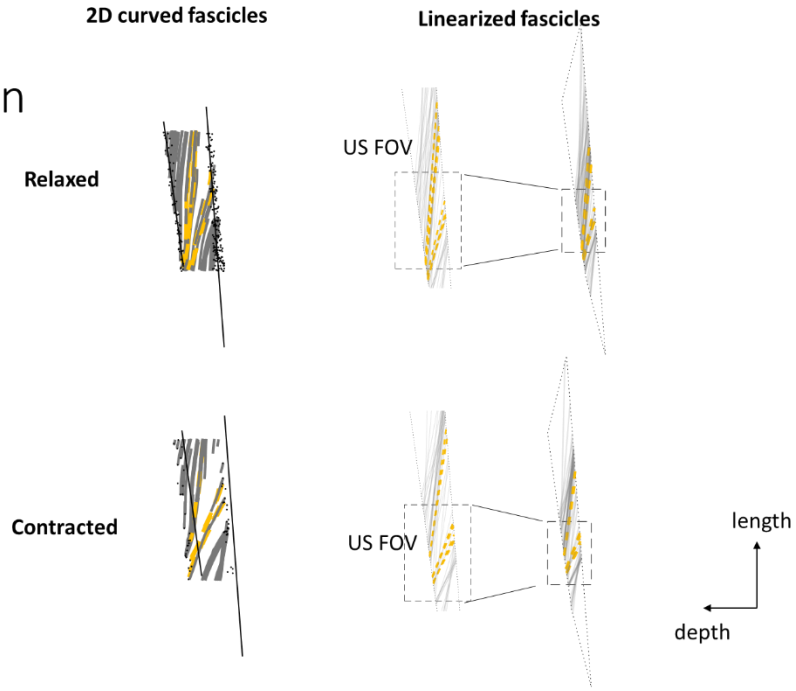

[0,-30] location

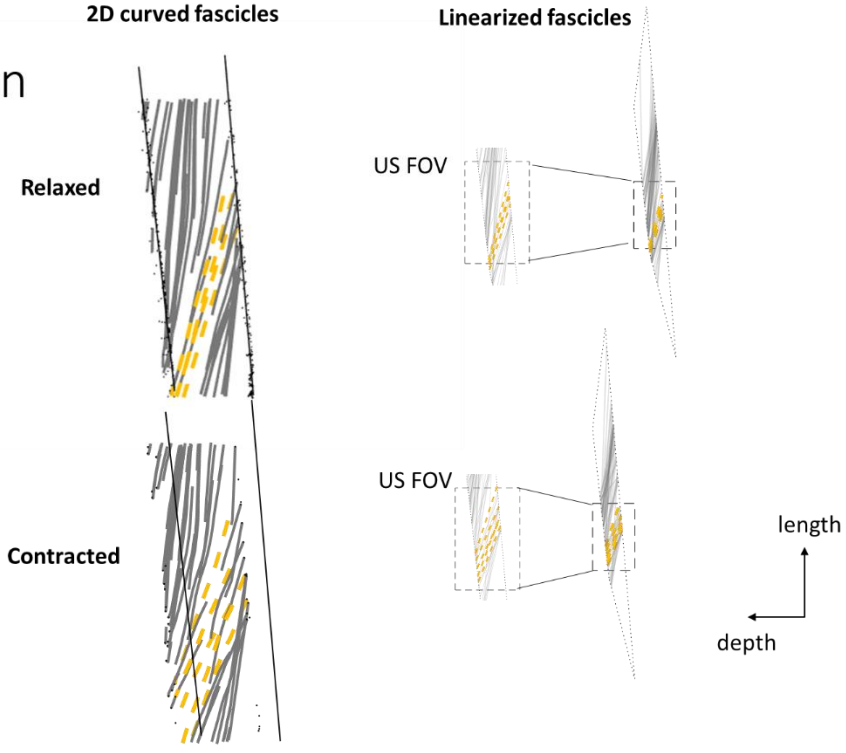

Appendix 2: Percentage difference between mean 2D and 3D architecture measurements by location

Linearized fascicle measurements (locations 1-5)

Architecture measurement	[0,30] location		[15,30] location		[0,15] location		[-15,0] location		[0,0] location	
	Initial	Final	Initial	Final	Initial	Final	Initial	Final	Initial	Final
# of 3D fascicles ≥75% present in FOV	5	8	0	0	8	8	8	11	5	5
# of fascicles ≥75% present in FOV when both relaxed and contracted	N/A	3	N/A	0	N/A	3	N/A	6	N/A	1
mean percentage of 3D FL in FOV	0.85347	0.898313	N/A	N/A	0.860203	0.919757	0.868679	0.8781	0.842365	0.8557
mean FL ± std.	60.38961	49.00548	N/A	N/A	54.60842	44.08608	55.56976	43.51854	58.8779	47.52781
mean PA ± std.	10.83507	12.69619	N/A	N/A	2.48793	4.829157	3.593438	7.001842	3.972017	3.982866
change in mean FL	18.62984	24.07697	N/A	N/A	19.12095	24.345	17.98488	23.68955	17.4212	21.99346
change in mean PA	2.749564	2.749564	N/A	N/A	0.796144	0.796144	1.240032	1.240032	1.186871	1.186871
mean FL of all fascicles in FOV	N/A	-11.3841	N/A	N/A	N/A	-10.5223	N/A	-12.0512	N/A	-11.3501
mean PA of all fascicles in FOV	N/A	5.447129	N/A	N/A	N/A	5.22405	N/A	5.704666	N/A	4.572262
# of 3D fascicles ≥75% present in FOV	62.86019	50.65369	61.5844	53.18533	67.89572	57.43826	62.69977	53.12866	72.66189	61.3381
# of fascicles ≥75% present in FOV when both relaxed and contracted	**18.26318**	**25.09827**	**26.11051**	**25.00336**	**17.49506**	**19.92223**	**17.01769**	**21.26628**	**15.12494**	**18.27134**

Linearized fascicle measurements (locations 6-10)

Architecture measurement	[15,0] location		[0,-15] location		[-15,-30] location		[0,-30] location		[15,5] location	
	Initial	Final	Initial	Final	Initial	Final	Initial	Final	Initial	Final
# of 3D fascicles ≥75% present in FOV	2	1	0	1	9	8	4	5	2	1
# of fascicles ≥75% present in FOV when both relaxed and contracted	N/A	0	N/A	0	N/A	3	N/A	2	N/A	0
mean percentage of 3D FL in FOV	0.803321	0.785714	N/A	0.829268	0.813065	0.907576	0.884941	0.918711	0.819285	0.828571
mean FL ± std.	67.61257	64.43687	N/A	40.73432	69.6837	44.03108	43.61763	36.06998	64.87971	64.08212
mean PA ± std.	1.090255	0	N/A	0	26.21622	20.69509	2.986348	3.599052	2.846525	0
change in mean FL	16.65616	18.51291	N/A	24.57048	17.31254	27.50247	22.44556	27.87749	17.58252	18.5166
change in mean PA	0.470044	0.470044	N/A	N/A	5.353787	5.353787	1.387958	1.387958	0.403153	0.403153
mean FL of all fascicles in FOV	N/A	-3.1757	N/A	N/A	N/A	-25.6526	N/A	-7.54765	N/A	-0.79759
mean PA of all fascicles in FOV	N/A	1.856756	N/A	N/A	N/A	10.18993	N/A	5.431937	N/A	0.934078
# of 3D fascicles ≥75% present in FOV	65.45071	61.61206	70.09499	56.36102	76.20344	66.65372	71.75521	58.92886	60.74887	59.50033
# of fascicles ≥75% present in FOV when both relaxed and contracted	17.70964	19.77545	15.23603	20.36307	31.45349	23.03332	46.84472	35.50766	19.16777	20.70662

3D fascicle measurements (locations 1-5)

Architecture measurement	[0,30] location		[15,30] location		[0,15] location		[-15,0] location		[0,0] location	
	Initial	Final	Initial	Final	Initial	Final	Initial	Final	Initial	Final
# of 3D fascicles ≥75% present in FOV	5	8	0	0	8	8	8	8	5	5
# of fascicles ≥75% present in FOV when both relaxed and contracted	N/A	3	N/A	0	N/A	3	N/A	3	N/A	1
mean percentage of 3D FL in FOV	0.85347	0.898313	N/A	N/A	0.860203	0.919757	0.860203	0.919757	0.842365	0.8557
mean FL ± std.	62.32803	49.50659	N/A	N/A	52.50051	43.82772	52.50051	43.82772	55.29641	44.37385
mean PA ± std.	10.1585	11.34222	N/A	N/A	2.738992	4.636502	2.738992	4.636502	6.425727	5.931739
change in mean FL	17.14186	23.67709	N/A	N/A	19.36394	23.48845	19.36394	23.48845	17.37804	23.40064
change in mean PA	1.805105	4.371412	N/A	N/A	2.206247	5.176067	2.206247	5.176067	4.936236	6.453954
mean FL of all fascicles in FOV	N/A	-12.8214	N/A	N/A	N/A	-8.67279	N/A	-8.67279	N/A	-10.9226
mean PA of all fascicles in FOV	N/A	-5.41709	N/A	N/A	N/A	-5.94567	N/A	-5.94567	N/A	-5.75597
# of 3D fascicles ≥75% present in FOV	60.55597	49.25971	61.58569	53.62995	61.55445	51.58272	61.55445	51.58272	61.70538	52.04633
# of fascicles ≥75% present in FOV when both relaxed and contracted	15.70053	22.29772	17.52207	24.33003	15.94714	20.55895	15.94714	20.55895	15.84463	20.67947

3D fascicle measurements (locations 6-10)

Architecture measurement	[15,0] location		[0,-15] location		[-15,-30] location		[0,-30] location		[15,5] location	
	Initial	Final	Initial	Final	Initial	Final	Initial	Final	Initial	Final
# of 3D fascicles ≥75% present in FOV	1	0	1	9	8	4	5	1	2	1
# of fascicles ≥75% present in FOV when both relaxed and contracted	0	N/A	0	N/A	3	N/A	2	0	N/A	0
mean percentage of 3D FL in FOV	0.785714	N/A	0.829268	0.813065	0.907576	0.884941	0.918711	0.785714	0.819285	0.828571
mean FL ± std.	76.79401	N/A	42.16455	58.85328	40.17697	44.66563	36.84192	76.79401	68.95659	76.79401
mean PA ± std.	0	N/A	0	10.63205	10.16507	2.324006	3.987215	0	4.153895	0
change in mean FL	23.33185	N/A	22.13028	15.94814	25.21728	19.88377	25.71593	23.33185	17.54686	23.33185
change in mean PA	0	N/A	0	2.548963	3.857928	1.236218	2.96873	0	1.447993	0
mean FL of all fascicles in FOV	7.007552	N/A	N/A	N/A	-18.6763	N/A	-7.82371	7.007552	N/A	7.83742
mean PA of all fascicles in FOV	-2.95951	N/A	-5.45387	N/A	-6.98124	N/A	-6.96344	-2.95951	N/A	-2.95951
# of 3D fascicles ≥75% present in FOV	54.66879	59.66437	49.43823	59.71806	47.78591	58.91665	49.7977	54.66879	62.6929	53.55258
# of fascicles ≥75% present in FOV when both relaxed and contracted	18.77027	16.02663	21.08667	16.74672	21.99892	16.50952	21.21359	18.77027	16.16885	18.70817

Percentage error of linearized fascicle measurements (locations 1-5)

Architecture measurement	[0,30] location		[15,30] location		[0,15] location		[-15,0] location		[0,0] location	
	Initial	Final	Initial	Final	Initial	Final	Initial	Final	Initial	Final
ave. FL	3%	1%	N/A	N/A	-4%	-1%	-6%	1%	-6%	-7%
ave. PA	-9%	-2%	N/A	N/A	1%	-4%	7%	-1%	0%	6%
change in mean FL	N/A	11%	N/A!	N/A	N/A	-21%	N/A	-39%	N/A	-4%
change in mean PA	N/A	201%	N/A	N/A	N/A	188%	N/A	196%	N/A	179%
mean FL (all fascicles in FOV)	-4%	-3%	0%	1%	-10%	-11%	-2%	-3%	-18%	-18%
mean PA (all fascicles in FOV)	-16%	-13%	-49%	-3%	-10%	3%	-7%	-3%	5%	12%

Percentage error of linearized fascicle measurements (locations 6-10)

Architecture measurement	[15,0] location		[0,-15] location		[-15,-30] location		[0,-30] location		[15,5] location	
	Initial	Final	Initial	Final	Initial	Final	Initial	Final	Initial	Final
ave. FL	3%	16%	N/A	3%	-18%	-10%	2%	2%	6%	17%
ave. PA	-16%	21%	N/A	-11%	-9%	-9%	-13%	-8%	0%	21%
change in mean FL	N/A	145%	N/A	N/A	N/A	-37%	N/A	4%	N/A	110%
change in mean PA	N/A	163%	N/A	N/A	N/A	246%	N/A	178%	N/A	132%
mean FL (all fascicles in FOV)	-4%	-13%	-17%	-14%	-28%	-39%	-22%	-18%	3%	-11%
mean PA (all fascicles in FOV)	-10%	-5%	5%	3%	-88%	-5%	-184%	-67%	-19%	-11%